

**Continuously variable lipid packing
as the principle of functional
membrane heterogeneity**



Dissertation

zur Erlangung des wissenschaftlichen Grades
PhD

vorgelegt der
Fakultät Mathematik und Naturwissenschaften
der Technischen Universität Dresden

von
Erdinc Sezgin
geboren am 11.03.1985 in der Türkei

Gutachter: Prof. Dr. Petra Schwille und Prof. Dr. Kai Simons

Abgabedatum: 30.11.2012

Datum der Verteidigung:

List of publications

The results presented in this thesis work have partly been communicated before in the articles listed below:

Erdinc Sezgin and Petra Schwille

Fluorescence techniques to study lipid dynamics. *Cold Spring Harb Perspect Biol.* **3(11)**, 144-154 (2011).

Erdinc Sezgin and Petra Schwille

Model membrane platforms to study membrane-protein interactions. *Molecular Membrane Biology* **25(5)**, 144-154 (2012).

Erdinc Sezgin, Hermann-Josef Kaiser, Tobias Baumgart, Petra Schwille, Kai Simons, Ilya Levental

Elucidating membrane structure and protein behavior using giant plasma membrane vesicles. *Nature Protocols* **7(6)**, 1042-1051 (2012).

Aliaksei Dubavik*, **Erdinc Sezgin***, Vladimir Lesnyak, Nikolai Gaponik, Petra Schwille and Alexander Eychmüller

Penetration of amphiphilic quantum dots through the model and cellular plasma membranes. *ACS Nano* **6(3)**, 2150-2156 (2012). (*Equal first author contribution)

Erdinc Sezgin, Ilya Levental, Günter Schwarzmann, Veronika Mueller, Alf Honigmann, Vladimir N. Belov, Christian Eggeling, Unal Coskun, Kai Simons, Petra Schwille

Partitioning, diffusion, and ligand binding of raft lipid analogs in model and cellular plasma membranes. *BBA-Biomembranes* **1818(7)**, 1777-1784 (2012).

James P. Saenz, **Erdinc Sezgin**, Petra Schwille and Kai Simons

Functional convergence of hopanoids and sterols in membrane ordering. *PNAS* **109(35)**, 14236-14240 (2012).

Abstract

Lipid rafts are nanoscale entities in the membranes of eukaryotic cells which provide a mechanism for the functional membrane segregation vital for several cellular processes. This lateral segregation of specific lipid and protein components provides the facilitative platforms for a variety of signaling and trafficking events at the plasma membrane and in the Golgi. Rafts are distinguished from the surrounding membranes by their physical properties and composition - they are relatively tightly packed and enriched in saturated lipids, sterols, and lipid-anchored proteins. Although the existence of rafts has been conclusively confirmed by several independent techniques, questions concerning various aspects of membrane heterogeneity are still to be addressed. Typical experiments investigating raft composition have been designed to evaluate the affinity of a given component for raft domains. In such experiments, the results are usually interpreted in a Boolean fashion, i.e., the component is either a raft molecule, or not. However, this binary point of view overlooks potential complexity that may underlie the nature of membrane heterogeneity.

In this work, we systematically investigated the nature of functional cellular membrane heterogeneity. We started by characterizing the model membranes and fluorescent lipid analogs widely used in research into membrane domains. After extensively evaluating the potentials/limits of these approaches and the artifacts that must be avoided or alternatively could be exploited, we applied these tools to understand whether the cell membrane has multiple kinds of raft domains with distinct compositions and physical properties, rather than only one. We found that cell membranes have the potential to form various kinds of functional domains having different physicochemical properties, compositions, and functional outputs. Therefore, we propose continuously variable lipid packing as the principle of the functional membrane lateral heterogeneity. According to this principle, the membrane is not composed of a single variety of raft domain with strictly defined properties coexisting alongside a specific and uniform non-raft environment; rather it is composed of entities having continuously variable lipid packing. Finally, we show that this spectrum of membrane packing modulates the orientation of membrane lipid receptors, which ultimately influences their specific bioactivity. Our results showing continuously variable lipid packing and its ability to fine-tune the activity of membrane molecules comprise a novel model for the structure and function of

eukaryotic membranes.

Contents

| | |
|---|------------|
| List of publications | iii |
| Abstract | v |
| Introduction and Outline | xi |
| | |
| I. Theoretical Background | 13 |
| 1. Introduction to Membrane Heterogeneity | 15 |
| 2. Fluorescence Techniques to Study Membrane Heterogeneity | 17 |
| 2.1. The Fluorescence | 18 |
| 2.2. Confocal microscopy | 19 |
| 2.3. Two-Photon microscopy | 20 |
| 2.4. Fluorescence Correlation Spectroscopy (FCS) | 22 |
| 2.5. Stimulated Emission Depletion (STED) Nanoscopy | 25 |
| 3. Fluorescent Probes to Study Membrane Heterogeneity | 27 |
| 3.1. Phase Specific Lipid Analogs | 27 |
| 3.2. Phase Sensitive Lipid Analogs | 28 |
| 3.3. New Lipids to Visualize the Cellular Lipidic Organelles | 30 |
| 4. Model Membranes to Study Membrane Heterogeneity | 31 |
| 4.1. Historical background | 31 |
| 4.2. Supported Lipid Bilayers (SLBs) | 33 |
| 4.3. Giant Unilamellar Vesicles (GUVs) | 34 |
| 4.4. Giant Plasma Membrane Vesicles | 35 |
| 4.5. Outlook - the future of model membranes | 36 |
| | |
| II. Investigations and Applications of Plasma Membrane Model Systems | 39 |
| | |
| 5. Giant Plasma Membrane Vesicles | 41 |
| 5.1. Introduction | 41 |
| 5.2. Plasma membrane vesicles | 42 |
| 5.3. Phase separation in GPMVs | 42 |
| 5.4. Alternative techniques | 43 |

| | |
|--|-----------|
| 5.5. Limitations of GPMVs as a plasma membrane model system | 44 |
| 5.6. Experimental design | 45 |
| 5.7. Purification and concentration of membranes | 45 |
| 5.8. Considerations for visualization of GPMVs by fluorescence microscopy | 46 |
| 5.9. Quantification of phase order in GPMVs | 47 |
| 5.10. Temperature-controlled imaging | 48 |
| 5.11. Characterization of component partitioning | 49 |
| 5.12. Controls | 50 |
| 5.13. Tips for GPMV yield | 51 |
| 5.14. Artifacts induced by vesiculation chemicals | 51 |
| 6. GUVs and GPMVs as Models to Study Cell Membrane Penetration: Amphiphilic Quantum Dot Penetration | 53 |
| 6.1. Introduction | 53 |
| 6.2. Materials and Methods | 54 |
| 6.2.1. Synthesis of CdTe/mPEG-SH nanocrystals | 54 |
| 6.2.2. Characterization of CdTe/mPEG-SH nanocrystals | 54 |
| 6.2.3. GUV preparation | 55 |
| 6.2.4. GPMV preparation | 55 |
| 6.2.5. Colloidal stability test | 55 |
| 6.2.6. Confocal microscopy imaging | 55 |
| 6.3. Results and Discussion | 56 |
| 6.4. Conclusions | 59 |
| 7. GPMVs for Investigating the Protein Partitioning in Cell Membrane: Raft Mediated Regulation of Lypd6 and LRP6 Activation | 61 |
| 7.1. Introduction | 61 |
| 7.2. Materials and Methods | 62 |
| 7.2.1. Cloning | 62 |
| 7.2.2. Secretion assay | 62 |
| 7.2.3. Luciferase assays | 63 |
| 7.2.4. Western blot analysis and immunoprecipitation | 63 |
| 7.3. Results and Discussion | 63 |
| 7.3.1. Lypd6 is GPI-anchored to the plasma membrane | 63 |
| 7.3.2. Lypd6 interacts with LRP6 independently of its GPI-anchor | 64 |
| 7.3.3. Lypd6 partitioning into rafts influences Wnt signaling activation | 64 |
| 7.3.4. Lypd6 regulates LRP6 distribution in plasma membrane phases | 66 |
| 7.4. Conclusion | 67 |
| 8. Investigation of Membrane Order Regulation in Prokaryotes with Model Membranes | 69 |
| 8.1. Introduction | 69 |
| 8.2. Materials and Methods | 69 |
| 8.2.1. Lipids and Probes | 70 |

| | |
|---|----|
| 8.2.2. Monolayers | 70 |
| 8.2.3. Preparation of liposomes and C-laurdan spectroscopy | 71 |
| 8.3. Results and Discussion | 72 |
| 8.3.1. The effects of cholesterol and diplopterol on the phase behavior and ordering of sphingomyelin in model membranes | 72 |
| 8.3.2. Cholesterol and diplopterol interact with sphingomyelin to form a liquid ordered phase in giant unilamellar vesicles | 73 |
| 8.3.3. Cholesterol and diplopterol modulate the order and phase behavior of lipid A in model membranes | 74 |
| 8.4. Conclusion | 76 |

III. The Nature of Membrane Lateral Heterogeneity 79

9. Partitioning, Diffusion, and Ligand Binding of Raft Lipid Analogs in Model and Cellular Plasma Membranes 81

| | |
|---|----|
| 9.1. Introduction | 82 |
| 9.2. Materials and Methods | 83 |
| 9.2.1. Fluorescent probes | 84 |
| 9.2.2. Determination of Lo partitioning and lipid analog brightness | 84 |
| 9.2.3. STED-FCS measurements | 85 |
| 9.3. Results and Discussion | 87 |
| 9.3.1. Partitioning in GUVs | 87 |
| 9.3.2. Differential partitioning of lipid analogs in GUVs and GPMVs | 88 |
| 9.3.3. Label size, hydrophobicity, and position affect analog partitioning | 88 |
| 9.3.4. Labeling affects binding of GM1 to CTxB | 90 |
| 9.3.5. Partitioning of lipid analogs is uncorrelated with its nanoscale diffusion in living cells | 91 |
| 9.4. Conclusion | 94 |

10. Continuously Variable Lipid Packing 97

| | |
|---|-----|
| 10.1. Introduction | 97 |
| 10.2. Materials and Methods | 98 |
| 10.3. Results and Discussion | 98 |
| 10.3.1. Order of phases can be tuned in GUVs and GPMVs | 98 |
| 10.3.2. Lipid packing affects the membrane related binding | 99 |
| 10.3.3. Lipid environment influences the geometry of membrane molecules | 101 |
| 10.3.4. Cells can tune their lipid packing | 102 |
| 10.4. Conclusion | 103 |

11. Conclusion 105

Appendix 107

| | |
|------------------------|------------|
| Bibliography | 109 |
| Acknowledgments | 131 |

Introduction and Outline

The cellular plasma membrane has long been pictured as two parallel layers of solely lipid components which creates a passive barrier between the inner cell and the outside. However, this idea has been replaced after the proteins has been found as important elements of the plasma membrane. Moreover, this picture was revolutionized by the introduction of heterogeneity in the membrane, the raft hypothesis. According to this concept, there are nanodomains in the cell membrane enriched in saturated lipids, cholesterol and certain proteins such as GPI-anchor proteins. Although the raft concept is largely accepted among the scientific community, there are still several questions to be answered and contradicting data to be unraveled concerning the nature of rafts (composition, dynamics, size etc.). The main issue in raft research is to apply the right tools (which include the techniques (microscopy, spectroscopy etc.), molecular probes and model membrane systems) for certain kind of questions. Each tool has certain advantages and disadvantages. They produce their own facts and artifacts.

This thesis work presents a systematic way to investigate the physicochemical nature of cellular membrane heterogeneity. It consists of three parts.

Part I constitutes the theoretical basis. The first chapter in this part will start with a general introduction to the question of membrane heterogeneity. The history, evolution and open questions will be addressed. This part is followed, in the second chapter, by the introduction to the fluorescent techniques to investigate the membrane heterogeneity. In this chapter, we will focus on the most widely used techniques for membrane research which also have been extensively used in this thesis. In the next chapter we will discuss the fluorescent probes to study membrane heterogeneity. Finally, in the last chapter of this part, widely used model membrane systems will be discussed and compared.

Part II which will focus on the investigations and the applications of plasma membrane models starts with a detailed chapter about Giant Plasma Membrane Vesicles (GPMVs) which constitutes an intermediate model membrane system between fully synthetic membranes and living cell membrane. Despite being shortly mentioned in Part I, we dedicate this chapter to GPMVs as they constitute a vital part of this thesis not least because the characterization of GPMVs resulted in very key questions of this thesis. In the next chapter, we will show the potential applications of Giant Unilamellar Vesicles (GUVs) and GPMVs as models to investigate the cell membrane penetration of amphiphilic quan-

tum dots which is vital for drug delivery applications. In the following chapter, we will present a study where we applied GPMVs to investigate membrane protein partitioning in rafts. Raft dependent regulation of LRP6 and Lypd6 proteins which take important part in Wnt signaling will be presented in this chapter. In the last chapter, we present the application of GUVs to figure out the membrane ordering regulation mechanism in prokaryotes.

After a thorough theoretical basis presented in Part I and extensive characterization of model membranes and probes along with several applications presented in Part II, in Part III, we will present our current view of membrane heterogeneity. The first chapter in this part will be focused on mainly the fluorescent lipid analog partitioning in GUVs and GPMVs. Moreover, a comparison between model membrane partitioning and the diffusion of the fluorescent lipid analogs in cell membrane will be presented. Observing, in this chapter, that the heterogeneity in the living cell membrane is beyond the phase separation in model membranes will take us to the last chapter where we discuss how we believe the heterogeneity of the cell membrane is (See Figure 1 to check the thesis at a glance).

Thesis at a Glance

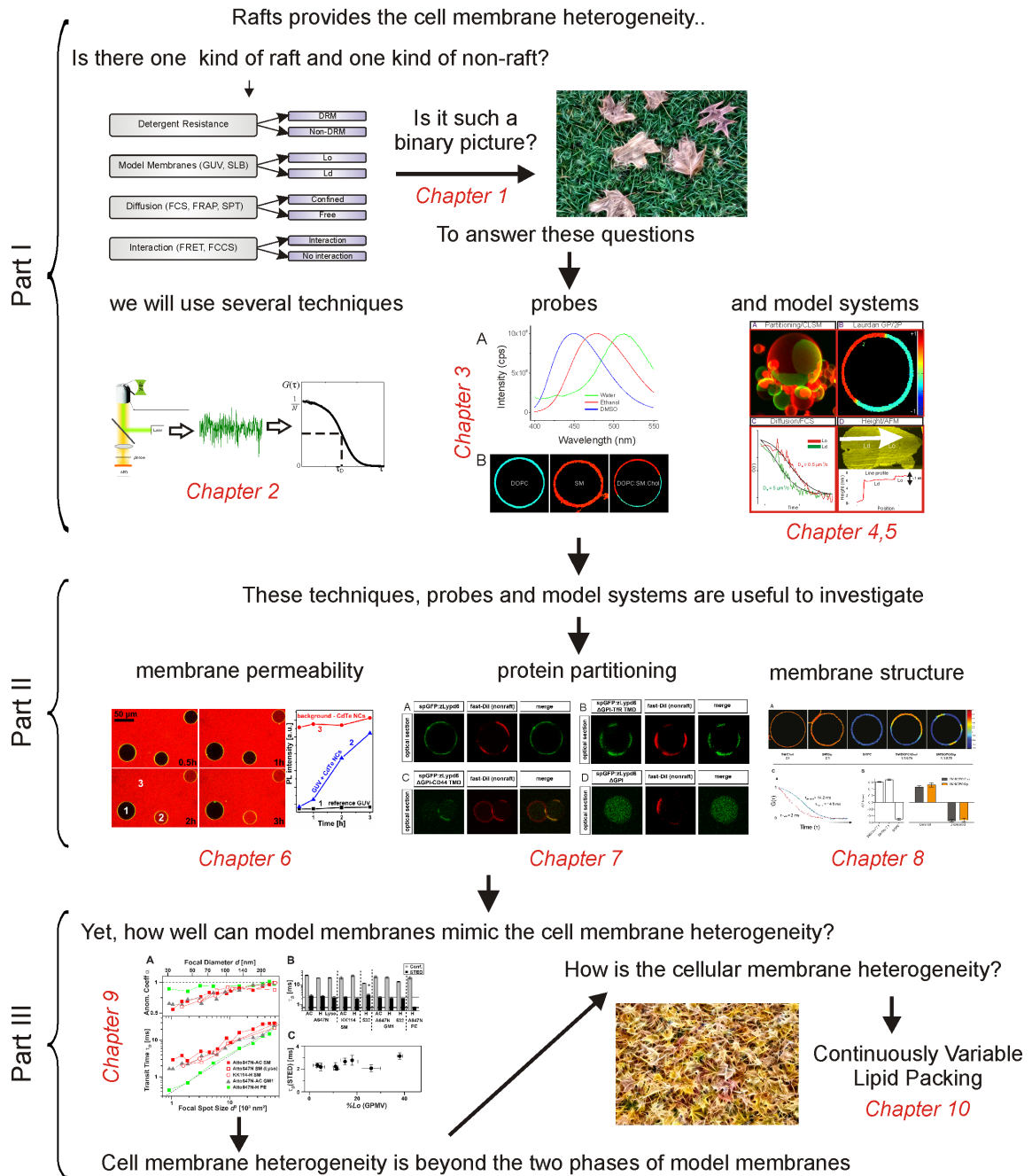


Figure 1. Thesis at a glance.

Part I.

Theoretical Background

Introduction to Membrane Heterogeneity

Since the introduction of the cell membrane concept [1, 2], the "Fluid Mosaic" model [3] has the most dramatic impact on the modern understanding of the cellular plasma membrane. It described the membrane as a homogeneous lipid environment with embedded proteins, which appeared to be remarkably accurate. The first major correction to the concept of a homogeneous fluid mosaic followed upon the discovery of detergent resistant membranes (DRMs), which required a model explaining a heterogeneous lipid structure of the plasma membrane [4]. The heterogeneous distribution of lipids in the apical, compared to the basolateral, plasma membrane in polarized epithelia was observed, strengthening the concept of heterogeneous membrane structure [5]. Although detergent resistant proteins were also observed in early 1990s [6], it was 1997 when the raft concept was introduced, proposing functional lipid-induced domains [7]. According to this concept, the membrane has small dynamic domains which are composed of tightly packed saturated lipids and enriched with cholesterol. Although there has been a notable opposition to the concept in the beginning, it diffused into the cell biology, biophysics and physical chemistry fields extremely fast (Figure 1.1). There has been around 1200 scientific articles on average per year related to "lipid rafts" published for the last 8 years.

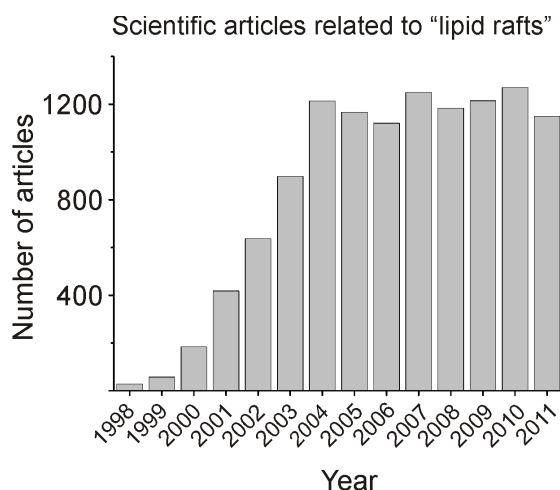


Figure 1.1. Number of articles published between 1998-2010 related to lipid rafts (data collected from ISI Web of Knowledge)

Having such an multidisciplinary impact, several tools were used to confirm and pinpoint the molecular details behind this phenomenon. Phase separation, for instance, was extensively investigated in synthetic membrane systems as models for lipid raft mediated membrane heterogeneity [8, 9]. Besides model membranes and detergent resistance assays, various microscopy and spectroscopy techniques were employed to address the key questions concerning this concept [10]. The diffusion characteristics of raft molecules in the cell membrane, interactions of different raft molecules, role of intracellular structures such as cytoskeleton and extracellular structures on raft formation/structure were among the questions intensively pursued. Although the questions remained the same, the answers usually were quite different when different methods/techniques were applied. This situation created vivid discussions about various different aspects of rafts such as mobility [11, 12], composition [13, 14] or size [13, 15, 16]. However, there was usually a pre-acceptance of a single kind of "raft" and a single kind of "non-raft". Therefore, all the techniques and the methods were set to give binary results when applied to this particular question (e.g., molecules are either in raft or in non-raft domains) (Figure 1.2). Collecting all the results obtained by using different techniques under the "raft" or "non-raft" umbrella created the confusion as there were many contradicting data. While there was such an effort to address the questions mentioned above, there has been a few reports questioning the validity of the "binary" pre-acceptance about the nature of membrane heterogeneity [17, 18] which is going to be the key question of this thesis.

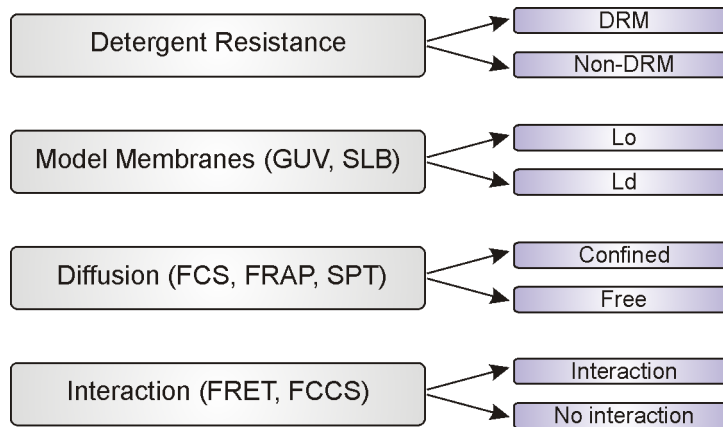


Figure 1.2. Binary interpretation of the results obtained by common techniques and methods.

Fluorescence Techniques to Study Membrane Heterogeneity

To elucidate cellular processes in their native dynamic environment has been one of the main issues in cell biology over the past decades. The lack of appropriate techniques has long been the main limiting step for the research on dynamic systems, because it was impossible to acquire real time information with the well-known biochemical techniques. The key challenge in dynamically observing biological systems is to combine the ability to resolve moderate to very low concentrations of molecules -because they are simply limited in living cells- on relevant timescales. Relevant timescales in cell biology can be minutes and hours, on a systemic level of cell metabolism, down to the micro- and even nanoseconds regime in which molecular and intramolecular rearrangements take place. With respect to lipidic systems, relevant dynamics range from the local movements of lipids by diffusion to the mechanical transformations of whole membranes, spanning several orders of magnitude in time to be covered. Like for other cellular processes, also the investigation of lipids and membranes in general benefited greatly from the introduction of fluorescence microscopy and spectroscopy to biology. After the 60s, great technological inventions based on the phenomenon of fluorescence were made, such as confocal microscopy, fluorescence recovery after photobleaching (FRAP), fluorescence correlation spectroscopy (FCS), Förstner resonance energy transfer (FRET), total internal reflection fluorescence (TIRF), and two-photon microscopy, that revolutionized not only imaging, but also yielded access to dynamics on previously inaccessible timescales. Another very big step was certainly taken after the introduction of fluorescent proteins, which again accelerated the use of these techniques in living cells and organisms. Nowadays, the technical advancements of fluorescence-based methods allow us to explore systems as small as single molecules with temporal resolution down to the nanoseconds regime. Lately, even the resolution limit of optical microscopy, for a long time being one of the fundamental barriers in elucidating cellular processes, has been overcome by smart applications of the phenomenon of fluorescence.

This chapter aims at giving a short overview on mainly fluorescence-based methods that have in recent years propelled lipid and membrane research to fully new levels. We will give a short introduction to the fluorescence technology extensively used in this thesis, referring to the techniques that allow addressing membrane heterogeneity.

2.1. The Fluorescence

The attempt to visualize the "living units" has progressed remarkably after Hooke's *Micrographia*. Starting from a simple light source, a mechanical stage and up to three glass lenses, microscopy nowadays culminated in so-called super-resolution techniques with particle localization accuracies down to the nanometer range. Certainly, the involvement of the phenomenon of fluorescence is one of the biggest steps in this long journey.

Fluorescence is such a ubiquitous phenomenon that it is impossible to speculate about its first systematic observation. The first reported documentation of fluorescence is thought to be Nicolas Monardes' observation of wood extract. In 1845, John Herschel observed the fluorescent property of quinine sulphate which is believed to be the onset of modern fluorescence spectroscopy. After many more observations by several light philosophers in the nineteenth century, it was Stokes who actually termed this phenomenon "fluorescence" in 1838. The first application in biology was probably in 1914 Stanislav von Provazek who used fluorescence as a cell stain. August Koehler and Oscar Heimstaedt were reportedly the first scientists who performed fluorescence microscopy in early 1900's. Today, a century later, fluorescence imaging and microscopy is one of the most powerful tools in the visualization and dynamic analysis of living structures, especially following the discovery of fluorescent proteins as cloneable markers, and the invention and widespread use of confocal microscopy. Minsky, its inventor, patented the idea of confocal microscopy already in the 1950s, and about 20 years later, the first commercial confocal microscopes appeared. Since then, many researchers and optical engineers step by step improved the technical realization [19–23]. The rapid developments in laser and detector technology, along with the onset of fiber optics certainly helped in the rapid dissemination of confocal microscopy into cell biology laboratories around the world [24].

When light interacts with matter, many photophysical phenomena may occur. Some molecules absorb light at a particular wavelength, while others predominantly scatter the light. Upon absorption, the molecules undergo vibrational relaxation on timescales between 10^{-14} and 10^{-12} s, and then return to ground state, either by emitting a photon at a longer wavelength after 10^{-9} to 10^{-7} ns, which is called fluorescence, or nonradiatively. Less probably, the molecules can jump to the quantum-mechanically forbidden triplet state or molecules transfer their energy to other molecules, by quenching or resonant energy transfer. After the molecules undergo the triplet state, they return to the ground state either by emitting light in longer time ranges than fluorescence or nonradiatively.

In the following sections, we will discuss, one by one, the most powerful fluorescence techniques to study membrane heterogeneity which were used in several parts of the work.

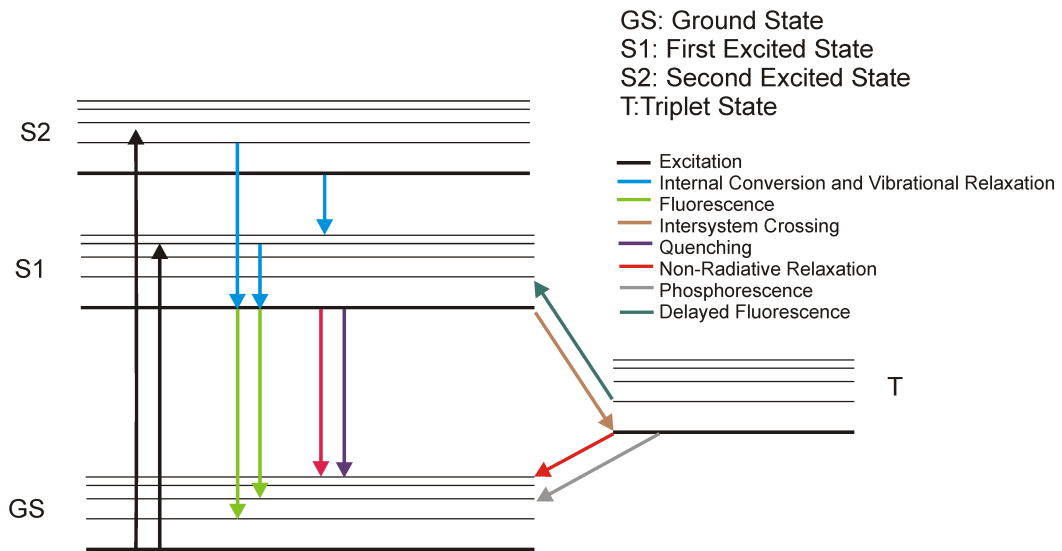


Figure 2.1. Jablonski diagram.

2.2. Confocal microscopy

Confocal microscopy may easily be the most widely applied imaging technique in cell and molecular biology field, since it allows live cell imaging with high spatial and temporal resolution, as well as optical sectioning and 3D reconstruction of images. To start with the techniques for cell dynamics, confocal microscopy should therefore be briefly mentioned since it forms the basis (and often, the gold standard) for most of the other techniques.

The confocal concept evolved as an alternative to wide field microscopy. For wide field microscopy, the so-called Koehler illumination guarantees a homogeneous illumination of the whole sample, which is then detected by area detectors. In contrast to this, confocal illumination occurs only at a resolution-limited point, which can then be sequentially scanned in three dimensions throughout the sample. As a technical difference, coherent light sources (lasers) are usually employed in confocal microscopy, while incoherent lamps are still mostly used in wide field microscopy. However, the basic difference between wide field and confocal is a so-called pinhole aperture which eliminates the out-of-focus light in the image plane, being the main source of background in wide field. The minimal size of the confocal illumination volume, and therefore the resolution that can be reached in confocal microscopy is usually determined by the so-called Rayleigh criterion. Here, resolution of the wide field is defined as the shortest distance d between two optically separable points;

$$d = \frac{0.61 \times \lambda}{NA} \quad (2.1)$$

where λ is the wavelength and NA the numerical aperture of the objective. When the advantage of selective detection (pinhole) and selective illumination (diffraction limited spot by coherent light source) are applied, the resolution reaches a better point;

$$d = \frac{0.4 \times \lambda}{NA} \quad (2.2)$$

Taking above equation into consideration, the theoretical resolution of a confocal system with an NA of 1.4, at a wavelength of 500 nm should be around 160 nm. However, all theoretical calculations consider a perfect optical system and a pinhole of a laser spot size (i.e., Airy disc size). Yet, there are many aberrations caused by imperfect optics such as spherical aberrations, chromatic aberrations, astigmatism, comma etc. Moreover, pinhole size can never be as small as laser spot size. The biggest problem in confocal microscopy is, however, the large discrepancy between lateral (xy) and axial resolution, resulting in image stacks that are usually quite blurred in z dimension.

Axial resolution is given by;

$$d = \frac{1.4 \times \lambda \times n}{NA^2} \quad (2.3)$$

where n is the refractive index of the medium. The axial resolution is usually 3-5 times worse than lateral resolution.

The limitation in axial resolution is a minor problem for pure membrane systems with little to no contribution of fluorescence light coming from the solution above and below the membrane. Thus, confocal microscopy has been particularly useful on supported membranes or Giant Unilamellar Vesicles (GUVs) [8]. On the other hand, for the study of cellular membranes with their rather high background from cellular autofluorescence and labeled molecules that cannot easily be retained at the cell surface (e.g., due to endocytosis), limited z resolution can be a significant technical problem in studying lipid dynamics. For this reason, other illumination strategies established for fluorescence microscopy, such as total internal reflection (TIR) are becoming increasingly popular for lipid and membrane research.

2.3. Two-Photon microscopy

The theoretical basis of two-photon excitation was laid in a study of the early 30's [25], although the experimental realization took almost three decades [26]. It was first used in LSM in the 70's [27] but a convincing two-photon excitation fluorescence microscopy

was only demonstrated in 1990 [28].

Two-photon microscopy, as the name implies, uses simultaneous absorption of two longer wavelength photons (at λ_1 and λ_2) to excite a fluorophore, which would be usually excited by a single photon at a shorter wavelength (λ_3). The relationship between the wavelengths is as follows;

$$\lambda_3 = \frac{1}{\lambda_1^{-1} + \lambda_2^{-1}} \quad (2.4)$$

Since the two photons have to be absorbed simultaneously to excite the fluorophore, the excitation is dependent on the square of the light intensity. This could be thought as an equivalent of the double selection in confocal imaging, achieved by a selective illumination by the light source and selective detection by a pinhole. Therefore, in the two-photon illumination mode, a pinhole is no longer necessary. Moreover, it minimizes the out-of-focus photobleaching since the excitation only occurs in the vicinity of the focal plane. Scattering is greatly reduced with two-photon excitation, and penetration depths for the long wavelength excitation are increased.

Because the emission does not have to pass through a pinhole, area detectors can be used and no de-scanning of the beam is necessary, making detection quite simple.

Another advantage of two-photon is its ability to excite fluorophores absorbing in the UV by two photons in visible range, which surpasses usual UV transmission problems with glass lenses. In combination with the reduced out-of-focus fluorescence, it also provides a suitable tool for UV uncaging *in vivo* without significant photo damage.

The photon density in two-photon excitation should be about one million times higher than is required for single photon excitation, because of the square dependence of the absorption on intensity. Therefore, pulsed lasers should be used with sufficient photon flux in the pulses while having fairly low average power. Titanium-sapphire lasers are extensively used for two-photon microscopes because they provide a wide range of excitation wavelengths between 700 nm to 1100 nm. Due to different photophysical selection rules, two-photon absorption spectra are not identical with twice the spectra for one-photon excitation, and have therefore to be independently determined.

Two-photon microscopy is very suitable to excite photo-sensitive, easily bleachable lipid probes in the blue to near-UV spectral range, such as Laurdan or C-Laurdan (see Section 3.2). These probes were used to detect the membrane domains in model membranes, as well as in living cells, by two-photon microscopy [9, 29–36]. Order of different membrane systems was investigated [37] and new probes to visualize the membrane order were tested by two-photon microscopy [38–40].

2.4. Fluorescence Correlation Spectroscopy (FCS)

Fluorescence correlation spectroscopy (FCS) is a method that has been extensively used and further developed by our group, being introduced and established as a very suitable approach to characterize model and cellular membranes [41, 42]. It is, in a way, a single molecule method, but provides sufficient statistical significance to also use it for general characterization of membranes, mainly through the diffusion properties of their constituents. It is thus related to FRAP, but provides several advantages, the most crucial of which is the dramatically improved sensitivity, allowing to work at significantly reduced fluorescence labeling densities. FCS has long been used to characterize domain-forming membranes [8], and recently, by combination with super resolution illumination [15], was able to resolve nanometer-sized entrapment sites of labeled raft-markers.

FCS measures small fluorescence intensity fluctuations in a defined volume. It provides accurate information about diffusion coefficients, concentrations, molecular brightness, intramolecular dynamics, and molecular interactions. It has been extensively used for a variety of biological applications, due to its great sensitivity. FCS has been combined with many different imaging methods, such as laser scanning confocal microscopy, two-photon microscopy, total internal reflection fluorescence microscopy, stimulated emission depletion nanoscopy and others, making it particularly feasible for cell biology.

FCS was first established in the 1970s [43–46] and technically greatly improved in the following years [47, 48]. Fluorescence intensity fluctuations, primarily addressed by FCS, can be caused by diffusion of the molecules through the observation volume, or by reversible brightness changes of the molecules because of some chemical or photophysical reactions [49]. FCS performs the statistical analysis of these fluctuations. In other words, it correlates a signal at a certain time t with the same signal after a lag time $t + \tau$, and takes the temporal average. This correlation can be described as self-similarity of the signal in time, which is represented by the autocorrelation function, a temporal decay function of average fluctuations. The basic formula for the fluctuation autocorrelation function is;

$$G(\tau) = \frac{\langle \delta F(t) \cdot \delta F(t + \tau) \rangle}{\langle F(t) \rangle^2} \quad (2.5)$$

where $\delta F(t) = F(t) - \langle F(t) \rangle$ is the fluctuation around the average intensity and $\langle \rangle$ denotes the temporal average; τ is the lag time. The denominator is for normalization.

The basic steps of FCS experiments are as follows. First, the sample is illuminated by the appropriate illumination technique. Generally, in the simplest representation of FCS, confocal illumination without beam-scanning is used. The fluorescence signal is

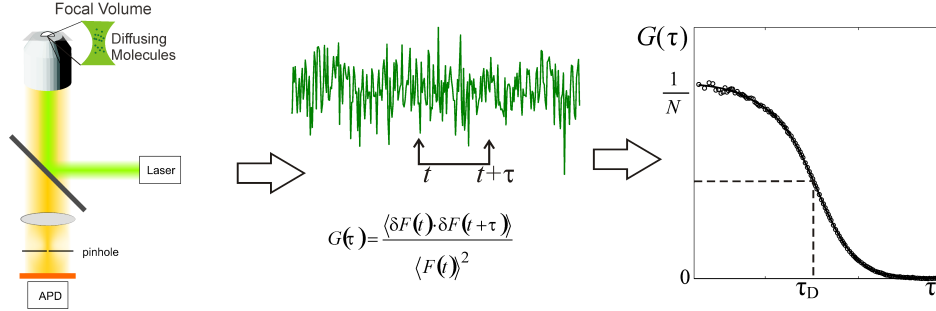


Figure 2.2. Fluorescence correlation spectroscopy.

collected by the objective and detected by sensitive photodetectors, often by avalanche photo diodes (APDs). After detecting the fluorescence intensity for a certain time, a hardware correlator usually correlates the signal from subsequent time points according to the correlation function mentioned above, and forms the experimental FCS curve. This correlation step can also be done retrospectively, if data is recorded in small enough ($< \mu s$) time bins. Then, the correlation curve as in Equation 2.5 is fitted by an appropriate fitting model to get the numerical values of diffusion times, concentrations and molecular brightness, or other parameters governing fluctuation decay.

As seen in the Figure 2.2, the amplitude of the curve is reciprocal to the concentration. The reason behind this is that for lag time zero, $G(\tau)$ is determined as;

$$G(0) = \frac{\langle (\delta F)^2 \rangle}{\langle F \rangle^2} \quad (2.6)$$

For random processes that are governed by Poisson statistics, the variance is;

$$Var(N) = \langle (\delta N)^2 \rangle = N \quad (2.7)$$

Because the fluorescence intensity is directly proportional to the number of molecules;

$$\langle F \rangle = q \langle N \rangle \quad (2.8)$$

when the intensity is normalized, we get;

$$\frac{\langle (\delta F)^2 \rangle}{\langle F \rangle^2} = \frac{\langle (\delta N)^2 \rangle}{\langle N \rangle^2} = \frac{\langle N \rangle}{\langle F \rangle^2} = \frac{1}{\langle N \rangle} \quad (2.9)$$

As stated above, the diffusion time and other variables are obtained from fitting the experimental data to the proper model function. From the diffusion time τ_D , the diffusion coefficient can be determined if the diameter of the focal volume is known;

$$\tau_D = \frac{\omega_0^2}{4D} \quad (2.10)$$

Here, ω_0 is the beam waist of focal volume, i.e., the radial distance of the optical axis, and D is the diffusion coefficient.

Besides the concentration and the diffusion time, the brightness of the molecule, η , can be calculated. This parameter is quite important for a good statistical accuracy, and can be used to assess the quality of FCS measurements in general. However, it can also reflect on the formation of higher molecular complexes and aggregates. η is directly proportional to the total photon count, and to the amplitude of the correlation function;

$$\eta = \frac{\langle F(t) \rangle}{N} = \langle F(t) \rangle \cdot G(0) \quad (2.11)$$

In practice, FCS is quite a complicated and delicate technique to apply, with many parameters that have to be taken into account and carefully controlled.

- If the concentration of the fluorophores is too high (greater than 100 nM) the contribution of correlated photons to the total intensity (or, the strength of the fluctuations) is only marginal, and precludes their analysis. If the concentration is too low (less than 1 pM) it gets difficult to register a molecule in the focal volume during a sensible measurement time. Background noise dominates the signal. In both cases, it is difficult to record decent FCS curves.
- Autofluorescence and (scattering) background may always affect the total fluorescence intensity, and there should be elaborate corrections for them. Besides, the sample should be kept in a non-autofluorescent medium.
- Low laser power should always be used to avoid photobleaching.
- The acquisition time should be long enough to collect enough photons to correlate, but not too long to avoid photobleaching.
- Fluorophore selection should be made carefully; more than other techniques FCS requires a high photostability.

The basic steps and tricks to do FCS on living cells are well described elsewhere [50].

2.5. Stimulated Emission Depletion (STED) Nanoscopy

All techniques discussed above are limited in their resolution by an optical barrier called the diffraction limit, or Abbe limit. It is usually given by approximately half the wavelength of the light at which illumination is performed. Although electron microscopy in principle allows shifting the wavelength to dimensions as low as single nanometers, it is not applicable to living cells. Therefore, many researchers have striven to overcome this barrier, and several techniques have been developed during the past years which yield access to dimensions far below the micrometer level. Here, we will discuss Stimulated Emission Depletion nanoscopy which is most commonly used super resolution technique for membrane research (also for this thesis work).

The concept of STED was formulated in the 90s and experimentally realized in later years [51–54]. Its underlying idea is to shape the volume which contributes to the fluorescent image of a focused laser beam by depleting fluorophores around the immediate vicinity of the focal spot, i.e., within the disturbing side lobes of the diffraction pattern. This concept is also referred to as "point spread function engineering". To get rid of fluorescence light in these unwanted areas, stimulated emission is performed through a donut-shaped illumination by a second laser operating at a suitable wavelength (the so-called STED laser). Stimulated emission is the process of efficiently and nondestructively bringing the molecule from the excited state to the ground state without fluorescence emission, by hitting the excited state fluorophores within their fluorescence lifetime by the red-shifted STED pulse. A phase mask is used to generate the STED donut-shape profile. This allows the peripheral excited molecules to be depleted, while keeping the STED intensity nearly zero (and thus, preserving the fluorescence) in the center of the focal spot. The particularly neat aspect of this scheme is the nonlinear dependence of the depletion level to the STED pulse intensity: When the STED pulse intensity is increased above a critical value, all molecules in the peripheral region are depleted. As the laser intensity increases further, the depletion region expands, but the center of the focal spot remains largely unaffected. Therefore, the fluorescently active inner area of the PSF may be reduced down to 20 nm, which is approximately 10 times less than that in confocal microscopy. The PSF for STED (Δr) is described with the formula;

$$\Delta r = \frac{\lambda}{2NA\sqrt{1+\zeta}} \quad (2.12)$$

where λ is the wavelength of the excitation light, NA is the numerical aperture of the objective and ζ is the saturation factor expressed as;

$$\varsigma = \frac{I}{I_s} \quad (2.13)$$

where I is the peak intensity of the STED laser and I_s is the saturation intensity of the fluorophore. Thus, depending on depletion laser intensity and the nature of the fluorophore, STED may offer a resolution of down to 20 nm. Although providing such an excellent theoretical resolution, the performance of STED in dynamic systems such as living cells is still limited. First, the depletion laser, especially when applied at high power, bleaches most of the fluorophores that are conventionally used in cells biology, like GFP, RFP or mCherry. The fluorophore library that can be used in STED is so far limited to a few organic dyes and a few YFP family members. However, new fluorescent proteins and organic dyes which are suitable for STED experiments are continuously being generated [55–57]. On the other side, the effect of aberrations on STED has been recently investigated [58] and a standard protocol for sample preparation for STED has been recently established [59].

There are several other techniques used to study membrane heterogeneity such as FRAP, FRET, Single Particle Tracking (SPT), PALM/STORM etc., however, we are not going to mention them here as they were not used in the work presented in this thesis.

Fluorescent Probes to Study Membrane Heterogeneity

After the invention of green fluorescent protein (GFP) as the first truly genetic fluorescent probe, visualizing proteins in their native environment became much more straightforward. From the perspective of the membrane researcher, this significantly improved our understanding of membrane proteins and their dynamics, but could help only marginally in better elucidating the functional dynamics of lipids. Therefore, fluorescent probes which could be observed by the techniques that can do dynamic measurements (Chapter 2) have been developed. In this chapter we will discuss the most extensively used fluorescent probes used to elucidate the membrane lateral organization. We separate these probes into two classes; phase specific analogs of which utility is based on preferential partitioning between coexisting domains and phase sensitive lipid analogs which changes their photophysical properties depending on the lipid environment.

3.1. Phase Specific Lipid Analogs

Easiest way to make a fluorescent lipid probe is coupling the synthetic fluorescence molecules to lipids *in vitro*, and then reconstitute them to the cell membrane. This method is getting more common in lipid field, enforcing the use of fluorescence also in lipid biology. Synthetic dye coupling has many advantages compared to fluorescent proteins, which nowadays represent the main strategy in protein labeling. First of all, one has theoretically a large choice of organic dyes in terms of their optical characteristics. It is possible, for instance, to use a far red dye, however, there is not yet a well-established monomeric far red protein. Second, the quantum efficiency and brightness of most of the organic dyes are higher than for fluorescent proteins. Cholesterol [60–63], Sphingomyelin [15, 62, 64], GM1 [15, 65, 66], PC, and PE [67, 68] are some of the lipids that are often conjugated to organic dyes. Additionally, fluorescently labeled membrane-binders, like cholera toxin, are used to label, e.g., the GMs on the cell surface [69]. However, taking into account that organic fluorophores are in comparison much larger handicaps to small lipid molecules than to proteins, and that the relatively tight packing of lipids in a membrane might be more easily disturbed by labeled lipids than in the case of soluble proteins, a careful control of the possible influence of labels on the functionality

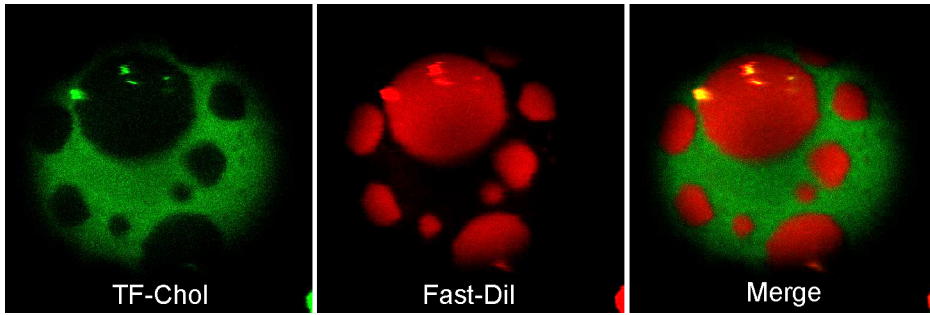


Figure 3.1. Lo and Ld phase specific markers in Giant Unilamellar Vesicles. Topfluor labeled cholesterol (TF-Chol) prefers Lo phase while Fast-Dil prefers Ld phase.

of lipids is of utmost importance. Besides fluorescent lipid conjugates, there are some lipophilic fluorescent molecules frequently used to yield information on a specific lipid environment. The most commonly used such dyes are the Di- family dyes. DiO, DiI and DiD are extensively used to label the non-raft (less ordered) domain (Figure 3.1).

3.2. Phase Sensitive Lipid Analogs

Besides the phase specific probes, there is a different class of the probes which efficiently penetrate into lipid membranes, and to some extent reflect on their physical properties, like viscosity, order, pH, or water content. Laurdan and Di-4-ANEPPHQD are the lipophilic dyes most commonly used to visualize the lipid environment. They partition equally in both phases, but their emission spectrum changes according to the polarity of the membrane environment. Providing that Ld phase is more aqueous than Lo phase, upon excitation the dye consumes some of its energy to reorient the water molecules in Ld phase, which shifts the emission to the red spectral region (emission maximum of 490 nm for Laurdan), while it is more blue shifted in Lo region (emission maximum of 440 nm for Laurdan) (Figure 3.2A). According to the ratio of fluorescence intensity in the blue-shifted (Lo phase) and the red-shifted region (Ld phase), one can calculate a order indicative value called Generalized Polarization (GP) calculated as;

$$GP = \frac{I_{440} - I_{490}}{I_{440} + I_{490}} \quad (3.1)$$

where I_x denotes the intensity at wavelength of x .

Alternatively, a spectral region instead of a single point can be taken into consideration for GP calculation. Then the equation becomes;

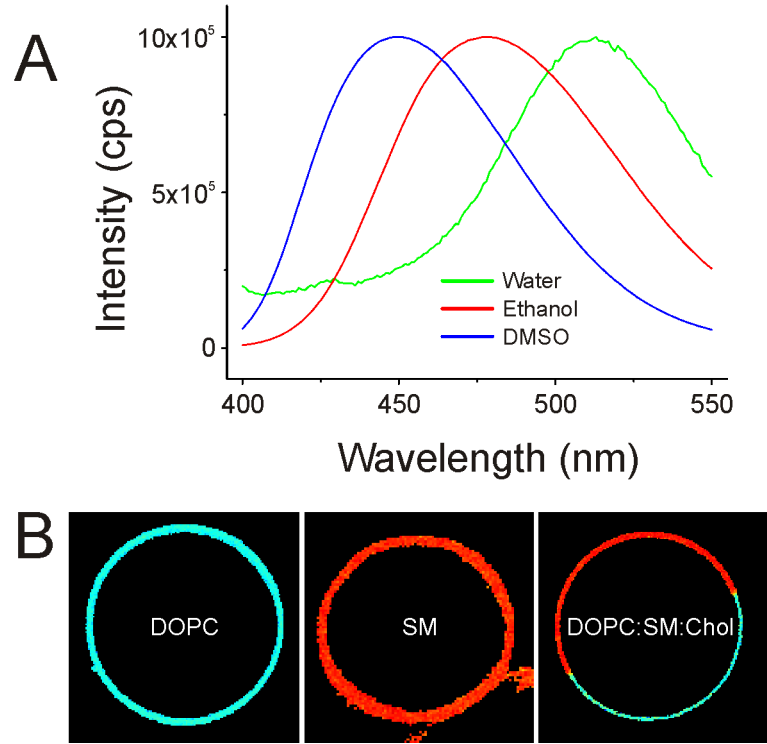


Figure 3.2. Phase sensitive probe C-Laurdan. (A) Its emission changes dependent on the environment. Emission is more red shifter in polar solvents and it gets more blue shifter in apolar solvents. (B) GP image of a GUV. Images are obtained with two photon microscopy with appropriate filters and GP is calculated as in Equation 3.2.

$$GP = \frac{\sum_{420}^{460} I_x - \sum_{470}^{510} I_x}{\sum_{420}^{460} I_x + \sum_{470}^{510} I_x} \quad (3.2)$$

Latter equation is more suitable for microscopy where the spectral information is limited by the filters. GP image can be calculated by splitting the emission according to the Equation 3.2 (Figure 3.2B).

In addition to generalized polarization, fluorescence anisotropy is another important phenomenon that can be exploited to monitor rotational diffusion of the molecules by using the polarization of light. Since rotational diffusion is very sensitive to the size of molecules, binding constants can be efficiently derived from fluorescence anisotropy measurements. There have been comparative studies on the feasibility of several dyes for fluorescence anisotropy. Alexa and Oregon dyes conjugates with biological molecules (e.g., lipids), for instance, were found to be suitable for this method [70]. Additionally, NBD and DHP lipid conjugates were used for fluorescence anisotropy to detect rafts in living cells [71]. Laurdan generalized polarization and fluorescence anisotropy were compared elsewhere [72].

3.3. New Lipids to Visualize the Cellular Lipidic Organelles

Besides lipid probes for the plasma membrane, there are also some tools to probe other lipidic environments in the cell, such as lipid droplets [73]. New fluorescent lipids were developed to visualize the intracellular and membrane lipids in their native environment without any external fluorescent labels [74, 75].

Model Membranes to Study Membrane Heterogeneity

Biophysical studies generally aim at a quantitative determination of key parameters to characterize a functional biological system. A characteristic of many, if not all, biological systems is their enormous complexity. Therefore, the reconstitution of cellular or molecular subsystems of reduced complexity in cell-free, well-controlled environments has been, and remains, an important task in biological science. This approach thus refers to the modern field of Synthetic Biology, as it implies that a specific biological phenomenon may be approached "bottom-up", from a minimal assembly of its functional parts [76–78]. In the present paper, we give a short overview over approaches to understand membrane related biological phenomena by employing suitable model systems simple enough to allow for quantitative analysis, but on the other side complex enough to retain the fundamental character of the phenomena to be observed. In addition to recent advances in microscopy and spectroscopy that have allowed investigation of membrane heterogeneity in live cells [10] (see Chapter 2), several advanced minimal model membrane systems have helped to address the issue from a "bottom up" paradigm. Here, we summarize the presently most widely used model membrane systems to investigate cellular membrane dynamics.

4.1. Historical background

The first experimental investigation of the remarkable physicochemical features of lipidic systems was documented by Benjamin Franklin, in order to understand the calming effect of "pouring oil on troubled water". He remembers the first sparks of his curiosity, when he made the observation that emptying the ship kitchen's greasy cleaning water significantly smoothed their wake [79]. In the description of the now-famous Clapham pond experiment, he noted how only a teaspoon of oil covered a significant region of the pond, making it look smooth as glass and explains the physical mechanisms of thin film formation on air-water interface [79]. Thus, the first research on lipidic surfaces started with half a membrane - a monolayer (i.e., a monomolecular film formed by lipids on an air-water interface) - well before the concept of a cell membrane was proposed in 1899 by Overton [1, 2]. Parallel with the discovery of the ultrathin structure of the plasma membrane in 1925 [80], Langmuir undertook the first quantitative characterization of monolayers

[81]. Decades later, liposomes, the first bilayer system, were discovered [82]. These discoveries led to the "Fluid Mosaic" model of the cellular plasma membrane [3], describing it as a homogeneous lipid environment with embedded proteins, which appeared to be remarkably accurate. The first major correction to the concept of a homogeneous fluid mosaic followed upon the discovery of detergent resistant membranes (DRMs), which required a model explaining a heterogeneous lipid structure of the plasma membrane [4]. The 1980s were the golden age of research on pure lipid model membranes, when the phase separation phenomenon was established for monolayers, and supported lipid bilayers were first prepared [83, 84]. A few years later, Giant Unilamellar Vesicles (GUVs) were introduced as a membrane model system that allowed microscopic investigation of cell-sized membrane vesicles [85]. Meanwhile, the heterogeneous distribution of lipids in the apical, compared to the basolateral, plasma membrane in polarized epithelia was observed, strengthening the concept of heterogeneous membrane structure [5]. Although detergent resistant proteins were also observed in early 1990s [6], it was 1997 when the raft concept was introduced, proposing functional lipid-induced domains [7]. To confirm and pinpoint the molecular details behind this phenomenon, phase separation was extensively investigated in synthetic membrane systems as models for lipid raft-mediated membrane heterogeneity [8, 9]. An important step to a more biological relevance of these phase-separating membrane models was the achievement of functional protein reconstitution into them [86–88]. The most recent manifestation of this quest is the observation of liquid-liquid phase separation in isolated plasma membranes (GPMVs) [67], thirty years after their discovery [89] (Figure 4.1).

In the following, we summarize the three most frequently used model membranes to quantitatively address the phase separation. The first two (supported membranes, GUVs) were initially lipid-only systems, used to determine the physical chemistry of lipids. To specifically investigate the interactions of proteins with these membranes, several protocols have been developed [86, 90, 91] in order to fully reconstitute the proteins into the membranes. GPMVs, on the other hand, represent a more top-down approach towards the study of lipid-protein systems, as they are derived from living cells by disrupting the membrane, and retain a large lipid complexity, along with an unknown number of integral and peripheral membrane proteins. Spanning from a single lipid bilayer (SLBs) to a complex cell membrane derived vesicle (GPMV), model membranes enabled membrane biologists to investigate the nature of the cell membrane heterogeneity in a system with desired complexity, composition and structure.

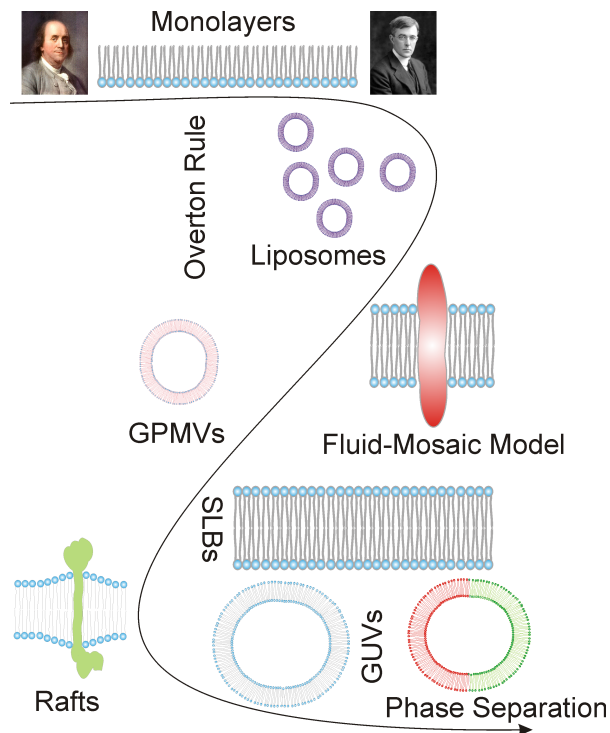


Figure 4.1. Development of model membrane systems.

4.2. Supported Lipid Bilayers (SLBs)

Supported lipid bilayers (SLBs) are flat membranes formed on a hydrophilic support (such as mica, glass or silica), containing a very thin (≈ 1 nm) layer of liquid between the support and the membrane. Thanks to the confinement on a solid support, changing physical conditions (e.g. buffer) without disrupting the membrane is much easier in SLBs than in free-standing membranes. Additionally, supported membranes are not only well accessible to all kinds of optical microscopy, but also to surface probe techniques such as atomic force microscopy (AFM), in contrast to free-standing bilayers (Figure 4.2). Thus, in contrast to free-standing membranes, SLBs provide access to parameters of membrane thickness and mechanical stability [92] by AFM, and allow to resolve membrane structures far below the optical resolution limit [93]. The first SLBs were achieved by the sequential transfer of monolayers from an air-water interface to a solid substrate [84]. Later attempts used the bursting of small vesicles (Small Unilamellar Vesicles (SUVs) or Large Unilamellar Vesicles (LUVs)) on a substrate. The vesicles are first adsorbed on the surface, then ruptured and spread into planar membranes [94]. The most recent technological development has seen SLBs deposited by spin coating membranes directly onto supports [95]. Although a solid-supported membrane is quite artificial compared to a free-standing one, the mobility of individual lipids can be preserved [96], making it

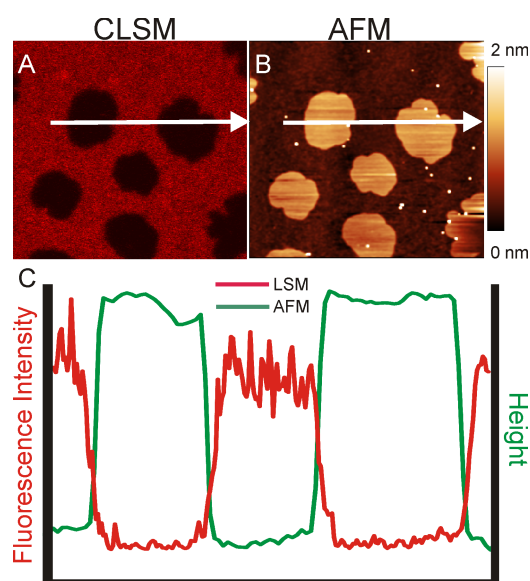


Figure 4.2. Phase separation in Supported Lipid Bilayers (SLBs). (A) Confocal image of a SLB prepared from DOPC/BSM/C18Cer/Chol mixture and stained with DiD (Ld marker). (B) Topological image of the same membrane obtained with AFM. (C) Intensity and height profile of the membrane above. The DiD containing Ld patches are thinner than the patches Lo regions (Image courtesy of Grzegorz Chwastek).

a well-controlled system for studying lipid/protein dynamics. Some technical improvements have been introduced to arrive at a relatively unbiased mobility even of integral proteins reconstituted into SLBs. For example, polymer cushions have been placed on the support to increase the hydration layer, to avoid non-specific trapping of proteins with large extramembrane domains at the support [97]. Recently, to eliminate the effect of the surface/lipid interaction, a lipid bilayer was suspended between narrowly separated solid supports or at a small orifice, allowing the formation of a free-standing planar bilayer. This assay has been employed for simultaneously measuring optical and electrical properties of the membrane [98, 99]. Similarly, bursting vesicles on porous substrates (like alumina or Si_3N_4) is an alternative way to eliminate the effect of support but preserving the experimental advantages of flat SLBs [100–102].

4.3. Giant Unilamellar Vesicles (GUVs)

In aqueous environments, lipid assemblies are easily transformed morphologically by changes of the physical parameters in the solution. Mild fluid convection, but also slowly alternating electric fields can lead to the vesiculation of a flat lipid multilayer, allowing the formation of unilamellar vesicles much larger than those prepared by sonication or injection methods, termed Giant Unilamellar Vesicles (GUVs >1000 nm). Originally, GUVs were formed using DC electric fields [85], though AC electric fields were later

found to increase formation efficiency [103]. The basic protocol for GUV preparation involves the spreading of a lipid mixture (in organic solvent) on a platinum electrode to form the lipid multilayer. Electrodes are then dipped into aqueous buffer and the electric field (usually between 2-3 V) is applied. GUVs can also be prepared by gentle hydration, where charged lipids are used to create electrostatic repulsion between the bilayers, which eventually facilitates unilamellar vesicle formation. For details on GUV preparation refer to refs [104, 105]. Besides having a great potential to selectively study single lipid species in a model membrane, it is also possible to form GUVs with complex lipid mixtures. This capability led to reconstitution of phenomena structurally and functionally similar to cellular lipid rafts in GUVs. One early assumption was that lipid rafts are related to more ordered, or more tightly packed, liquid membrane phases from the bulk membrane. The first attempts to observe phase separation in GUVs were made with binary mixtures of saturated phospholipids, namely DPPC/DLPC and DPPC/DPPE [9]. These mixtures indeed phase separate under near-physiological conditions, however while one of phases retains the liquid-crystalline properties of biological membranes, the other is a solid crystal (in membranes, termed the "gel" phase) with little translational or rotational diffusion. Due to the limited biological relevance of the gel phase, another component was added to recapitulate liquid-liquid phase coexistence. The key ingredient turned out to be cholesterol - ternary mixtures of a saturated lipid, an unsaturated lipid and cholesterol readily resulted in coexisting liquid ordered (Lo) and liquid disordered (Ld) domains [29] (Figure 4.3). In addition to their crucial role in defining the physical chemistry of raft-mimetic Lo phases, GUVs have been widely used as platforms to investigate the role of individual lipids in protein activity or interactions.

4.4. Giant Plasma Membrane Vesicles

Although non-lipid cellular components (such as functional membrane proteins) can be reconstituted into GUVs, these experiments are rather work-intensive and still only capable of reproducing a limited complexity, compared to the physiological situation. This is particularly true for the extensive variety of lipids in a native cellular membrane. An optimal complement to simple GUV models is a free-standing membrane which retains at least the compositional lipid complexity of a live cell membrane. Such a system is provided by so-called membrane blebs, which can be grown and harvested from native cellular membranes [106]. Blebs are pure cell membrane regions, detached from the cell cortex, which can naturally form during cell division, apoptosis or cell migration, or are induced by some chemical or physical destruction of the cytoskeleton. In dividing cells, blebs provide an attractive system for studying the cell mechanics and biophysics of membrane-cytoskeleton interactions in live cells [107]. Chemically-induced cell mem-

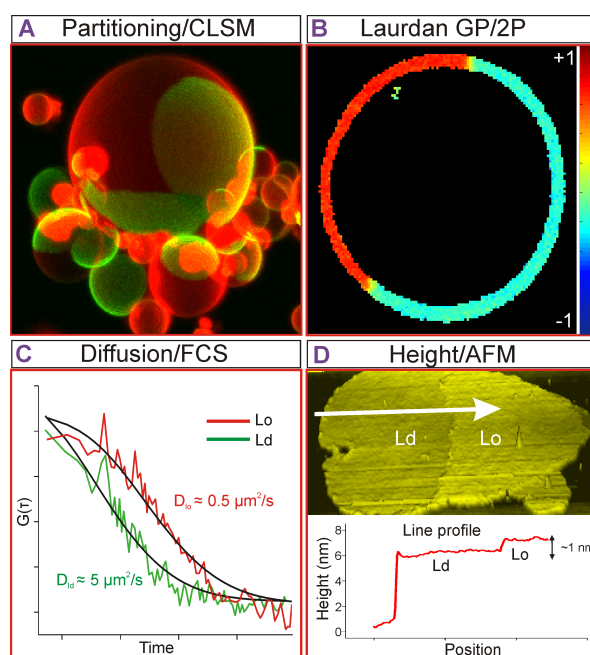


Figure 4.3. Phase Properties in GUVs. (A) 3D confocal image of phase separation in GUVs composed of DOPC/BSM/Chol (2:2:1; dyes are same as Figure 2A). (B) Laurdan GP image of a phase separated GUV (same composition as [A]). Ordered phases have higher GP values. (C) Diffusion of a fluorescent molecule in Lo and Ld phases of Giant Unilamellar Vesicles (GUVs) quantified by fluorescence correlation spectroscopy (same composition as [A]). Diffusion is approximately an order of magnitude slower in the Lo phase. (D) Height profile of a burst GUV (same composition as [A]) obtained by AFM. The Lo phase is thicker than Ld phase by about 1 nm.

brane vesiculation (so-called plasma membrane vesicles (PMVs)) was first observed in 1976, and used as a method to isolate plasma membrane [89]. Recently, phase separation was observed in Giant Plasma Membrane Vesicles (GPMVs) [67](Figure 4.4), mirroring the behavior of the three component GUVs described above in a system retaining the compositional complexity of the native plasma membrane. Measurements of temperature [108] and composition dependence of phase separation in GPMVs [109] have further confirmed these similarities. A similar method was developed to separate intact Plasma Membrane Spheres (PMS) from the cell interior [110], and phase separation was shown by confocal imaging and fluorescence correlation spectroscopy.

As GPMVs hold utmost importance for this thesis, we will discuss it in detail in the next chapter separately.

4.5. Outlook - the future of model membranes

As summarized in Table 4.1, there exist advantages and disadvantages of each membrane model system discussed above. Each system has its own difficulties and limitations and unfortunately, also produces its own artifacts. Moreover, all the model membranes men-

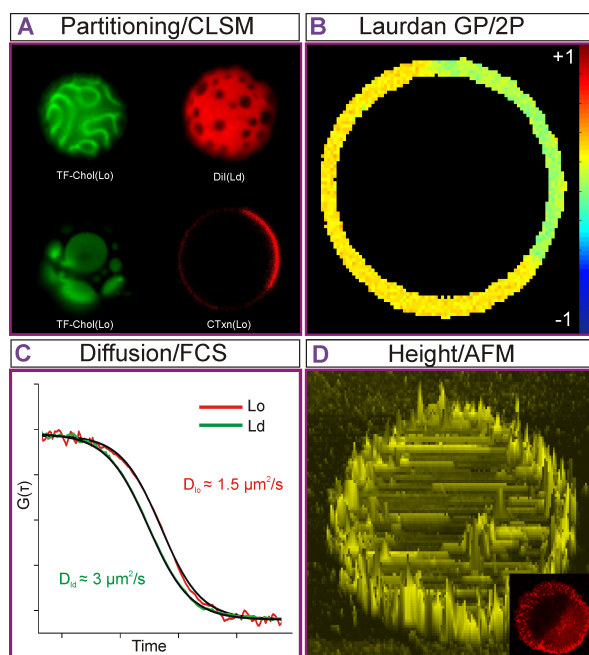


Figure 4.4. Phase Properties in Giant Plasma Membrane Vesicles (GPMVs). (A) Phase separation of GPMVs at 10°C stained with TopfluorCholesterol (ordered phase), DiI (disordered phase) or Alexa647- Cholera toxin (ordered phase). (B) Laurdan GP image of a phase separated GPMV at 10°C. The order difference between coexisting phases is less pronounced than in GUVs shown in 4.3. (C) The diffusion of a fluorescent molecule in two phases of GPMVs measured by FCS. Diffusion in the ordered phase is slower, but much closer to the disordered phase than in GUV shown in Figure 4.3. (D) AFM image of a burst GMPV. The surface is covered by proteins. (The inset shows the corresponding confocal image of the membrane stained with DiI disordered phase).

tioned above are at thermodynamic equilibrium, which does clearly not reflect the state of a living cell membrane. Similarly, membrane asymmetry, i.e. different compositions of the two opposing leaflets of a bilayer, is a central feature of biological membranes [111], while only the first steps have been taken to establish and investigate asymmetric model membranes [90, 111, 112] since the introduction of Montal-Muller membranes [113]. Thus, the development and study of asymmetric membranes away from equilibrium presents the next challenge in the processive development toward truly biomimetic model membranes.

| Model Systems | Advantages | Disadvantages |
|----------------------|--|---|
| SLBs | Compositional control Simple buffer exchange High stability Eligible to surface techniques | Support effects Limited complexity Difficult to incorporate proteins |
| Suspended SLBs | Compositional control Simple buffer exchange Free-standing membranes Eligible to surface techniques | Limited complexity Difficult to incorporate proteins |
| GUVs | Compositional control Free-standing membranes | Limited complexity Difficult to incorporate proteins Difficult buffer exchange Low stability |
| GPMVs | Near-physiological complexity Proteins included Free-standing membranes | No compositional control Difficult buffer exchange Low stability |

Table 4.1. Comparison of Model Membranes.

Part II.

Investigations and Applications of Plasma Membrane Model Systems

Giant Plasma Membrane Vesicles

The observation of phase separation in intact plasma membranes isolated from live cells is a breakthrough for research into eukaryotic membrane lateral heterogeneity. These observations are made in giant plasma membrane vesicles (GPMVs), which can be isolated by chemical vesiculants from a variety of cell types and microscopically observed using basic reagents and equipment available in any cell biology laboratory. Microscopic phase separation is detectable by fluorescent labeling, followed by cooling of the membranes below their miscibility phase transition temperature. Here, we present the GPMV preparation protocol for phase separation studies, compare GPMVs with alternative techniques and discuss several artifacts that GPMV system includes.

5.1. Introduction

The proposal of functional rafts in eukaryotic membranes [7] prompted a period of extensive research, revealing many physiological contexts that appear to employ this mechanism of membrane organization for modulation of cell function. The modern conception of this phenomenon [114] is that preferential associations between raft lipids (i.e. sterols, glycosylated sphingolipids, and lipids with saturated acyl chains) and certain proteins (saturated lipid anchored-proteins, as well as some transmembrane ones) promote lateral heterogeneity and segregation in the plane of the membrane. This heterogeneity can be manifested in a hierarchy of organizational states, from molecular level complexes [11, 15] and functional domains on the order of hundreds of nanometers [115] in live cells to microscopic phases [67, 110] in isolated membrane systems - the specific state of any given membrane depends on a complex combination of its physical properties (e.g. temperature) and biochemical composition.

The recent discovery of phase separation in Giant Plasma Membrane Vesicles (GPMVs) isolated directly from live cells has convincingly validated the raft hypothesis by confirming its central tenet, i.e. the capacity of eukaryotic membranes for forming coexisting liquid domains [67]. Nevertheless, the precise nature of rafts' mechanistic involvement in specific cell functions remains speculative (see Chapter 1). To address this shortcoming, GPMVs comprise an intermediate model system which maintains the compositional com-

plexity and protein content of biological membranes and is capable of forming coexisting, microscopic, lipid-driven domains without the many confounding variables (protein synthesis and active transport, cytoskeletal support, active signaling networks) of live cells. These advantages combine to make GPMVs a versatile tool for quantitative investigation of raft-associated phenomena, specifically the structure and physical properties of coexisting domains, protein partitioning between them, and domain-dependent protein and lipid function.

5.2. Plasma membrane vesicles

Although the observation of phase separation in GPMVs has recently invigorated the raft field, chemically-induced plasma membrane vesiculation was first observed in the 1970's [89]. This protocol produces efficient yields of large (up to 10 μm), nearly pure plasma membrane vesicles without any internal membranous structures observable by electron microscopy (EM); indeed there are no EM-discernible intravesicular structures, suggesting the absence of assembled cytoskeleton or nuclear material [116]. Despite these advantages of yields and purities, PMVs were largely ignored as a plasma membrane model system for biochemical investigation, likely due to the chemical modifications inherent in isolation. Exceptions included the groups of Baird, Holowka, and Webb, which used these vesicles for characterization of plasma membrane lipid composition and physical properties [117], domain formation [118], and the structural/biochemical properties of the IgE receptor [119]. More recently, these vesicles have been used as cell membrane models to test the membrane permeability of various molecules which are potentially important for drug delivery applications [120, 121].

5.3. Phase separation in GPMVs

The original observation of phase separation in GPMVs also contained the critical observation that membrane components, including both proteins and lipids, were sorted preferentially into one or the other of the coexisting phases [67], often according to predictions from biochemical raft preparations (i.e. detergent resistance) [122]. Due to this enrichment of many putative raft components in the more ordered phase of GPMVs, this phase is often referred to (and will be referred to here) as the "raft phase". However, this terminology should not be taken as an indication of equivalence between the raft phase in GPMVs and the nanoscale, dynamic rafts postulated in live cells (this issue will be discussed in Chapter 10) - not least because GPMVs are at thermodynamic equilibrium, a situation clearly not reflective of biology (see Section 5.5). Furthering the analogy between the raft phase in GPMVs and biochemical raft preparations, there

was a qualitative correlation between both the temperature and cholesterol dependence of detergent resistance and phase separation [123]. These studies were followed up by partitioning experiments to define the structural determinants of lipid and protein partitioning to the raft phase. For lipids, the general paradigm of a sphingosine backbone and longer, more saturated acyl chains being raftophilic seems to be applicable; however, significant perturbations can be induced by the polar headgroup and addition of a bulky fluorescent tracer [106, 122]. While proteins anchored to the membrane by a GPI-anchor (usually containing two saturated acyl chains) were consistently enriched in the raft phase [122, 124], most transmembrane proteins require post-translational modification by a saturated fatty acid (palmitoylation) for raft phase partitioning [124]. As noted below, palmitoylation is sensitive to the preparation conditions, possibly explaining the lack of correlation between raft phase partitioning and detergent resistance of several transmembrane proteins [108]. Finally, the remarkable observation of critical behavior in GPMVs provides a possible link between the microscopic phase segregation observed at non-physiological conditions (i.e. low temperature, isolated membrane), and the nanoscopic organization present in live cells [125].

5.4. Alternative techniques

Prior to development of GPMVs, the standard and nearly exclusive criterion for assigning raft association was insolubility in cold (4°C) non-ionic detergents [126]. Such preparations clearly do not reflect the organization of an unsolubilized membrane at physiological temperature and tend to be highly variable due to the complex molecular interactions between detergents and membrane components. Finally, different detergents yield insoluble fractions of different compositions [127, 128], demonstrating that detergent-resistance alone is an inadequate, or at least incomplete, method for defining raft composition.

Giant Unilamellar Vesicles (GUVs) synthesized from pure lipid components show liquid-liquid phase coexistence due to the preferential association of sterols with saturated lipids, especially sphingolipids, to form the liquid ordered (Lo) phase, which is immiscible with the unsaturated lipid-rich liquid-disordered (Ld) phase [29, 129, 130] (see Chapter 4). This collective segregation has been the primary 'minimal' model of raft separation in eukaryotic membranes and has helped to elucidate the physicochemical principles and molecular interactions behind raft formation; however, the biological relevance of such model systems is inherently limited by their compositional simplicity and (typically) lack of integral membrane proteins.

Finally, a recently developed technique, Plasma Membrane Spheres (PMS), allows swelling of the plasma membranes away from the rest of the cellular components - large scale separation of the membrane can be then be induced by crosslinking of raft glycosph-

ingolipids [110]. Although this method includes many of the advantages of GPMVs, it is somewhat limited because only certain cell types exhibit the swelling behavior required to form PMS and these must contain enough GM1 glycolipid such that crosslinking induces raft coalescence.

5.5. Limitations of GPMVs as a plasma membrane model system

The obvious and most significant limitations of GPMVs are the covalent modifications induced by chemical vesiculants. The more common preparation involves a combination of formaldehyde and dithiothreitol, which are non-specific crosslinkers and reducers, respectively. Adaptations of this protocol [17, 124] have circumvented these undesirable side-effects by N-ethyl maleimide, which irreversibly reacts with terminal sulfhydryls (typically cysteine side chains), covalently blocking these groups without crosslinking. Beyond the simple chemical modifications required for vesicle formation, there is a myriad of possible cellular events that occur during the vesicle isolation procedure - because these are so complex and nearly impossible to predict, these comprise the broadest limitation of GPMVs. A known example is the loss of membrane leaflet asymmetry, typically defined by the exposure of the anionic lipid phosphatidylserine (PS). While GPMV membranes are asymmetric to some degree (e.g. proteins likely retain their native topology), PS is clearly exposed on the exoplasmic leaflet [67], in contrast to live cell plasma membranes. The mechanism (i.e. active scrambling or passive lipid flipping) and extent of loss of bilayer asymmetry is not known, nor is the effect of scrambling on phase separation. Similarly, the potential of lipid and protein modifying enzymes and/or membrane trafficking to affect membrane composition is clearly not negligible (e.g. PIP2 appears to be depleted [109]), and cannot be ruled out. Finally, GPMVs represent the cellular membrane in a state of thermodynamic equilibrium, whereas the live cell membrane is a highly dynamic and out-of-equilibrium environment whose composition is constantly modified by vesicle trafficking, enzyme activity, interaction with cytoskeletal components, etc. Therefore, GPMVs can be indicative, but not definitive, about raft organization or domain preference of a given molecule in the living cell.

Despite these limitations, GPMVs constitute a powerful model system with which phase separation can be easily visualized, the order of the coexisting phases can be measured, and component partitioning between coexisting domains can be directly and quantitatively evaluated. Because of this simplicity, this model system provides an essential ingredient of the general toolbox for research into membrane organization, and a way forward for investigation of membrane heterogeneity.

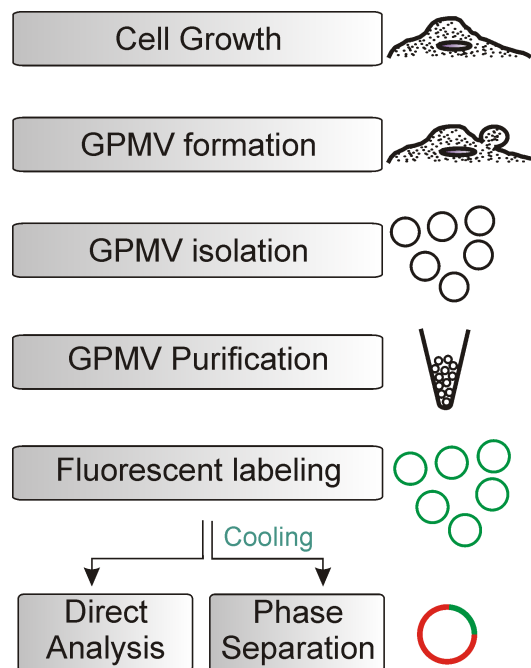


Figure 5.1. Overview of GPMV preparation protocol. Giant plasma membrane vesicles can be isolated from a variety of cell types by addition of vesiculation chemicals followed by separation of vesicles from attached cells. These GPMVs can then be used for fluorescence imaging of proteins and/or membrane domains. Green circles represent fluorescently labeled vesicles, whereas those with red and green areas represent phase-separated GPMVs.

5.6. Experimental design

GPMVs can be isolated from a variety of mammalian cell types, however adherent cells generally provide better yields and purities because these cells remain attached to the dish during vesiculation while the vesicles themselves are released into the supernatant. The basic protocol for preparing GPMVs is simple - cells are treated with Ca^{2+} -containing buffer supplemented with vesiculation agents at 37 °C. GPMV formation then proceeds over the course of approximately one hour. A graphical overview of the complete protocol is depicted in Figure 5.1.

5.7. Purification and concentration of membranes

After formation, GPMVs can be separated from adherent cells by transferring the supernatant by pipette. Although most cells remain attached to the plate (Figure 5.2), cellular debris in the supernatant can be separated from GPMVs by differential centrifugation—cell debris pellets almost completely at $\approx 100g$, whereas vesicles can be collected by centrifugal forces of 20,000g [131]. This procedure results in the recovery of 20% of original plasma membrane material [131]. These steps are only necessary if the membrane

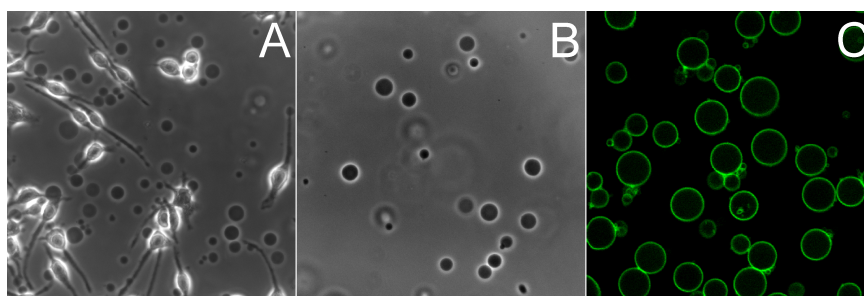


Figure 5.2. GPMV visualization. (A,B) GPMVs are observable by bright-field microscopy either in the presence of cells (A) or after isolation (B). (C) GPMVs can be observed by fluorescence microscopy after labeling the membranes with a fluorescent amphiphilic dye (FAST-DiO). Scale bars, 20 μm .

material is used for biochemical experiments where purity is an important concern - for microscopy, GPMVs can be easily distinguished from cellular debris, thus obviating the need for purification. Vesicles can be concentrated for microscopy by allowing them to sediment at 4 °C and then removing the supernatant or pipetting the sample directly from the bottom of the container.

For biochemistry, lipid and protein concentrations can be measured by standard methods. Additionally, the relative concentration of membranes in GPMV suspensions can be estimated by spectroscopy. The emission spectrum ($\lambda_{ex} = 385 \text{ nm}$) of unlabeled bilayer membranes typically has a relatively strong emission peak at 425 nm (Figure 5.3A) - the intensity of this peak correlates well with the amount of membrane in the sample, as judged by standard biochemical assays [132]. Since background fluorescence above 450 nm is independent of the sample concentration, the relative intensity of the peak at 425 nm can be used to normalize sample membrane concentrations [132].

5.8. Considerations for visualization of GPMVs by fluorescence microscopy

GPMVs can be visualized by bright field microscopy due to the refractive index difference between the cytoplasm inside the GPMVs and the buffer outside (Figure 5.2A,B). Alternatively, GPMVs can be imaged using fluorescence microscopy (Figure 5.2C) by one of three methods: (1) labeling cellular plasma membranes with fluorescent markers prior to vesicle isolation; (2) direct labeling of isolated vesicles; or (3) transfection of cells with fluorescent chimeras of plasma membrane proteins. Each method has distinct advantages. Direct labeling of isolated vesicles is the simplest method - addition of lipophilic dyes directly to vesicle suspensions leads to rapid incorporation into membranes. The drawback of this approach is high background fluorescence from unincorporated dye and, more importantly, poor control of relative fluorescent analog loading. This drawback is important because high levels of fluorescent lipid analogs would be expected to affect the

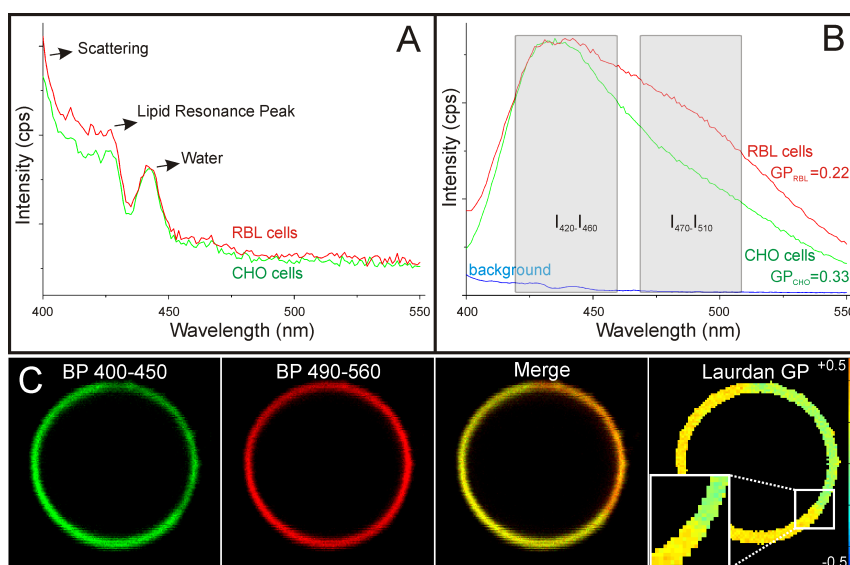


Figure 5.3. C-laurdan characterization of GPMVs. (A) The membrane concentration of GPMV suspensions can be normalized by spectroscopy of unstained membranes. Upon excitation at 385 nm, GPMV suspensions give a characteristic scattering spectrum with a water Raman scattering peak at 440 nm and a lipid scattering peak at 425 nm. This lipid peak is directly proportional to the membrane concentration of the sample and can be used to normalize across samples/preparation conditions. Shown are emission spectra from unstained GPMVs isolated from two common cell culture lines, rat basophilic leukemia (RBL; red) and Chinese hamster ovary (CHO; green) cells. (B) Lipid packing/order can be quantified by fluorescence spectroscopy of an environment-sensitive fluorophore (C-laurdan). Shown are the C-laurdan emission spectra of GPMVs isolated from cell culture lines shown in A. The different degree of spectral red shift (i.e., the higher emission intensities of RBL GPMVs between 470 and 510 nm) indicates that GPMVs from RBL cells are less ordered than those from CHO cells. Wavelength ranges used to calculate generalized polarization (GP) by equation (1) are shown as gray boxes. (C) The order of coexisting phases in phase-separated GPMVs can be quantified using two-photon microscopy of the same dye by filtering emission light to select wavelengths representative of ordered (green) and disordered (red) phase emission. These can then be processed to yield maps of the GP, a relative index of membrane order (right). c.p.s., counts per second.

biophysical properties of the membranes. Additionally, it is important to be aware of potential artifacts induced by photo-oxidation of fluorescent dyes, which has been shown to affect phase separation [133]. Labeling cells prior to isolation yields more uniform labeling with less background fluorescence, but requires more dye and several pre-isolation labeling steps. Finally, expression of fluorescent proteins offers the least perturbing approach to visualizing the membrane (since the fluorescent moiety is typically far away from the membrane portion of the protein), but yields much lower fluorescent signal due to the limited expression and transfection efficiency.

5.9. Quantification of phase order in GPMVs

A potential application for GPMVs is to quantify the physicochemical properties of isolated plasma membranes and/or relative differences between the coexisting raft and non-

raft phases. An important property defining the state of membranes is the conformational order of the acyl chains in the hydrophobic core of the bilayer. This order can be explicitly measured in pure lipid systems by NMR; in biological membranes a simple approach to approximate the relative order/lipid packing of membranes is the use of polarity-sensitive dyes, the most widely used being Laurdan. This fluorescent lipid shows a water-induced emission shift between the relatively ordered (tightly packed, less aqueous) phase where the emission peak is at 440 nm and the relatively disordered (loosely packed, more aqueous) phase with maximal emission at 490 nm (Figure 5.3B). A normalized polarity index, generalized polarization (GP), is used to express the relative emission shift, reflective of membrane packing/order which is calculated as shown in Equation 3.2. In GPMVs with coexisting fluid phases, microscopy of Laurdan can be used to simultaneously measure the order of both phases by splitting the fluorescence emission signal with band-pass filters selective for the ordered and disordered phase emissions (Figure 5.3C). These images can then be processed to generate order maps, using correction factors to enforce agreement between micro- and spectroscopic data, as described [134].

5.10. Temperature-controlled imaging

The most important advantage of GPMVs compared with both pure lipid model systems and live cells is the ability to investigate microscopic phase separation in a membrane reflective of the true composition of biological plasma membranes. This phase behavior is inherently temperature-dependent, and thus it is often necessary to cool the system well below room temperature to observe phase separation in GPMVs. This requirement presents an experimental challenge, because most commercial temperature-controlled imaging systems are designed for warming samples to physiological temperatures, rather than cooling. Several different strategies have been implemented for accurate and rapid control of sample temperature (Figure 5.4). Cooled water from a water pump (Figure 5.4A) is circulated through the pipes. Additionally an electronic system (Figure 5.4B) cools down the peltier element in thermal insert (Figure 5.4C,D) where the sample is placed. If water immersion objectives are used, a ring for objective cooling (Figure 5.4E) may also be necessary. All the strategies to cool down the vesicles involve the construction of a sealed chamber consisting of two coverslips separated by a water-repellent sealant (e.g., paraffin wax) and containing the GPMV suspension (Figure 5.4F). This chamber is typically imaged using an inverted microscope, because the vesicles quickly sink to the bottom of the chamber. In one construction, this chamber is attached directly to the underside of a metallic thermal insert, thus ensuring tight thermal coupling between the temperature controller and the sample (Figure 5.4F,G). In this arrangement, the objective needs to be either thermally isolated from the sample (i.e., air-immersion objective)

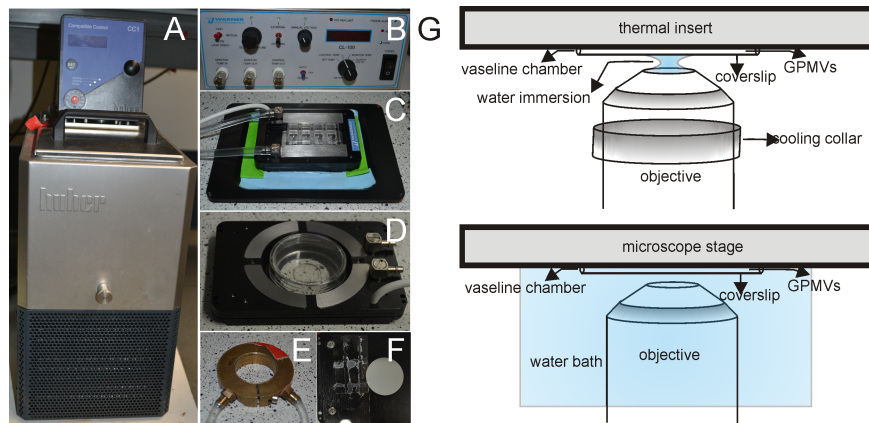


Figure 5.4. Temperature-controlled imaging. To observe phase separation in GPMVs, it is often necessary to cool the sample. (A) Water pump, (B) temperature control unit (C) thermal insert for 8 well LabTek chambers, (D) thermal insert for 35 mm MatTek chambers, (E) cooling ring for objective, (F) a construction involves a small volume (10–25 μl) of sample between two coverslips separated by wax sealant, (G) schematic image of this chamber mounted directly on a thermal insert. The imaging chamber is not placed in the well designed for imaging, but rather attached directly to the underside of the cooled microscope stage. (H) An alternative construction.

or if a fluid-immersion objective is desired for higher resolution, it should be cooled to the sample temperature to avoid heat flow and resulting temperature gradients which lead to convective flow. Another option to simultaneously cool the objective and sample is to immerse both in a water-filled chamber cooled by submerged coils (Figure 5.4H).

5.11. Characterization of component partitioning

One of the most important uses of GPMVs is determination of lipid and protein partitioning between raft and non-raft phases [108, 124, 135], providing a simple and quantitative method for estimating raft association. The method involves imaging the fluorescently labeled protein or lipid component concurrently with a reference marker with well-characterized phase partitioning (Fig. 5A,B). Counterstaining of apposing phases with different fluorescent markers (as in Figure 5.5A) is an important control for the presence of coexisting selective phases. Appropriate markers for the raft phase are the B subunit of cholera toxin (binds the raft glycolipid GM1), some cholesterol analogs (e.g. Bodipy-cholesterol), naphthopyrene, and/or GPI-anchored proteins, while non-raft phases are typically marked by unsaturated lipid analogs. Using a reference marker for either phase, the relative concentration of the component of interest can then be quantified in both phases by a fluorescence intensity line scan through the two phases (white arrow in Fig. 5B). Raft phase partitioning can then be expressed as an equilibrium partition coefficient ($K_{p,raft} = I_{raft}/I_{non-raft}$) or as the percentage of protein in the raft phase ($\%raft = I_{raft}/(I_{raft} + I_{non-raft})$) (as in Figure 5.5C). Figure 5.5D-F shows the

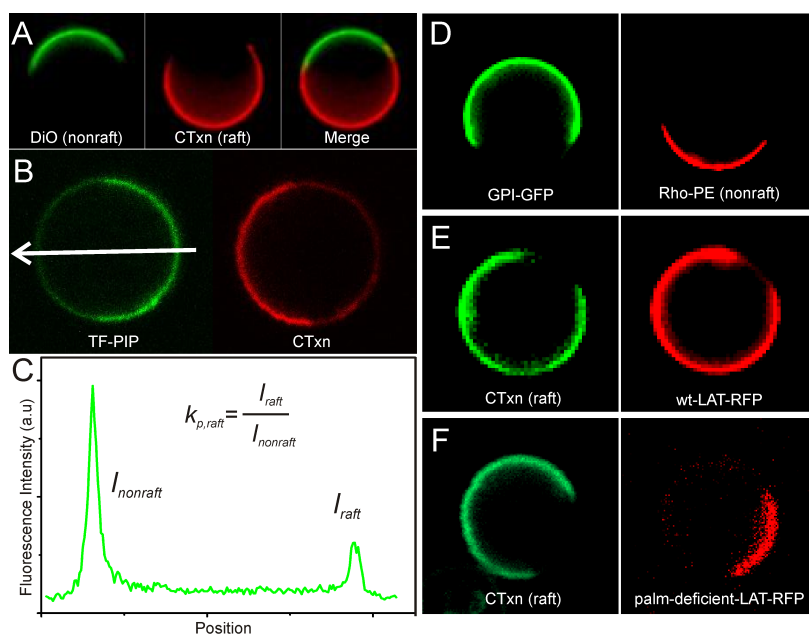


Figure 5.5. Quantification of component partitioning. (A) Phase identity in separated GPMVs can be confirmed by well-characterized markers. Unsaturated lipidic dyes (e.g., FAST-DiO—left) and glycosphingolipid-binding proteins (CTxn; e.g., the B-subunit of cholera toxin—middle) are bona fide markers of the nonraft and raft phases, respectively. (B,C) The partitioning of a component of interest (b) (TopFluor (TF)-PIP₂; left; white arrow represents the line used for the intensity scan in part (c)) between the coexisting phases identified by a well-established marker (right) can be quantified by a fluorescence intensity line scan through the two phases (c). The ratio of fluorescence in the raft and nonraft phase gives a quantitative measurement ($K_{p,raft}$) of phase preference. (D-F) The partitioning of some well-characterized membrane proteins in NEM GPMVs is shown: GPI-anchored GFP (d) and the doubly palmitoylated transmembrane linker for activation of T-cells (LAT) (E) are strongly enriched in the raft phase. (F) The palmitoylation deficient mutant of LAT (LAT-C26A) is depleted from the raft phase.

partitioning of various proteins that could be used as controls for phase separation and appropriate partitioning.

5.12. Controls

Counterstaining of apposing phases with different fluorescent markers (Figure 5.5A) is an important control for the presence of coexisting selective phases. Appropriate markers for the raft phase are the B subunit of cholera toxin (binds the raft glycolipid GM1), some cholesterol analogs (e.g., Bodipy-cholesterol), naphthopyrene, and/or GPI-anchored proteins, whereas nonraft phases are typically marked by unsaturated lipid analogs. 5.5D-F shows the partitioning of various proteins that could be used as controls for phase separation and appropriate partitioning.

5.13. Tips for GPMV yield

The vesicle yield correlates directly with the number of cells used for the preparation, thus the maximal density of cells that are compatible with the experiment should be used. For microscopic experiments, a 35-mm dish of cells at 70% confluence should be sufficient for a number of individual samples. For biochemistry, e.g. Western blotting, it is often necessary to start with a 10-cm dish. GPMV formation is a function of incubation temperature - at 37 °C, blebbing is completed within 1 h. Colder temperatures, e.g. room temperature or even 4 °C, still allow vesicle formation, but require longer incubation times (overnight for 4 °C). Shaking the cell plates during GMPV preparation can increase vesicle yield, but this comes at the cost of decreased purity, as more whole cells will detach from the dish. Finally, the concentrations of the vesiculation chemicals can be varied by an order of magnitude in both directions while still allowing GPMV formation [17]. These parameters (chemical concentration, incubation time, incubation temperature, shaking) should be optimized for each specific cell type, although the conditions described here have proven successful for a number of different cultured cell lines.

5.14. Artifacts induced by vesiculation chemicals

The most efficient, cleanest, and therefore most common preparation for GPMVs involves the mixture of 25 mM formaldehyde and 2 mM DTT as the vesiculants. Unfortunately, this preparation induces several unwanted artifacts: (1) non-specific crosslinking of lipids and proteins by the aldehyde, which precludes many types of protein analysis (e.g. PAGE); (2) cleavage of protein disulfides and thioesters, leading to depalmitoylation [124]; (3) specific coupling of phosphatidylethanolamines to proteins [17]. This last effect seems to have the biggest impact on phase behavior/properties in the GPMVs, increasing the miscibility transition temperature (i.e. the highest temperature at which coexisting domains are observable) by 15 °C. To avoid many of these artifacts, non-crosslinking vesiculants like N-ethyl maleimide are suggested; however, these present experimental challenges because they require cooling the sample to below 5 °C to observe microscopic phase coexistence. Other chemicals that cross the plasma membrane and covalently block free sulfhydryls have been used for GPMV preparation [116] - their effects on phase behavior have not been measured.

GUVs and GPMVs as Models to Study Cell Membrane Penetration: Amphiphilic Quantum Dot Penetration

In this work we investigate the membrane permeability of the amphiphilic CdTe nanocrystals stabilized by thiolated PEG by using GUVs and GPMVs. We show that the CdTe/mPEG-SH quantum dots synthesized penetrate through the lipid bilayer of GUVs and GPMVs which constitute basic free-standing model systems to mimic cell membranes lacking endocytosis machinery. This finding is crucial for drug delivery applications of quantum dots.

6.1. Introduction

Owing to their unique photophysical properties semiconductor nanocrystals (NCs) or quantum dots (QDs) are promising tools for bio-labeling instead of, or in combination with, fluorescent organic dyes and biomolecules [136, 137]. In comparison to organic fluorophores, QDs possess many advantages, such as broad absorption with narrow emission spectra, wide spectral range, long lifetimes, high molar extinction coefficients, and photo- and chemical stability [138]. Nevertheless, some issues still need to be addressed for their successful application as biomarkers. One of them is the intracellular delivery of colloidal nanoparticles. While organic dyes used for tracking intracellular events are able to permeate cell membranes, the size and surface properties of QDs prevent their diffusion across the lipid bilayer [139]. QDs often end up in endocytic compartments instead of their delivery into cell organelles. Therefore, strategies to escape the endocytic pathway, described e.g. for negatively charged CdTe/TGA QDs [140], and to diffuse through the cell membrane as individual units should be developed. One of the most useful model systems to study membrane related processes in a controlled fashion is GUV system (see Chapter 4). However, since they have limited compositional elements (only a few lipids), a more advanced membrane system, GPMVs, has been developed. Very recently both GUVs and GPMVs have been revealed as valuable model membrane systems to study the membrane penetration process [121, 141, 142]. In this work, we report on further improvements of the synthesis of amphiphilic CdTe QDs which was introduced in ref. [143]. Using low-molecular-weight methoxypolyethylene glycol termi-

nated with a HS-group (mPEG-SH) as the stabilizer leads to an inherent amphiphilicity of the nanoparticles[143, 144]. Employing solvents of high polarity and high boiling temperatures in the synthesis yields nanocrystals exhibiting emission maxima ranging from 540 to 640 nm and photoluminescence quantum yields (PL QY) of up to 30%. Moreover, for the first time we show that the QDs synthesized are able to permeate through the membranes of GUVs and GPMVs and might then be perspective candidates for tracking whole cells and intracellular processes owing to the ability to escape from the endocytic uptake mechanism.

6.2. Materials and Methods

6.2.1. Synthesis of CdTe/mPEG-SH nanocrystals

All chemicals used were of analytical grade or higher. The short chain stabilizer $H_3C - (O - CH_2 - CH_2)_7 - SH$ was synthesized according to the method reported in refs. [143, 145]. The preparation of amphiphilic QDs was carried out both in dimethylacetamide (DMA) and in dimethylformamide (DMF) solutions. In a typical synthesis, 0.16 g (0.69 mmol) of $Cd(CH_3COO)_2$ and 0.33 g (0.9 mmol) of mPEG-SH was dissolved in 30 mL of DMA (or DMF) followed by deaeration by argon bubbling for 30 min. Under vigorous stirring, H_2Te gas generated by the reaction of 0.1 g (0.228 mmol) of Al_2Te_3 lumps with an excess of 0.5 M H_2SO_4 solution was injected into the reaction mixture with a slow Ar flow. The molar ratio of $Cd^{2+}/Te^{2-}/mPEG-SH$ was 1/1/1,3. Formation and growth of the nanoparticles proceeded upon reflux. The reaction was terminated after the PL maximum reached 640 nm (4 h - in DMA, 36 h - in DMF). Purification of the QDs was achieved by precipitation of the as-prepared colloidal solution of the CdTe nanoparticles from DMA or DMF by the addition of a toluene/hexane mixture (colloid/toluene/hexane = 1/1/3) followed by dissolution of the precipitate in pure solvent (e.g. water or toluene). As a reference sample for the membrane permeability experiment, hydrophilic CdTe nanoparticles stabilized by thioglycolic acid (TGA) were prepared according to the procedure reported in ref. [146]. Prior to the GUV permeation experiment the CdTe/TGA nanoparticles were purified by the reprecipitation procedure described in ref [147].

6.2.2. Characterization of CdTe/mPEG-SH nanocrystals

UV-Vis absorption spectra were collected with a Cary 50 spectrophotometer (Varian). Fluorescence spectra were measured at room temperature using a FluoroMax-4 spectrofluorimeter (HORIBA Jobin Yvon). All spectra were taken at room temperature. The PL QYs of the QDs solutions were determined according to the procedure described

in ref. [148] by comparison with Rhodamine 6G and Rhodamine 101 dyes in ethanol assuming their PL QYs to be 95% and 96%, respectively. Samples for transmission electron microscopy (TEM) were prepared by dropping diluted nanoparticle solutions in toluene onto copper grids coated with a thin Formvar-carbon film with subsequent evaporation of the solvent. TEM images were obtained on a Tecnai T20 microscope (FEI), operating at 200 kV. The zeta-potentials were measured on a Beckman Coulter Delsa Nano C particle analyzer. The values were averaged from three measurements.

6.2.3. GUV preparation

Dioleoyl phosphatidylcholine (1,2-dioleoyl-sn-glycero-3-phosphocholine) (DOPC) (Avanti, AL, USA) and the membrane dye 3,3'-dioctadecyloxacarbocyanine perchlorate (DiO) (Invitrogen, CA, USA) were mixed in chloroform. Then this mixture was deposited on platinum wires. After chloroform evaporation, the platinum wires were dipped into sucrose solution and exposed to 10 Hz AC for 1 hour and following 2 Hz AC for 30 min with a 2 V voltage. For microscopy, GUVs were mixed with phosphate buffered saline (PBS) in Bovine Serum Albumin (BSA) coated LabTek chambers. Afterwards, amphiphilic CdTe/mPEG-SH QDs and hydrophilic CdTe/TGA QDs colloids (final concentration of 0.25 μM) were added to the chambers. The mixtures were incubated at room temperature.

6.2.4. GPMV preparation

Chinese Hamster Ovary (CHO) cells were cultured in alpha MEM medium supplemented with 10% Fetal Calf Serum up to 70-80 % of confluence. GPMVs were isolated by chemically inducing cell blebbing with 25 mM PFA and 2 mM DTT in GPMV buffer (150 mM NaCl, 10 mM Hepes and 2 mM CaCl_2 (pH 7.4)) for 1 h at 37 °C. The membrane dye TopFluor PIP (Avanti, AL, USA) was added to GPMVs in a concentration of 0.1 μM . They were observed in BSA coated Labtek chambers similar to GUVs. The mixtures were incubated at 4 °C.

6.2.5. Colloidal stability test

Equal concentrations of amphiphilic and hydrophilic QDs were mixed with several biological buffers and subsequently imaged by confocal microscopy.

6.2.6. Confocal microscopy imaging

Confocal microscopy images were acquired using a Zeiss LSM 510 microscope equipped with a 40X NA 1.2 UV-VIS-IR C-Apocromat water-immersion objective and a 488 nm

Argon-Ion laser. NFT 545 and NFT 635 filters were used to separate the green signals from the membrane dyes and from orange or red fluorescing QDs, respectively. For additional filtering, band pass 505-530 for green, long pass 585 for orange and band pass 615-685 for red emissions were employed. Imaging was performed in 0.5, 1, 2, 3 hours after QDs injection and after overnight incubation.

6.3. Results and Discussion

As shown in recent work on green emitting amphiphilic nanoparticles [143], CdTe/mPEG-SH QDs synthesized both in DMA and in DMF exhibit the same spontaneous 3-phase transfer from toluene via water to chloroform confirming their unique amphiphilic properties. Syntheses performed in toluene and water limit the growth of the NCs to 2 nm in size. Employing solvents with higher boiling temperature (tbp of DMF = 153.1 °C, tbp of DMA = 166.1 °C) [149] yields CdTe QDs with average diameters of up to 4 nm emitting in the wide spectral region from 540 to 640 nm. Interestingly, in DMA the growth of the nanoparticles is 9 times faster than that in DMF (the PL maxima of 640 nm were reached in 4 h for the reaction in DMA and in 36 h for DMF) while the difference between the boiling temperatures of these solvents is only 13 °C. This observation suggests that besides the temperature of the reaction mixture, the solvation capability of the medium towards the precursors and the evolving nuclei plays an important role as well. DMA and DMF are known as coordinating solvents which act as electron-donors and thereby are good cation solvators [149]. Thus, DMA having the higher boiling point, a larger donor number and dielectric constant in comparison with DMF (27.8 and 26.6 $kcal\Delta mol^{-1}$, 37.78 and 36.71, respectively [149]), facilitates the growth of CdTe nanocrystals. Such a large growth rate leads to a quite broad size distribution of the CdTe/mPEG-SH QDs in comparison with that from an aqueous synthesis.

For membrane penetration experiments orange QDs emitting with a maximum at 610 nm and red QDs emitting with a maximum at 634 nm were chosen in order to distinguish their luminescence from the green emitting membrane dye DiO. As a control sample, hydrophilic CdTe NCs stabilized with TGA having a similar size (ca. 3 nm) were used. The optical characteristics of the orange emitting samples are shown in Figure 6.1 . CdTe/TGA QDs carry deprotonated carboxyl groups on their surface and hence possess negative charge. Zeta potential measurements reveal a value of -65 mV. On the contrary, amphiphilic CdTe nanoparticles have a slightly positive zeta potential of 4 mV, which favors their versatile solubility and should prevent their aggregation via electrostatic interaction in biological media. As opposed to ligand exchange procedures, the stable bonding of the stabilizer to the nanocrystal surface imparts a high colloidal stability against deterioration. The short chain length of the $H_3C - (O - CH_2 - CH_2)_7 - SH$

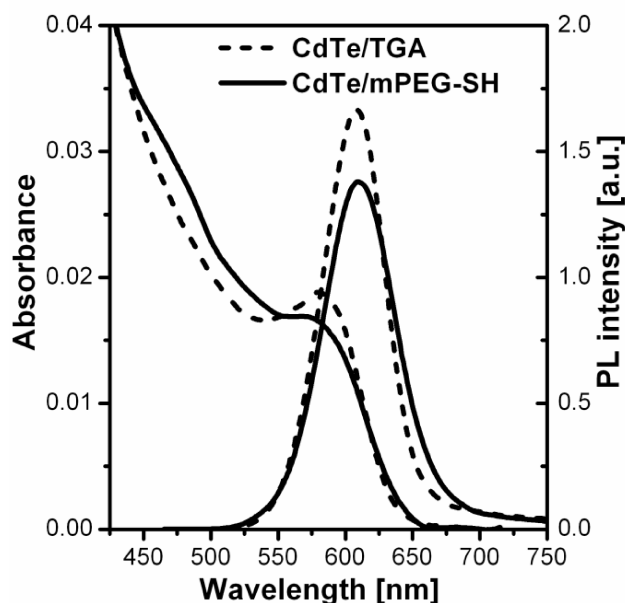


Figure 6.1. Absorbance and PL (ex. = 450 nm) spectra of the amphiphilic CdTe/mPEG-SH NCs and the hydrophilic CdTe/TGA NCs colloids used for the membrane penetration experiment.

molecule assures the quite small sizes of the resulting nanoparticles which is also beneficial for biological applications. The diameter of the amphiphilic QDs used for the penetration test was calculated to be of 8.7 nm including the fully extended mPEG-S-chains.

In order to test the ability of the QDs to permeate through lipid bilayers, GUVs prepared via electroformation were incubated in PBS containing diluted QD colloids of the same concentration. The images obtained during 3 hours of confocal microscopy observation are shown in Figure 6.2 where the red background stems from the QD fluorescence and the black circles are interiors of the GUVs. The uptake was quantified during a period of 3 hours by acquiring the intensity profile of the inner part of the GUVs. The intensity of the QD fluorescence background and the empty GUVs have also been quantified as references (see Figure 6.2). More than 100 GUVs have been observed in order to estimate the uptake efficiency after 3 hours and overnight incubation. Approximately 40 % of the GUVs contained QDs after 3 hours while after overnight incubation this number increased to 60%. Many parameters such as membrane curvature, size of the vesicle, unilamellarity of the membrane, lipid packing may account for the heterogeneous penetration. It should be noted that even after overnight exposure the QDs still have retained their emission. In the control experiment performed with CdTe/TGA NCs colloids penetration was not observed presumably because of their aggregation (Figure 6.3) which was also reported previously [150].

We further tested the colloidal stability of both QDs in various buffers including PBS,

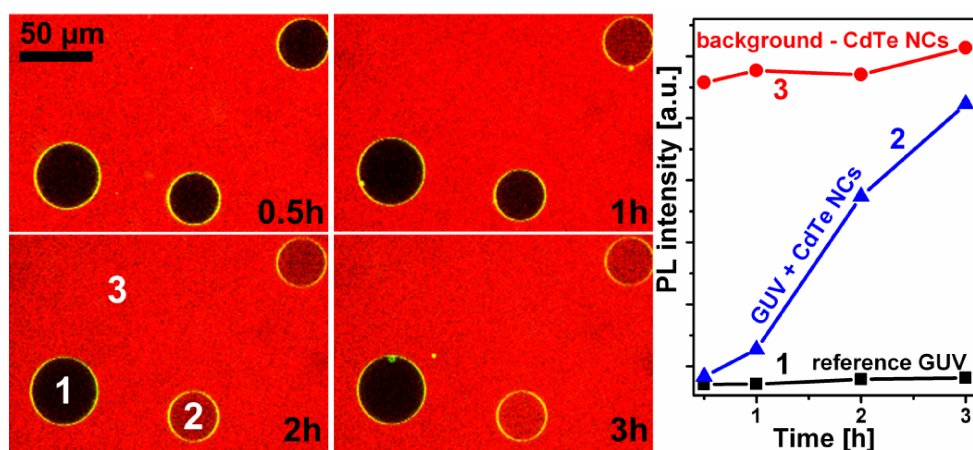


Figure 6.2. Confocal microscopy images acquired after 0.5, 1, 2 and 3 hours of incubation of GUVs with CdTe/mPEG-SH QDs in PBS (left); corresponding emission intensity profiles of the regions of interest shown on the left (right).

GPMV buffer, MEM cell medium and air buffer which are the main buffers used for cellular maintenance. The experiments revealed that the amphiphilic CdTe/mPEG-SH NCs remain homogeneously dispersed in all the biological buffers while the hydrophilic CdTe/TGA QDs tend to aggregate in all of them (Figure 6.3). It is considered that aggregation/clustering on the cell surface results in endocytosis [151]. Most probably this is the main reason why the hydrophilic nanoparticles cannot escape the endocytic uptake. Our data show that the amphiphilic QDs have the ability to diffuse through the GUV membrane owing to their colloidal stability in biological media and to their versatile solubility, in contrast to hydrophilic particles.

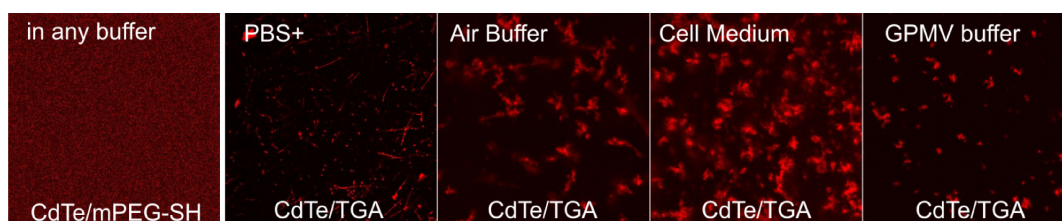


Figure 6.3. Confocal microscopy images demonstrating the colloidal stability of the amphiphilic CdTe/mPEG-SH QDs and the tendency to aggregation of the CdTe/TGA particles in various cellular buffers and medium.

In order to further investigate the penetration of the amphiphilic QDs we used GPMVs composed of a natural cell membrane. Clear visualization of the QD permeation was achieved employing a two channel detection approach. Thus, vesicles have been observed via the green emission of the TF-PIP dye adsorbed on their surface (Figure 6.4), whereas the QD distribution in the system has been monitored via the red band pass. As seen from the resulting merged image, the vesicles take up the amphiphilic NCs during incubation.

Although the penetration was slower than GUVs, we observed approx. 40% of GPMVs containing QDs after 10 hours of incubation.

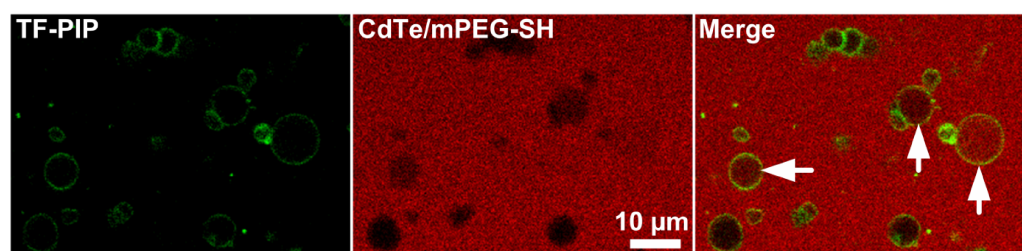


Figure 6.4. Confocal microscopy images, acquired after 3 hours of incubation, demonstrating penetration of the CdTe/mPEG-SH NCs into GPMVs visualized by merging the TF-PIP dye green fluorescence and the QD red emission. Arrows show the vesicles containing QDs.

6.4. Conclusions

In this study, we have further improved the synthesis of amphiphilic CdTe/mPEG-SH nanocrystals via the use of the high-boiling coordinating solvents dimethylacetamide and dimethylformamide. The optimized procedure yields QDs emitting in the wide visible region of 540-640 nm with enhanced quantum yield of up to 30%. The permeability test performed using GUVs and GPMVs for the first time demonstrated the ability of amphiphilic nanoparticles to penetrate through lipid bilayers which makes them promising agents for tracking whole cells and intracellular processes. Moreover, their high colloidal stability in various biological media and stable emission properties can be exploited for a better delivery of agents for therapeutic applications. The data acquired also provide new insight into the interaction of nanoparticles with an artificial lipid membrane as well as with natural cell membranes.

GPMVs for Investigating the Protein Partitioning in Cell Membrane: Raft Mediated Regulation of Lypd6 and LRP6 Activation

In this work, we use GPMVs along with other biochemical methods in order to investigate the impact of membrane heterogeneity on lipoprotein receptor-related protein 6 (LRP6) activity which is vital for Wnt signaling. We found out that LY6/PLAUR domain containing 6 (Lypd6), a member of the Ly6 protein family, is a GPI anchored protein which is located in the ordered domains in the cell membrane. Lypd6 is required for recruiting LRP6 to the rafts, where LRP6 becomes phosphorylated upon Wnt stimulation.

7.1. Introduction

Wnt/ β -catenin signaling controls embryonic development via regulating cell proliferation, cell fate determination and tissue patterning in many species from cnidarians to vertebrates and is required for maintenance of adult tissue homeostasis and regeneration of various animal tissues and organs [152–154]. Thus, pathway misregulation causes cancer, genetic disorders, degenerative and many other human diseases [155, 156]. Wnt signaling can be initiated by different interactions between various ligands and receptors, which can activate either β -catenin-dependent (canonical) or -independent (noncanonical) pathways. The signaling is initiated by interaction of the Wnt ligands, or alternative ligands like Norrin and possibly R-Spondin, with the Frizzled receptors and the co-receptor low density lipoprotein receptor-related protein 5/6 (LRP5/6) [157]. One early response to ligand-receptor interaction is phosphorylation of the intracellular domain of LRP5/6, which has been reported to preferentially occur in ordered membrane domains and the secreted Wnt antagonist Dkk1 inhibits the formation of a complex between LRP6 and CK1 α by eliminating LRP6 from these domains, thus, leading to its internalization [158]. However, it remains unclear how LRP6 accumulates in the raft domains.

Here, we find that Lypd6, a Ly6 protein family member, is GPI-anchored to the plasma membrane and this type of membrane anchorage is necessary for its partitioning to the lipid rafts in the membrane microdomains. Moreover, our data strongly suggest that Lypd6 regulates LRP6 distribution on the plasma membrane by concentrating it in the

rafts and hence enhancing its phosphorylation.

7.2. Materials and Methods

GPMVs were prepared as described in Section 6.2.4.

7.2.1. Cloning

Zebrafish Lypd6 (BC081426) open reading frame (ORF) was amplified from a cDNA mixture of gastrula and somitogenesis stage embryos. spGFP-zLypd6 (full length zebrafish Lypd6 fused in frame with mmGFP5 between amino acids 22 and 23), spGFP-zLypd6 Δ GPI (deletion construct of zebrafish Lypd6 lacking the carboxy terminus after amino acid 146, fused in frame with mmGFP5 between amino acids 22 and 23), spGFP-zLypd6 Δ GPI-TfR TMD (replacement construct of zebrafish Lypd6 with the carboxy terminus after amino acid 146 replaced by the first 97 amino acids of the Transferrin receptor (TfR) including the transmembrane domain (TMD), fused in frame with mmGFP5 between amino acids 22 and 23) and spGFP-zLypd6 Δ GPI-CD44 (replacement construct of zebrafish Lypd6 with the carboxy terminus after amino acid 146 replaced by the TMD of CD44, fused in frame with mmGFP5 between amino acids 22 and 23) were cloned into pCS2P+ expression vector. A rescue construct of zebrafish Lypd6 was cloned into pCS2P+ expression vector by mutating the first 25 nucleotides, which prevents the MO from binding but does not alter the amino acid sequence.

7.2.2. Secretion assay

HEK293T cells were transfected with either spGFP-Lypd6 (150 ng) or spGFP-Lypd6 Δ GPI (140 ng) along with equimolar amounts of spGFP-GPI and spGFP as controls, respectively. Cells were treated with phosphatidylinositol-specific phospholipase C (PIPLC) for 12 hours at 37°C at 24 hours post transfection. Conditioned media were collected from all four samples and concentrated using SpeedVac. Cells were lysed with passive lysis buffer (Promega). Media and lysates were loaded on a protein gel and blotted for GFP. Morpholinos, microinjection and whole mount in situ hybridization Capped sense RNA was synthesized in vitro using mMessage mMachine kits (Ambion). RNA and/or morpholinos were injected into the cytoplasm of 1-cell stage zebrafish embryos using standard procedures. Embryos were fixed at the indicated stages and mRNA in situ hybridization was performed as described previously [159].

7.2.3. Luciferase assays

HEK 293T cells were transiently transfected with the TCF/Lef firefly luciferase reporter pGL3 BAR (pBAR, 20 ng) (Biechele and Moon, 2008) and pGL4.73 hRLuc/SV40 (RLuc, 5 ng) (Promega, Madison) in triplicates. Firefly and renilla luciferase activities were measured 24 hours after transfection using the Dual-Luciferase Reporter Assay System (Promega) and firefly activity was normalized to renilla luciferase levels.

7.2.4. Western blot analysis and immunoprecipitation

For Western blotting, samples were dissolved in SDS gel-loading buffer containing β -mercaptoethanol, separated by SDS-PAGE gel and transferred to PVDF membrane (Invitrogen). The following antibodies were used: mouse anti-c-Myc monoclonal (Life Technologies, 1:2000), rabbit anti-GFP (Abcam, 1:2000), rabbit anti-Flag (Sigma, 1:1000), anti-HA (Abcam, 1:2000), rabbit anti-Phospho-LRP6 (Ser1490, Cell Signaling, 1:1000), rabbit anti-LRP (Cell Signaling, 1:1000), rabbit anti-Transferrin receptor 2 (Abcam, 1:2000) and mouse anti-Caveolin1 (BD Transduction Laboratories, 1:2000). Immunoprecipitation experiments were performed as described previously [160].

7.3. Results and Discussion

7.3.1. Lypd6 is GPI-anchored to the plasma membrane

Lypd6 belongs to the Ly6 family of proteins, which is characterized by an LU domain with conserved cysteine residues and whose members are either secreted or GPI-anchored to the plasma membrane [161, 162]. Bioinformatic analyses showed that zebrafish Lypd6 contains both a potential signal peptide sequence which is predicted to be cleaved from the protein and a C-terminal GPI anchor attachment site, referred to as the omega site. To verify Lypd6's subcellular localization, we generated tagged constructs by inserting GFP between the signal peptide (sp) and the rest of protein (spGFP-Lypd6, Figure 7.1A). This construct localized to the plasma membrane both in zebrafish embryos and cultured mammalian cells while a truncated version lacking the carboxy terminus starting at the omega site (spGFP-Lypd6 Δ GPI) did not (Figure 7.1B). Consistent with their predicted GPI-anchorage spGFP-Lypd6 and a spGFP-GPI control construct could not be detected in the media conditioned by transfected cells, while spGFP-Lypd6 Δ GPI and a spGFP control construct could (Figure 7.1C). However, when cells were treated with phosphatidylinositol-specific phospholipase C (PIPLC), which cleaves the GPI-anchor of cell surface anchored proteins, both spGFP-GPI and spGFP-Lypd6 were detected in the media (Figure 7.1C). These data indicate that Lypd6 contains a functional GPI-anchor attachment site which locates it to the plasma membrane.

7 GPMVs for Investigating the Protein Partitioning in Cell Membrane: Raft Mediated Regulation of Lypd6 and LRP6 Activation

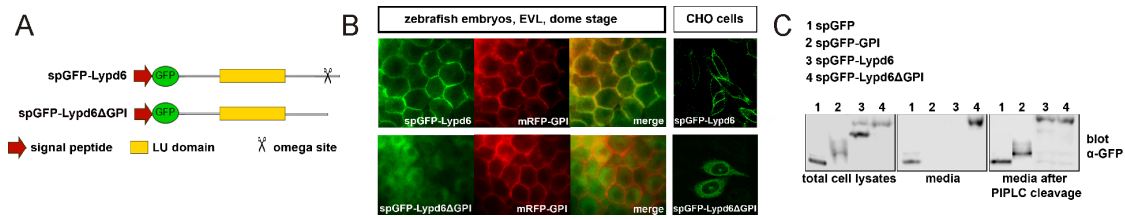


Figure 7.1. *lypd6* is GPI-anchored to the plasma membrane. (A) Domain structure of N-terminally GFP-tagged wild-type *Lypd6* (spGFP-*Lypd6*) and C-terminally truncated *Lypd6* (spGFP-*Lypd6*ΔGPI), (B) Localization of GFP tagged zebrafish wt and C-terminally truncated *Lypd6* in enveloping cells (EVL) of sphere stage zebrafish embryos and in Chinese hamster ovary (CHO) cells, (C) Release of spGFP-*Lypd6* and spGFP-GPI from the plasma membrane upon treatment with phosphatidylinositol-specific phospholipase C (PIPLC). spGFP-*Lypd6*ΔGPI and spGFP are detectable in the conditioned media without PIPLC treatment.

7.3.2. *Lypd6* interacts with LRP6 independently of its GPI-anchor

We next asked whether *Lypd6* physically interacts with the members of the Wnt receptor complex. *Lypd6* co-immunoprecipitated (co-IPed) with LRP6, but not with the LDL receptor (LDLR), which is related to LRP6 but has no role in β -catenin signaling (Figure 7.2A). However, a construct where the GPI anchor attachment site was replaced with the transmembrane domain of human CD44 (spGFP-*Lypd6*ΔGPI-CD44TMD) also interacted with LRP6, indicating that LRP6-*Lypd6* interaction does not depend on how *Lypd6* is anchored to the plasma membrane (Figure 7.2A). Interestingly, *Lypd6* could also be co-IPed with the β -catenin pathway coupled Frizzled (Fz) receptor Fz8 dependent of exogenous Wnt stimulation, but not with the ligand Wnt8. Wnt3a stimulation triggers formation of a complex between LRP6 and Frizzled. Receptor complex formation is followed by phosphorylation of LRP6 at serine and threonine residues found in its intracellular domain [163] and subsequent internalization of LRP6 via caveolin-mediated endocytosis [157]. Hence, we first asked whether *Lypd6* is necessary for Wnt-induced LRP6 phosphorylation. Upon Wnt3a stimulation, while total LRP6 levels remained constant, phosphorylated LRP6 at S1490 (P-LRP6) increased in the cells where *Lypd6* was overexpressed (Figure 7.2B). Intriguingly, phosphorylation of LRP6, was reduced in the cells where spGFP-*Lypd6*ΔGPI-CD44TMD was overexpressed, showing that this construct acts as a dominant-negative construct. These findings show that *Lypd6* binds to LRP6 independent of how it is attached to the plasma membrane but it is capable of stimulating LRP6 phosphorylation only when it is GPI-anchored to the membrane.

7.3.3. *Lypd6* partitioning into rafts influences Wnt signaling activation

Endogenous LRP6 is found in both ordered glycolipoprotein membrane microdomains, termed lipid rafts, and disordered regions, i.e. non-rafts, independent of Wnt3a stimulation. Phosphorylation of LRP6, however, occurs preferentially in the lipid rafts [158].

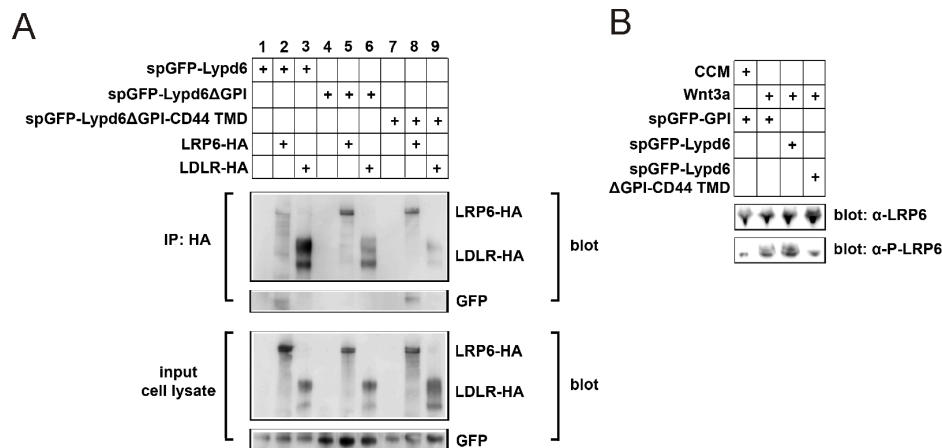


Figure 7.2. Lypd6 interaction with LRP6. (A) spGFP-zLypd6 and spGFP-zLypd6ΔGPI-CD44 TMD co-immunoprecipitate (co-IP) with LRP6-HA, but not LDLR-HA in HEK293T cells. spGFP-zLypd6ΔGPI does not co-IP with LRP6-HA or LDLR-HA, (B) spGFP-zLypd6ΔGPI-CD44 TMD blocks Wnt3a-induced phosphorylation of LRP6 at S1490 in HEK293T cells assayed at 6h post stimulation with Wnt3a CM.

How raft-specific LRP6 phosphorylation is regulated remains unknown. We thus wondered whether Lypd6 might facilitate raft-specific LRP6 activation.

GPI-anchored proteins often preferentially partition into the raft domains. To test whether Lypd6 partitions into rafts, we employed giant plasma membrane vesicles (GPMVs) which enable observation of lipid phase separation in intact plasma membranes isolated from live cells. GPMVs are cell-derived liposomes that can be isolated after chemically induced membrane blebbing and which to a large extent maintain the lipid and protein diversity of the plasma membrane [67, 106]. We found that Lypd6 partitioned preferentially into the lipid rafts in GPMVs derived from CHO cells, which were transfected with spGFP-Lypd6 and stained for the fluorescent non-raft lipid marker Fast DiI (Figure 7.3A). Unlike spGFP-Lypd6, a construct in which the GPI anchor was replaced with the transmembrane domain of the human Transferrin receptor (TfR), a non-raft marker protein, (spGFP-Lypd6ΔGPI-TfR TMD) and the transmembrane-anchored spGFP-Lypd6ΔGPI-CD44TMD partitioned into the non-raft phases (Figure 7.3B-C). As expected, the truncated construct spGFP-Lypd6ΔGPI was not detectable on the surface of GPMVs (Figure 7.3D) but inside the vesicles.

As fusion with the TfR transmembrane domain caused a relocation of the Lypd6 from raft to non-raft domains, we asked how this affected Lypd6's ability to modulate Wnt/ β -catenin pathway activation. We found that, unlike the wild type Lypd6, the transmembrane anchored version (spGFP-Lypd6ΔGPI-TfR TMD) did not enhance but reduced the Wnt8-induced pBAR activation both in HEK cells (Figure 7.4A) and in embryos (Figure 7.4B). These data indicate that the TfR TMD fusion acts as a dominant-negative construct, suggesting that localization of Lypd6 to lipid raft domains is necessary

7 GPMVs for Investigating the Protein Partitioning in Cell Membrane: Raft Mediated Regulation of Lypd6 and LRP6 Activation

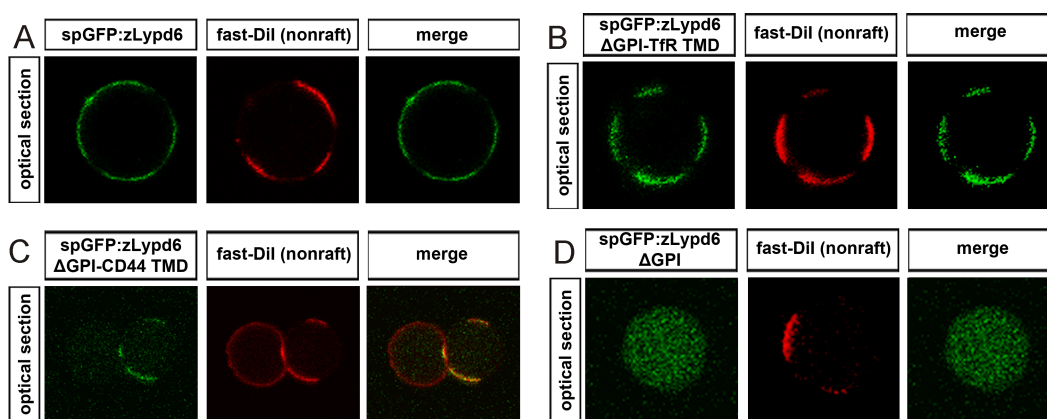


Figure 7.3. Membrane partitioning of various tagged Lypd6 constructs in GPMVs derived from CHO cells: (A) GPI-anchored spGFP-zLypd6 preferentially goes into the lipid rafts ($74 \pm 6\%$) and does not overlap with the fluorescent non-raft lipid marker Fast DiI (red). (B) Transmembrane-anchored spGFP-zLypd6 Δ GPI-TfR TMD prefers the non-raft phase ($93 \pm 4\%$) and largely overlaps with Fast DiI. (C) Transmembrane-anchored spGFP-zLypd6 Δ GPI-CD44 TMD partitions to the non-raft phase ($95 \pm 2\%$) and overlaps with Fast DiI on the plasma membrane of GPMVs derived from CHO cells. (D) GPI anchor lacking version spGFP-zLypd6 Δ GPI does not localize to the surface of GPMVs.

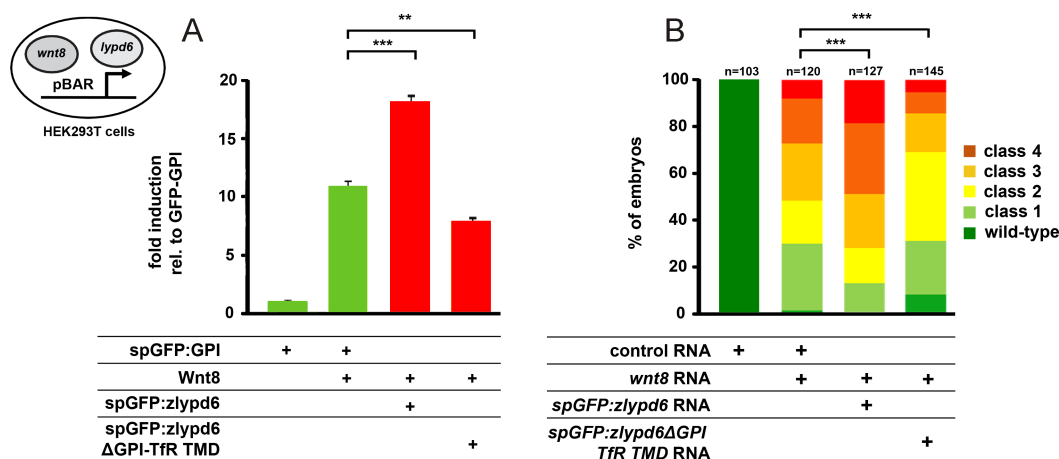


Figure 7.4. (A) pBAR luciferase reporter activity in HEK293T cells transfected with Wnt8 (20 ng) plus spGFP-zLypd6 (100 ng) or spGFP-zLypd6 Δ GPI-TfR TMD (95 ng) or equimolar amounts of spGFP-GPI control. spGFP-zLypd6 Δ GPI-TfR TMD acts as a dominant negative and reduces reporter activity. ***, $p < 0.001$, **, $p < 0.01$, Student's t-test, (B) Range of phenotypes in Wnt8-overexpressing embryos injected with wnt8 (20 pg) plus spGFP-zLypd6 (150 pg) or spGFP-zLypd6 Δ GPI-TfR TMD (140 pg) or equimolar amounts of spGFP-GPI control RNA. spGFP-zLypd6 Δ GPI-TfR TMD significantly rescues Wnt8-induced phenotypes. ***, $p < 0.001$, Chi-Square test.

for its function as an enhancer of Wnt/ β -catenin signaling.

7.3.4. Lypd6 regulates LRP6 distribution in plasma membrane phases

Because Lypd6 partitions into the rafts where LRP6 has previously been shown to be phosphorylated, we asked whether it is necessary to recruit LRP6 to the lipid rafts. Due

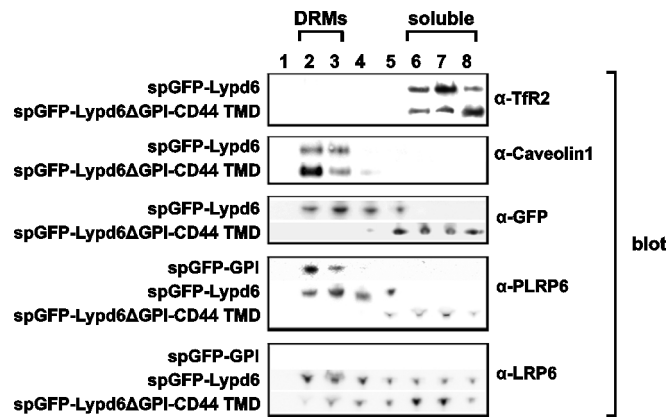


Figure 7.5. DRM flotation on an OptiPrepTM step gradient. Detection of endogenous Transferrin, Caveolin-1, P-LRP6 and LRP6 and overexpressed GFP tagged Lypd6 in spGFP-zLypd6 (2 ng) or spGFP-zLypd6ΔGPI-TfR TMD (1.85 ng) or equimolar amounts of control spGFP transfected cells treated with Wnt3a.

to their molecular composition, high lipid-to-protein ratio and packing structure, lipid raft domains tend to remain intact and stay insoluble in non-ionic detergents at low temperatures and they can be aggregated into detergent resistant membranes (DRMs), while the fluid membrane dissolves [164]. Using DRM flotation on an OptiPrepTM step gradient, we separated the DRMs marked by Caveolin1 (Figure 7.5, second row) from the soluble membranes marked by TfR2 (Figure 7.5, first row). We found that the GPI-anchored spGFP-Lypd6 was enriched in the DRMs while the transmembrane anchored spGFP-Lypd6ΔGPI-CD44TMD was shifted towards the detergent soluble phase and showed almost no phase overlap with spGFP-Lypd6 (Figure 7.5, compare α-GFP, third row). Strikingly, LRP6 phosphorylation preferably occurred in the place where Lypd6 was present and that it was also reduced when Lypd6 was forced to be expressed in the soluble phases (Figure 7.5, fourth row, compare with the third row). These data suggest that Lypd6 controls LRP6 distribution on the membrane and recruits it to the lipid rafts, which is critical for it to become phosphorylated.

7.4. Conclusion

Here, by employing GPMVs, we found that the GPI-anchored Ly6 family protein Lypd6 partitions into the rafts and that this partitioning depends exclusively on its GPI-anchor. Lypd6 physically interacts with LRP6 and recruits it to the lipid rafts, where LRP6 becomes phosphorylated in response to Wnt stimulation.

Investigation of Membrane Order Regulation in Prokaryotes with Model Membranes

Ordered phases are one of the biochemically active membrane states, which up to now were thought to be a unique property of interactions between Eukaryotic membrane lipids. The ordering properties of sterols form the basis for the formation of Lo phase bi-layers. Through a biophysical examination of diplopterol, the simplest bacterial hopanoid, and cholesterol, we demonstrate that hopanoids are bacterial sterol surrogates possessing the ability to order saturated lipids and to form a "raft" phase. Furthermore, diplopterol can buffer pH-induced changes to the order of lipid A, a major component of the bacterial outer membrane. These observations can explain major features of the environmental distribution of hopanoids and prove that cholesterol-like ordering could have evolved prior to the oxygenation of Earth's surface.

8.1. Introduction

The capacity for sterols to modulate the ordering of lipids forms the basis for a membrane organizing principle in eukaryotes [7]. The emergence of sterol-like ordering was likely a critical step in the evolution of biological membranes, allowing cells to control fluidity without compromising membrane integrity, and providing a means to compartmentalize membranes into functional domains [114, 165, 166]. It is not known, however, to what extent such membrane ordering properties span the domains of life. Prokaryotes generally lack sterols, however some bacteria produce hopanoids [167, 168], which are structurally similar (Figure 8.1A) [169] and their cyclization is catalyzed by related enzymes [170]. These similarities inspired the hypothesis that hopanoids are bacterial "sterol surrogates" [171], and led us to examine whether hopanoids might share the properties of sterols in membranes.

8.2. Materials and Methods

GUVs were prepared as described in Section 6.2.3. Fluorescence Correlation Spectroscopy measurements were carried out as will be described in detail in Section 9.2.2.

8.2.1. Lipids and Probes

SM, kdo-lipid A, DPPC, POPC, DPPC, DPPG, POPG, DOPG, and cholesterol were purchased from Avanti Polar Lipids. Diplopterol was purchased from Chiron AS. Atto532 labeled sphingomyelin was purchased from AttoTech. C-laurdan was a gift from Prof. B. R. Cho (Seoul, Korea). Stock concentrations of lipids were measured by phosphate assay. Cholesterol and diplopterol were weighed out on a precision scale and solubilized in a known volume of chloroform/methanol (2:1).

8.2.2. Monolayers

Monolayers were prepared as described previously [172]. Briefly, chloroform/methanol (2:1) solutions of pure lipids and mixtures were prepared at 0.5 mg/ml lipid concentrations. Monolayers were prepared by injecting 10-20 μ l of lipid solution onto an aqueous subphase maintained at 25 °C by a built-in water jacket supplied by a temperature controlled circulating water bath. The subphase was comprised of 150 mM NaCl, 3.3 mM sodium citrate, 3.3 mM sodium phosphate, 3.3 mM glycine, and 0.1 mM ethylenediaminetetraacetic acid (EDTA), with pH titrated to 7.4, 5.1, or 3.1 by HCl or NaOH. Isotherms were recorded using a 70 cm^2 teflon Langmuir trough fitted with a motorized compression barrier equipped with pressure sensor and Wilhelmy plate (Nima Technology). The mean molecular areas (MMA) for each mixture were estimated from the averages of isotherms from three monolayers that were prepared independently. The theoretical mean area per molecule (lipid) for each mixture was calculated as follows:

$$A_i = X_1A_1 + X_2A_2 \quad (8.1)$$

where: A_i = MMA of the mixture, X_1 , X_2 = the mole fraction of lipid 1 and 2, and A_1 , A_2 = the MMAs of lipid 1 and 2 at surface pressures 5, 10, 15, 20, and 25 mN/m. The percent change in molecular area (condensation effect) was calculated as follows:

$$c = 100(A_i - A_o)/A_i \quad (8.2)$$

where: c = % condensation, A_o = the observed MMA at 5, 10, 15, 20, and 25 mN/m, and A_i = the theoretical MMA of the two lipids.

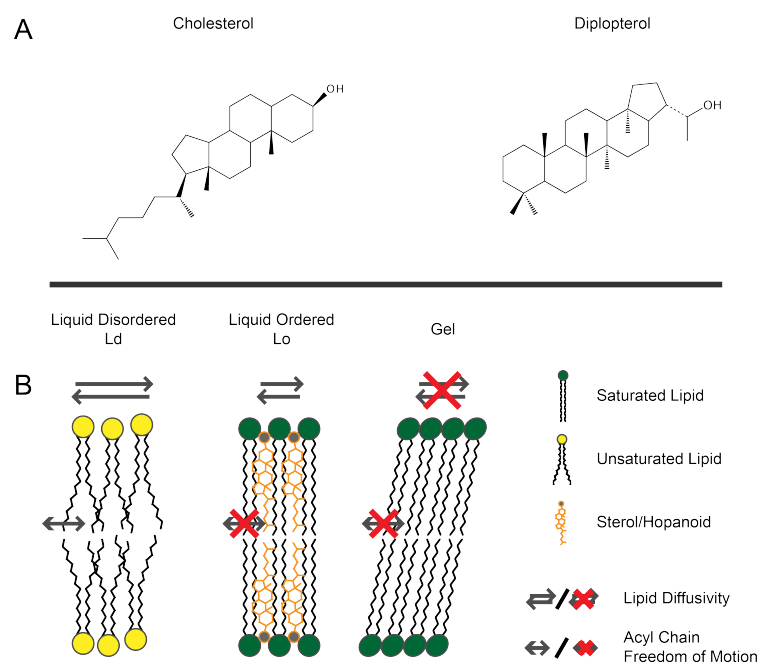


Figure 8.1. (A) Structures of cholesterol and diplopterol and (B) a conceptual cartoon illustrating liquid disordered (Ld), liquid ordered (Lo), and gel phase membranes.

8.2.3. Preparation of liposomes and C-laurdan spectroscopy

Lipids in 2:1 chloroform/methanol were mixed, dried under vacuum for 4 hours. Lipids were then hydrated in HBS (50 mM Hepes, 150 mM NaCl, 0.2 mM EDTA, pH 7.2) at 68 °C for 20 minutes. The resulting liposomes were subjected to 10 freeze-thaw cycles, followed by sonication for 5 minutes to promote formation of unilamellar membranes. Bi-layer formation was confirmed in unlabelled liposomes by the presence an emission peak at 425 nm ($\text{ex} = 385 \text{ nm}$) [106]. Liposome preparations containing 200 μM lipid were stained with 100 nM C-laurdan and incubated at room temperature for 20 minutes to equilibrate. Liposomes of each mixture were independently mixed and prepared in triplicate. Spectra were recorded with 1 nm resolution on a Fluoromax-3 fluorescence spectrometer (Horriba) with temperature maintained at either 25 or 50 °C by a temperature controlled circulating water bath. Excitation of C-laurdan was 385 nm. Spectra were recorded from triplicate preparations of each mixture and averaged. The GP values for C-laurdan were calculated from two emission bands 420- 460 nm and 470 - 510 nm according to Equation 3.2. C-Laurdan microscopy was carried out as described in Section 5.9.

8.3. Results and Discussion

8.3.1. The effects of cholesterol and diplopterol on the phase behavior and ordering of sphingomyelin in model membranes

Sterols and sphingolipids are closely associated in eukaryotic membranes and the nature of their interactions has been extensively characterized. Therefore we chose to test whether diplopterol behaves similarly to cholesterol in this well-defined system. Sterols interact with sphingolipids *in vitro* to form a liquid ordered (Lo) phase that represents a thermodynamic intermediate between liquid disordered (Ld) and crystalline gel phases (Figure 8.1B) [173]. The interactions leading to the formation of a Lo phase derive from the ability of sterols to simultaneously inhibit the formation of the gel phase (by intercalating between sphingolipids and preventing their crystallization) and to order saturated acyl chains. To test whether these properties are also exhibited by hopanoids, we examined the effect of diplopterol on N-stearoyl-D-erythro-sphingosylphosphorylcholine (SM), a synthetic sphingolipid. Monolayer experiments provide an approach to study the gel-liquid phase transition of SM. Lipids are spread out over an air-water interface to form a monolayer and lateral pressure (measured as surface tension) is measured while the area of the monolayer is decreased. The measurements are depicted as an isothermal plot of pressure versus mean molecular area (MMA - *Angstroms*²/*molecule*) of the lipid mixture (Figure 8.2A). Lipids such as SM that form a gel phase at physiological temperatures show a characteristic inflection point in the isotherm plot, which reflects a sharp phase transition from liquid to gel phase. This phase transition is eliminated in the presence of cholesterol (Figure 8.2). We observed the same effect of diplopterol on SM (Figure 8.2A), demonstrating a shared ability to inhibit gel phase formation.

To determine whether diplopterol shares an ability with cholesterol to order SM we measured ordering by (C-laurdan) spectroscopy. The generalized polarization (GP) index calculated from C-laurdan emission spectra is correlated with lipid order (see Section 3.2). We calculated the ordering effect of cholesterol or diplopterol as the difference in the GP index (ΔGP) of liposomal membranes containing pure SM and mixtures containing cholesterol or diplopterol. Measurements were made above the gel-liquid transition temperature of SM to ensure that we were observing an ordering effect on bilayers in a liquid state and not a fluidizing effect on gel phase bilayers. Our results indicate that diplopterol exhibits an ordering effect on SM comparable to the effect of cholesterol (Figure 8.2B). This result is further corroborated by monolayer experiments in which the observed MMA of mixtures containing cholesterol or diplopterol with SM was less than the MMA predicted from the sum of the individual components; indicating an energetically favorable condensing interaction (Figure 8.2A). Interestingly, compared with

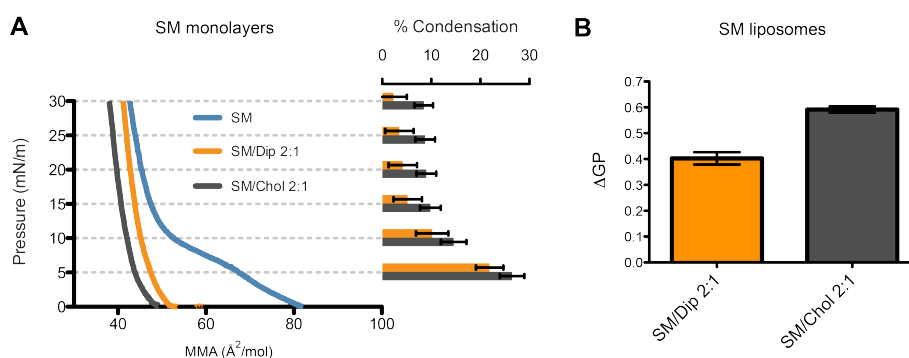


Figure 8.2. The effects of cholesterol and diplopterol on SM. (A) Monolayers of SM and mixtures containing cholesterol (chol) or diplopterol (dip) were compressed at 25 °C. The condensation effect of chol and dip on SM was calculated as shown to the right of the isotherm traces. (B) The membrane ordering effect (ΔGP) of chol or dip on SM was determined by C-laurdan spectroscopy on liposomes labeled with 0.2 mol % C-laurdan and composed of SM, SM/chol (2:1 mol%) and SM/dip (2:1) at 50 °C. The ΔGP was calculated as the difference in GP between liposomes containing pure SM and mixtures of either SM/chol or SM/dip.

cholesterol, diplopterol exhibits a weak ordering effect on lipids containing unsaturated acyl chains.

8.3.2. Cholesterol and diplopterol interact with sphingomyelin to form a liquid ordered phase in giant unilamellar vesicles

Having demonstrated a shared ability for diplopterol and cholesterol to inhibit gel phase formation and order SM, we directly assayed whether diplopterol induces the formation of a L_o phase. In model systems composed of synthetic lipids SM and 1,2-dioleoyl-sn-glycero-3-phosphocholine, cholesterol induces the formation of two immiscible liquid phases: an ordered phase (L_o) enriched in SM and sterol, and a disordered phase (L_d) enriched in DOPC [174]. We investigated the coexistence of L_o and L_d phases in GUVs using C-laurdan microscopy. Mixtures containing SM/DOPC and either cholesterol or diplopterol yielded phase separated GUVs with ordered and disordered phases (Figure 8.3A,B), suggesting that the hopanoid ring structure is capable of inducing phase separation. The relative order (e.g. C-laurdan GP) of GUVs comprised of SM/cholesterol and SM/diplopterol were roughly equal, and within the range characteristic of L_o bilayers (Figure 8.3A,B) [34]. By comparison, the GP of DOPC GUVs was negative indicating a liquid disordered (L_d) membrane. These observations were confirmed by quantifying the diffusivities of the membranes by FCS (See Chapter 2). The diffusivity of Atto532 labeled sphingomyelin in GUVs containing cholesterol or diplopterol with SM was identical and nearly an order of magnitude slower than for DOPC GUVs (Figure 8.3C). These results demonstrate that diplopterol is capable of interacting with SM to form a L_o phase with order and fluidity that are essentially identical to the cholesterol-SM L_o phase.

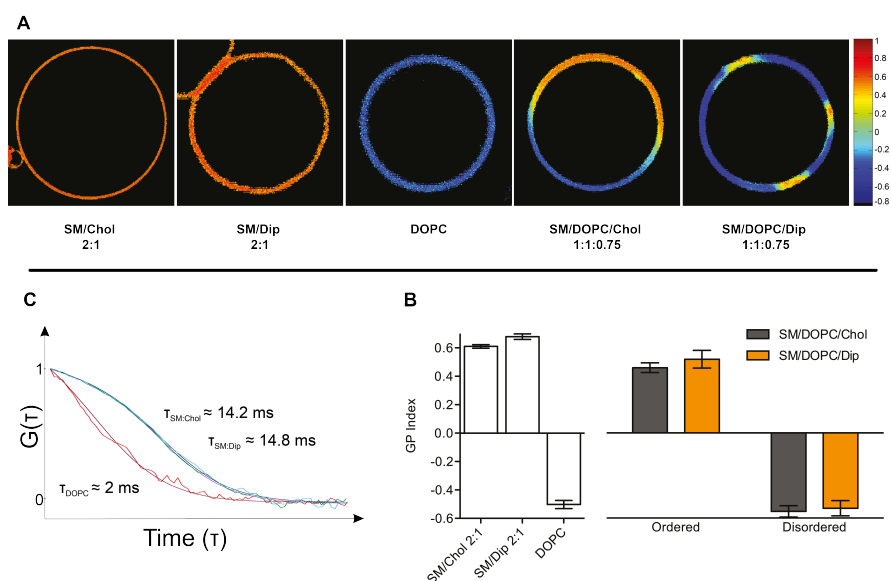


Figure 8.3. Diplopterol forms a liquid ordered phase. (A) Confocal images of GUVs at 22 °C and labeled with 0.2 mol % C-laurdan. The composition (mol %) of GUVs is given below each image and GP values are depicted by color. (B) Average GP of one- and two-component GUVs and of ordered and disordered domains from three-component GUVs ($n = 4$). (C) Autocorrelation curves and estimated diffusion times of Atto532 labeled sphingomyelin (0.001 mol%) in SM/Chol, SM/Dip and DOPC GUVs at 22 °C.

8.3.3. Cholesterol and diplopterol modulate the order and phase behavior of lipid A in model membranes

Thus, we now have evidence that diplopterol and cholesterol share a conserved ability to order saturated lipids and to promote the formation of a Lo phase while preventing the formation of a gel phase. The physiological relevance of this property in bacteria, however, remains unaddressed. The cellular abundance of hopanoids in bacteria varies by nearly two orders of magnitude between organisms [168] and approaches roughly 50% of the lipid content of some bacteria [175]. We observed that the ordering effect of diplopterol was apparent at molar concentrations as low as 5 % , indicating that hopanoids could play a role in membrane ordering at physiologically relevant abundances. Hopanoids in bacteria have been observed in the outer membranes [176–178], where lipid A is the major component of the extracellular leaflet of the bilayer [179]. This lipid bears several structural similarities to SM, including amide-linked saturated acyl chains and hydroxylations (Figure 8.4A). This similarity led us to conjecture that diplopterol could also affect lipid A-containing membranes. It was previously demonstrated that lipid A undergoes a pH dependent change in order, becoming less fluid at lower pH and approaching a gel state [180]. Such extreme pH-induced changes in ordering of lipid A could be detrimental to the integrity and biochemical functionality of the bacterial outer

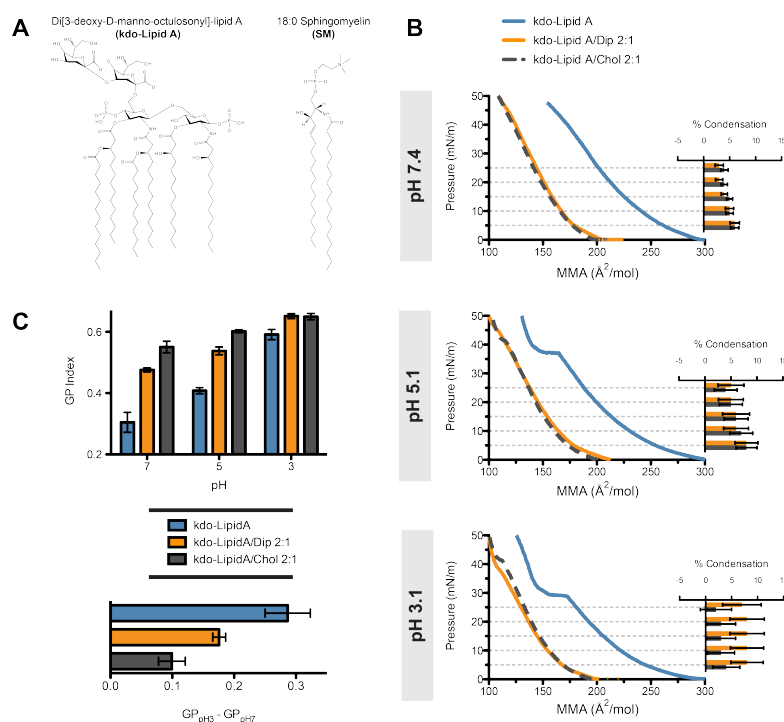


Figure 8.4. Ordering effect of diplopterol (dip) and cholesterol (chol) on kdo-lipid A. (A) comparison of the structures of kdo-lipid A and SM. (B) Isotherms of Lipid A mixtures and calculated condensation effect of chol and dip on kdo-lipid A at 25 °C and pH 7.4, 5.1, and 3.1. (C) The membrane order (GP) of liposomes labeled with 0.2 mol % C-laurdan containing kdo-lipid A, kdo-lipid A/dip, and kdo-lipid A/chol. The pH-induced change in relative membrane order was calculated as the difference in GP ($GP_{pH3} - GP_{pH7}$) between pH 3 and 7 for the three mixtures at 25 °C.

membrane. Indeed, two recent studies showed that mutants of hopanoid-producing bacteria with disrupted hopanoid synthesis exhibited retarded growth at low pH [181, 182]. We therefore tested the possibility that hopanoids play a role in modulating the order of lipid A in response to changing pH. To determine if diplopterol or cholesterol could influence the pH-induced phase transition of lipid A we examined their effect on synthetic Di[3-deoxy-D-manno-octulosonyl]-lipid A (kdo-lipid A; Figure 8.4A) in monolayers at neutral and acidic pH. At pH 7.4 kdo-lipid A yielded a monotonically increasing change in surface pressure with decreasing molecular area, demonstrating that it is in a fluid state with no phase transition occurring (Figure 8.4B). As predicted, at pH 5 and 3 we observed the emergence of a phase transition, identified by a "shelf" in the isotherms (Figure 8.4B). The addition of diplopterol or cholesterol eliminated this phase transition. Additionally, both of these lipids exhibited a condensing effect on kdo-lipid A (Figure 8.4B), consistent with our previous results demonstrating their ability to condense SM. Together, these observations indicate that both diplopterol and cholesterol are capable of simultaneously condensing lipid A and inhibiting its gel phase formation, thus buffering the effects of low pH on lipid A.

Finally, we measured the order of kdo-lipid A-containing membranes using C-laurdan spectroscopy. At pH 7, liposomes comprised of kdo-lipid A alone were less ordered than with either diplopterol or cholesterol, and values of the latter two mixtures were within the range expected for Lo membranes (Figure 8.4C). Thus, in terms of order, lipid A/diplopterol membranes at neutral pH are analogous to SM/cholesterol membranes. At pH 5.1 and 3.1 the GP of pure lipid A in comparison to pH 7 increased to 0.4 and 0.6, respectively, indicating increasing membrane order. On the other hand, the lipid A mixtures with diplopterol and cholesterol exhibited a smaller change in the GP. These results again demonstrate that diplopterol and cholesterol have the ability to moderate pH-induced changes in ordering. This capability of hopanoids could play a key role in modulating the ordering of the outer membrane of hopanoid-producing bacteria in environments with variable pH and could explain the prominence of hopanoids in bacteria that live in acidic environments [167, 168, 183], environments that experience large pH shifts such as soils [184, 185], and the rarity of hopanoids in pH buffered environments such as the oceans [186, 186, 187]. It may also explain the previously mentioned sensitivity of hopanoid deficient mutants to low pH [181, 182].

8.4. Conclusion

Here, we demonstrate for the first time that the hopanoid ring structure, like the sterol ring structure, is capable of interacting with saturated lipids to form a Lo phase and to modulate the order of lipid A. The similarities between hopanoids and sterols were first considered over 30 years ago by pioneers in the field [169], and they were subsequently dubbed as "bacterial sterol surrogates" [171]. However, the significance of the Lo phase as a unique product of lipid ordering and the biological implications of the Lo phase for membrane organization were not known at that time. The ordering properties of hopanoids in some bacteria could potentially confer the ability to subcompartmentalize their membranes into functional domains [188]. Evidence for lipid dependent functional domains has been reported for *Bacillus subtilis* [189], and there is evidence for lateral membrane heterogeneity in *Gloeobacter violaceus* [190], a hopanoid-producing cyanobacterium. Interestingly, it has been suggested that the averaged order of eukaryotic plasma membranes and bacterial inner membranes lacking hopanoids converge [132]. These studies imply that bacteria that lack hopanoids may employ alternate mechanisms for achieving lateral heterogeneity and modulating membrane order. Since the biosynthesis of hopanoids does not require molecular oxygen [191–194], our results demonstrate that the capacity to order membranes could have preceded the emergence of free oxygen on Earth's surface. Furthermore, the shared ability of hopanoids and sterols to mediate Lo phase formation suggests that this property might be a conserved feature of all membrane

polycyclic isoprenoids. This possibility prompts the need to extend our observations to other hopanoids (such as the bacteriohopanepolyols), and other cyclic lipids including tetrahymanol. If ordering and the promotion of coexisting liquid phases are conserved properties of these lipids, the invention of isoprenoidal cyclase enzymes could mark an important event in the evolution of biological complexity: the evolution of a second biochemically active liquid membrane phase and the ability to regulate membrane order by decoupling lipid lateral diffusivity from acyl chain freedom of motion.

Part III.

The Nature of Membrane Lateral Heterogeneity

Partitioning, Diffusion, and Ligand Binding of Raft Lipid Analogs in Model and Cellular Plasma Membranes

Several simplified membrane models, as discussed in Chapter 4 featuring coexisting liquid disordered (Ld) and ordered (Lo) lipid phases have been developed to mimic the heterogeneous organization of cellular membranes, and thus, aid our understanding of the nature and functional role of ordered lipid–protein nanodomains, termed “rafts”. In spite of their greatly reduced complexity, quantitative characterization of local lipid environments using model membranes is not trivial, and the parallels that can be drawn to cellular membranes are not always evident. Similarly, various fluorescently labeled lipid analogs have been used to study membrane organization and function *in vitro* (See Chapter 3), although the biological activity of these probes in relation to their native counterparts often remains uncharacterized. This is particularly true for raft-preferring lipids (“raft lipids”, e.g. sphingolipids and sterols), whose domain preference is a strict function of their molecular architecture, and is thus susceptible to disruption by fluorescence labeling. Here, we analyze the phase partitioning of a multitude of fluorescent raft lipid analogs in GUVs and GPMVs. We observe complex partitioning behavior dependent on label size, polarity, charge and position, lipid headgroup, and membrane composition. Several of the raft lipid analogs partitioned into the ordered phase in GPMVs, in contrast to fully synthetic GUVs, in which most raft lipid analogs mis-partitioned to the disordered phase. This behavior correlates with the greatly enhanced order difference between coexisting phases in the synthetic system. In addition, not only partitioning, but also ligand binding of the lipids is perturbed upon labeling: while cholera toxin B binds unlabeled GM1 in the Lo phase, it binds fluorescently labeled GM1 exclusively in the Ld phase. Fluorescence correlation spectroscopy (FCS) by stimulated emission depletion (STED) nanoscopy (see Chapter 2) on intact cellular plasma membranes consistently reveals a constant level of confined diffusion for raft lipid analogs that vary greatly in their partitioning behavior, suggesting different physicochemical bases for these phenomena.

9.1. Introduction

The minimal systems approach aims to uncover the principles underlying biological processes by minimizing the number of variables, thus decreasing complexity, while retaining the functionality of the system [76]. For research on biological membranes, several minimal systems exist to study both isolated lipid behavior and the interplay of lipids and proteins [96]. GUVs (see Chapter 4) are widely used model membranes [85, 103, 195] that have found a large variety of applications [29, 41, 86, 129, 130, 174, 196, 197], due to their ease of preparation and strict control of membrane composition. Yet, having a limited number of components, GUVs cannot fully recapitulate many important properties of cellular membranes, most notably due to the lack of leaflet asymmetry and membrane spanning proteins that comprise a major fraction of all biological membranes. An intermediate model system between fully synthetic GUVs and live cell membranes are GPMVs (see Chapter 5), microscopic spheres of plasma membranes harvested from live cells following chemical treatment [89, 198]. GPMVs more closely resemble native biological membranes, because they maintain lipid and protein diversity, but have the disadvantage of rather high compositional variation and complexity.

The most widely investigated physicochemical phenomenon of biomimetic membranes is the liquid-liquid phase coexistence occurring when saturated lipids and sterols condense to form a liquid ordered (Lo) phase, which separates an unsaturated lipid-rich liquid disordered (Ld) phase. Lo/Ld phase separation in GUVs and GPMVs has been extensively characterized [29, 67, 86, 109, 123, 125, 129, 130, 135, 174, 196, 197, 199] (see Chapter 4) and proposed as a physical basis underlying the raft concept in cell membranes [7, 29, 200].

Measurements of membrane nanostructure require specific visualization of lipids and proteins, realized by adding a fluorescent label to the molecule of interest. The discovery of the green fluorescent protein (GFP) enabled direct observation of proteins both in their native environment and in the synthetic systems described above [67, 122, 123]. In the case of lipids, such a universal probe is not available. To sensitively and selectively probe the lipid environment [74, 201], coupling synthetic fluorescent moieties to lipids and incorporating these analogs into cell membranes has become a common protocol for optical investigation of membranes (see Chapter 3). However, the addition of bulky tags, often containing hydrophilic groups, may drastically affect native lipid behavior [199]. This is particularly true of raft lipids (i.e. those that would be expected to enrich in the raft phase based on their enrichment in detergent resistant membranes - sphingolipids, sterols, etc), which require specific structural features to allow their condensation into an ordered domain. Correspondingly, apart from a few examples [202–204], most fluorescent raft lipid analogs do not enter the raft-mimetic Lo phase of model

membranes [65, 68, 199, 202, 205–208].

As a complement to minimal membrane model systems, local heterogeneity in the membranes of live cells has been probed by measuring the diffusion of lipids and proteins (e.g. by single particle tracking (SPT) [209] and Fluorescence Correlation Spectroscopy (FCS) [86] since the introduction of the raft hypothesis [7, 210]. In contrast to SPT, where a labeled molecule is tracked with very high positional accuracy to reveal the local membrane structure, FCS on cellular membranes suffered from the relatively large size of the confocal observation spot compared to the size of putative lipid nanodomains. Recently, the addition of FCS to STED nanoscopy [51, 54, 211] (used to tune focal spots down to 30 nm in diameter) revealed transient local confinement of fluorescent sphingolipid and ganglioside (but not phosphoglycerolipid) analogs in the plasma membrane of living cells [15, 212]. Despite the large difference in nanoscopic diffusion between fluorescent sphingo- and phosphoglycerolipids, both lipids have been shown to mainly partition into the Ld phase of model membranes [98, 212]. Consequently, it remains to be shown how the transient nanoscopic interactions probed by STED-FCS relate to ordered phases in model membranes and functional "rafts" in live cells.

Due to the mis-partitioning of most fluorescent lipid analogs in model membranes, the justification of using GUVs as model systems and fluorescent lipid analogs as probes of heterogeneous membrane organization *in vivo* has been challenged. In this report, we extend previous observations and perform a systematic comparison of phase partitioning, diffusion and binding characteristics of a multitude of differently labeled and either commercially available or specifically synthesized raft lipid analogs in cellular and model membranes. We compare phase partitioning in fully synthetic GUVs and cell-derived GPMVs, and relate it to nanoscopic diffusion characteristics in the plasma membrane of living cells as measured by STED-FCS. We also study the influence of tagging the ganglioside GM1 with an organic dye on its ability to bind its native ligand, cholera toxin B (CTxB). We show that many of the fluorescent raft lipid probes partition to the raft-mimetic ordered phase in GPMVs, in contrast to GUVs. Moreover, we show that binding of GM1 to CTxB changes dramatically upon labeling. Finally, our data show that phase association of raft lipid analogs in model membranes does not correlate with confined diffusion measured by STED-FCS which points that the heterogeneity in living cell membrane is much more complex than two phase partitioning in model membranes.

9.2. Materials and Methods

GUVs and GPMVs were prepared as described in Section 6.2.3 and Section 6.2.4 respectively. Confocal Microscopy was carried out as described in Section 6.2.6. C-Laurdan measurements were done as described in Section 5.9.

9.2.1. Fluorescent probes

We labeled sphingomyelin (SM) and the ganglioside GM1 either at the headgroup (H) or at the water-lipid interface by replacing the native long acyl chain with a short acyl chain carrying the dye (AC) with different dyes: NBD, TopFluor (TF), Bodipy-FL (BD-FL), Bodipy-TMR (BD-TMR), Atto532, Atto647N and KK114 [213]. TF-SM and NBD-C12-SM were purchased from Avanti Polar Lipids (AL, USA) and BD-FL labeled SM and GM1 and NBD-C6-SM from Invitrogen (CA, USA). NBD-C6-GM1 and the Atto532, Atto647N and KK114 labeled lipid analogs were synthesized as outlined previously [15, 212–215]. The cholesterol analogs were purchased from Avanti (TF) or Invitrogen (BD-TMR). For the lipid dye structures refer to Appendix. Fast DiO, Fast DiI and DiD C18 were purchased from Invitrogen (CA, USA) and Alexa647 or Alexa555 labeled cholera toxin B (CTxB) from Sigma-Aldrich (MO, USA). C-Laurdan was a gift from Dr. B. R. Cho (Seoul, Korea).

9.2.2. Determination of Lo partitioning and lipid analog brightness

We determined the fraction of lipid analogs partitioning into the Lo phase from intensity line profiles of confocal images Figure 9.1 using ImageJ-Line profile, as described [124]. The fluorescence intensities of the Lo and Ld phase, F_{Lo} and F_{Ld} respectively, were determined from the peaks of the line scan, where the different phases were identified by the Ld phase markers Fast DiO, Fast DiI or DiD. Opposite sides experienced the same polarization of the exciting lasers and were thus chosen to eliminate any bias in fluorescence intensity due to differences in laser excitation efficiency. The background values obtained from the pixels outside the vesicles were subtracted from peak values. The Lo-partitioning coefficient (%Lo) is then;

$$Lo\% = \frac{F_{Lo}}{F_{Lo} + F_{Ld}} \quad (9.1)$$

This relationship would not hold if the molecular brightness (cpp, counts per particle) of a given analog was dependent on the membrane environment, i.e. if the fluorescent yield was different in the two phases. For all the lipid analogs tested, we performed FCS in pure Lo (DOPC/BSM/Chol (10:50:40)) and pure Ld (DOPC/BSM/Chol (80:10:10)) GUVs to measure the brightness of particles in each phase (cpp_{Lo} and cpp_{Ld}) (Figure 9.2). These compositions are representative of the coexisting phases in the DOPC/BSM/Chol (2:2:1) GUVs used for the partitioning experiments and were estimated using published phase diagrams and tie lines [216]. FCS experiments were carried out as described previously [88]. Briefly, the focal spot was placed either on the top or bottom of the GUVs

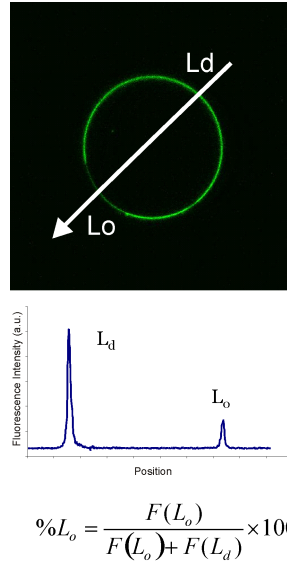


Figure 9.1. Calculation of Lo% using intensity profiles through scanning confocal fluorescence images. Representative scanning confocal fluorescence images of phase separated vesicles incorporating a fluorescent lipid analog (upper panel) and an intensity profile (lower panel) along the line marked in the upper panel. The distribution of these molecules is revealed by the fluorescence intensity (green). The fluorescence intensities of the Lo and Ld phase, $F(L_o)$ and $F(L_d)$ respectively, were determined from the peaks of the line scan, where the different phases were identified by the Ld phase markers DiO, DiI or DiD (fluorescence of these markers not shown). Opposite sides experienced the same polarization of the exciting lasers and were thus chosen to eliminate any bias in fluorescence intensity due to differences in laser excitation efficiency. The ratio of F_{L_o} and F_{L_d} allow calculating the Lo partitioning coefficient Lo% as shown in the equation. The Lo% values of >10 vesicles were used to get an average Lo% value for a lipid analog.

with the optical settings kept the same for Lo and Ld vesicle measurements. Brightness values were obtained by fitting the autocorrelation curves with a two-dimensional one-component diffusion model;

$$G(\tau) = \frac{1}{N} \left(1 + \frac{\tau}{\tau_D}\right)^{-1} \quad (9.2)$$

Normalized Lo partitioning values ($(Lo\%)_n$) were then calculated accounting for the relative brightness of the lipid analogs in two phases;

$$Lo\%_n = \frac{Lo\% \times (cpp_{Ld}/cpp_{Lo})}{Lo\% \times (cpp_{Ld}/cpp_{Lo}) + (100 - Lo\%)} \quad (9.3)$$

9.2.3. STED-FCS measurements

STED-FCS data were recorded on a microscope outlined previously in detail [15, 212, 217]. Briefly, pulsed diode lasers at 633 nm (≈ 80 ps pulse width, LDH-P-635, PicoQuant,

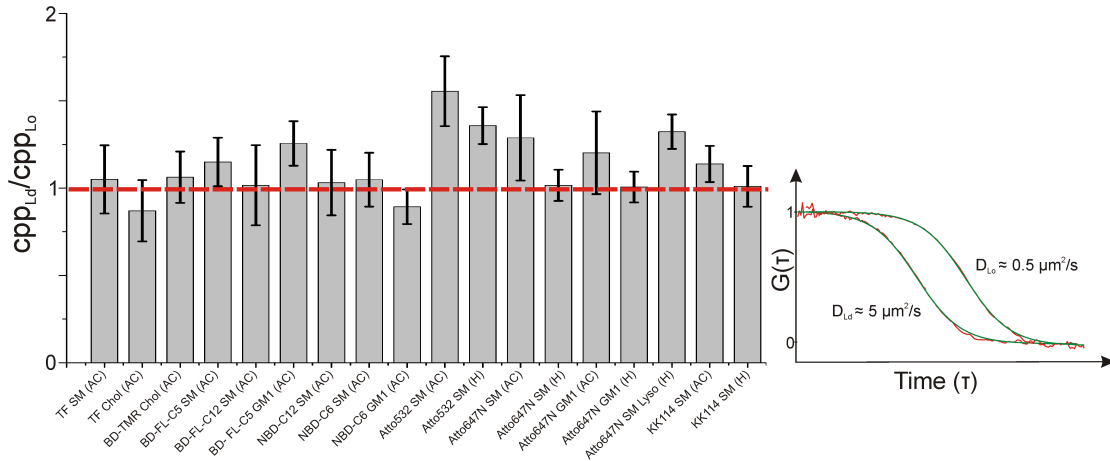


Figure 9.2. Brightness of the lipid analogs.

Berlin, Germany) or at 532 nm (≈ 80 ps pulse width, Pico-TA 532, PicoQuant) were used for excitation of Atto647N or KK114 and Atto532 fluorescence, respectively, and the STED beams were provided by a Titanium:Sapphire laser system (MaiTai, Spectra-Physics, Mountain View, CA, USA) operating at 770-780 nm with a repetition rate of 76 MHz, either directly for Atto647N or KK114 and at 612 nm for Atto532 by an optical parametric oscillator (APE, Berlin, Germany) fed by the same Titanium:Sapphire laser system. Fluorescence excitation and collection was realized using an oil immersion objective (PLAPON 60X, NA = 1.42, Olympus, Japan; or HCXPLAPO NA = 1.4, Leica Microsystems). The 50:50 split fluorescence signal was detected by two single-photon counting modules (avalanche photo diode SPCM-AQR-13-FC, Perkin Elmer Optoelectronics, Fremont, CA, USA) and the recorded fluorescence counts were further processed by a hardware correlator card (Flex02-01D, Correlator.com, NJ, USA). Mammalian PtK2 cells were prepared, and incorporation of the lipids into the plasma membrane via a BSA-lipid complex was performed as previously described [15, 217]. STED-FCS measurements were performed at room temperature by placing the foci on random positions in the lower plasma membrane facing the coverslip, and by completing all measurements before significant internalization or any morphological changes in the cell could take place. The measurement times were kept short (≈ 15 s) to avoid biasing distortion of the correlation data due to very infrequent transits of bright particles such as cell debris [15, 217]. Fitting of the FCS data was performed by using a two-dimensional diffusion model assuming a Gaussian-shaped fluorescence detection profile.

$$G(t_c) = 1 + (1/N)(1 + (t_c/\tau_D)^\alpha)^{-1} \quad (9.4)$$

Here, $\tau_D = d^2/(8\ln 2D)$ denotes the average transit time through the focal spot of diameter (or full-width-at-half-maximum) d , D the apparent diffusion coefficient and α the anomaly coefficient, which is = 1 for normal free Brownian diffusion and < 1 for heterogeneous diffusion, for example, due to trapping. Additional terms due to dark (triplet) state populations were regarded as detailed in references [15, 217].

9.3. Results and Discussion

9.3.1. Partitioning in GUVs

GUVs composed of DOPC/BSM/Chol (2:2:1) displayed separation into an Ld and an Lo phase at room temperature, revealed by a heterogeneous distribution of the dyes Fast DiO, Fast DiI or DiD-C18 (Figure 9.3A). All of these dyes are known to incorporate into the membrane and specifically mark the Ld phase [199]. This domain assignment was confirmed by Generalized Polarization (GP) experiments using the membrane marker C-Laurdan: the Lo phase is characterized by relatively high GP values, compared to the Ld phase [29] (Figure 9.3C). We determined the Lo partitioning (%Lo) of various fluorescent analogs of sphingomyelin (SM), GM1 and cholesterol (Chol), which were either labeled with the dye NBD, TopFluor (TF), Bodipy-FL (BD-FL), Bodipy-TMR (BD-TMR), Atto532, Atto647N or KK114, from intensity line profiles of scanning confocal fluorescence images (Figure 9.1 and Figure 9.3). The fluorescent raft lipid analogs were either labeled on the headgroup (H) or by replacement of the native acyl chain with a short acyl chain carrying the dye (AC) (for structures see Appendix). Non-labeled SM, GM1, and cholesterol would be predicted to enrich in the Lo phase based on their preference for raft domains in live cells, as assayed by detergent resistance [218]. The orientation of the tie lines in tertiary mixtures confirms this assumption for SM, and to a much smaller extent, cholesterol [130]. Lo enrichment of GM1 is predicted by binding of its ligand cholera toxin [218]. Based on this information, deviation from Lo preference for SM, GM1, and cholesterol analogs can be attributed to the influence of the label.

Figure 9.3A (upper panel) shows representative fluorescence scanning images of a GUV incorporating the dye DiD and a SM analog (BD-FL C12 SM). This analog preferentially partitions into the phase marked by DiD, i.e., the Ld phase. Using the procedure described in Equations 9.1 and 9.3, we determined %Lo \approx 30%. Table in Appendix lists the %Lo values for all fluorescent raft analogs tested here. 17 of the 18 analogs tested (TF-Chol excepted) were enriched in the disordered phase (%Lo $<$ 50%) in GUVs, in agreement with previous observations for other lipid analogs [60–62, 66, 68, 206, 208, 214, 219]. The mis-partitioning of raft analogs labeled by acyl chain replacement (AC) is expected, because the addition of the bulky fluorescent side-chain may change the packing abilities

of the lipid. In the case of headgroup labeling, mis-partitioning may be explained by a label-induced change of the headgroup conformation and/or by the dye label tilting towards the membrane, again introducing a steric hindrance. This can be explained by a label-induced change of the headgroup conformation and/or by the dye label tilting towards the membrane, again introducing a steric hindrance.

9.3.2. Differential partitioning of lipid analogs in GUVs and GPMVs

GPMVs derived from RBL cells showed phase separation similar to that of GUVs (Figure 9.3A bottom). However, nearly all analogs were much more ordered phase preferring in GPMVs ($\%Lo(GPMV) > \%Lo(GUV)$, Figure 9.3B) regardless of the chemical preparation used to derive the vesicles (i.e. PFA/DTT or NEM; all data shown is from PFA/DTT GPMVs). This model system-dependent partitioning is likely due to the difference in order/packing of the lipids in the coexisting phases of the GUVs compared to GPMVs [9, 35, 220]. Similar to previous reports [34], we used C-Laurdan microscopy to measure the molecular packing (and thus order) of the Ld and Lo phases in the vesicles (Figure 9.3C). In the DOPC/BSM/Chol GUVs, the Ld phase was much more disordered, and the Lo phase much more ordered, than in the GPMVs. Consequently, the order difference between the coexisting phases was much larger for these GUVs than for the GPMVs (as observed in previous experiments [34]), likely amplifying the inherent disorder preference of many lipid analogs in the case of the GUVs. The quite small order difference between domains in GPMVs is presumably due to its complex lipid and protein content, likely resulting in a more biologically appropriate molecular partitioning than modeled in GUVs.

9.3.3. Label size, hydrophobicity, and position affect analog partitioning

Having determined that GPMVs seem to provide a more physiological system to measure lipid analog partitioning between coexisting liquid phases, we attempted to determine the dependence of this partitioning on specific structural factors such as label type, label position, and lipid headgroup. Lo partitioning of SM was in general lowest for the most bulky and charged dye labels Atto647N, KK114 and Atto532 ($\%Lo$ values down to $< 2\%$ and $< 4\%$ in GUVs and GPMVs, respectively - Atto647N is positively charged and KK114 and Atto532 have a negative net charge) and highest for the smaller and uncharged dye labels NBD, TF and BD-FL ($\%Lo$ up to 65% in GPMVs; TF and BD-FL are zwitterionic with a very small charge separation). Therefore, it seems that it is advantageous to use smaller and uncharged dye labels. In agreement with this conclusion, a lipid labeled with an uncharged NileRed derivative has previously been shown to be Lo preferring [221] (this derivative did not represent a functional lipid,

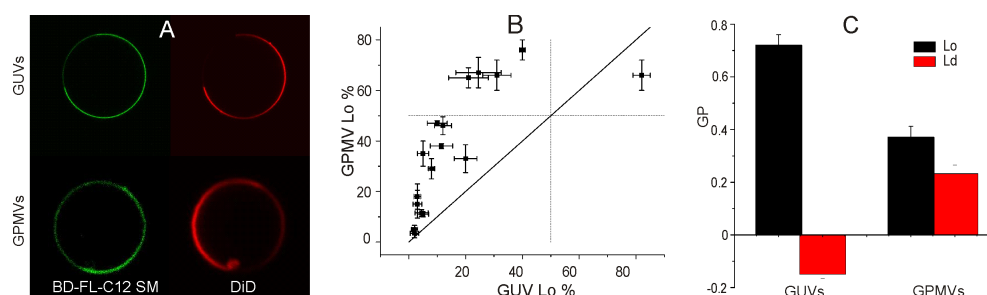


Figure 9.3. Phase partitioning of fluorescent raft lipid analogs in GUVs and GPMVs. (A) Representative scanning confocal fluorescence images of phase separated GUVs and GPMVs stained with BD-FL-C12 SM and the Ld-phase marker DiD. The distribution of both molecules is revealed by the respective fluorescence intensities (green: BD-FL-C12 SM, red: DiD) and the %Lo values determined from the intensity ratios along the line profiles as shown in Figure 9.1. BD-FL-C12 SM prefers the Ld phase in GUVs (%Lo \approx 30%) and the Lo phase in GPMVs (%Lo = 65%). (B) Correlative plot of %Lo determined for the 18 different raft lipid analogs in GUVs and GPMVs. Most analogs prefer the Ld phase (%Lo < 50%, dashed lines) in GUVs; this mis-partitioning is less pronounced in GPMVs. (C) GP values of Ld (red columns) and Lo (black columns) domains in GUVs and GPMVs quantified by C-Laurdan microscopy. Larger GP values are indicative of higher molecular packing/order. Absolute ordering and the difference in order between phases is much more pronounced in GUVs than in GPMVs. Error bars represent standard deviations of the respective values determined from >10 vesicles/sample.

such as a sphingolipid). Label steric size and charge are not the only determinants of partitioning, since SM labeled with the smallest and completely uncharged moiety NBD was less Lo preferring (%Lo < 50% in GPMVs) than slightly larger and zwitterionic analogs (TF and Bodipy). This effect may be attributed to the hydrophilic nature of NBD, which is evidenced by the relatively poor integration of NBD-labeled lipids into membranes [15]. Further, NBD-labeled lipid analogs have been shown to partition to the hydrophobic/hydrophilic interface of the membrane [222], thereby disrupting the local packing of the membrane. However, this effect cannot be generalized since NBD-labeled GM1 prefers the ordered phase (see Appendix). Moreover, hydrophobicity of the dye does not completely determine Lo preference: the most hydrophobic label of all (Atto647N) drives SM into the disordered phase, while the same lipid labeled with the similarly bulky but very hydrophilic dye Atto532 (shown to be hardly membrane anchored [15]) was much more Lo preferring (%Lo in GPMVs nearly 50%). Using the Atto647N, KK114 and Atto532 labeled SM and GM1 derivatives, we studied the influence of the dye position (acyl chain replacement (AC) versus headgroup attachment (H)) on the phase affiliation. The position had no observable influence for Atto532- and Atto647N-SM (even when comparing it to the headgroup labeled Lyso derivative): Lo partitioning was always low. However, headgroup-labeling slightly improved the Lo affinity for Atto647N-GM1 and KK114-SM (up to 3-fold larger %Lo than for AC). Finally, we evaluated the effect of labeling at different positions on the acyl chain by comparing SM labeled with BD-FL and NBD at the end of a short versus a long acyl tail (C5 or C6 versus C12). In GUVs, the

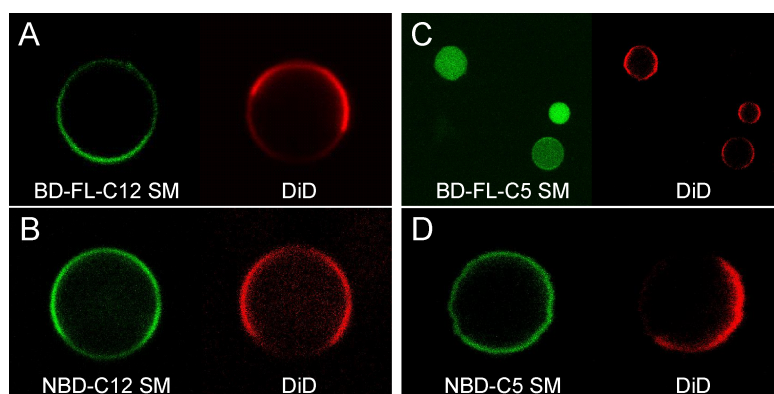


Figure 9.4. Phase partitioning of acyl-chain labeled SM depends on the dye label and linker length. Representative scanning confocal fluorescence images of phase separated GPMVs stained with the Ld marker DiD (red) and (A) BD-FL-C12 SM, (B) NBD-C12 SM, (C) BD-FL-C5 SM and (D) NBD-C6 SM (green). While BD-FL-C12 SM prefers the Lo phase (%Lo = 66%), NBD-C12 SM is slightly more Ld preferring (%Lo = 35%) and NBD-C5 SM is almost uniformly distributed (%Lo = 46%). BD-C5 SM penetrated through the membrane and completely internalized.

longer acyl chain (C12) derivative was slightly more Lo preferring for BD-FL but less for NBD. In GPMVs, C6 versus C12 had no significant effect on NBD (%Lo \approx 46% compared to 35%) but we observed a surprising behavior for the BD-FL-SM analogs (Figure 9.4): in contrast to the C12 derivative with a %Lo > 60%, the BD-FL-C5 analog penetrated through the GPMV membrane and accumulated inside the vesicles. We conclude that partitioning of a lipid analog is a complex combination of a multitude of factors, such as the polarity, size and charge of the label, the label position and headgroup size of the lipid, that influence the ability of the analog to be inserted into the more restrictive ordered phase. However, it seems that the use of small and uncharged dye tags is more likely to preserve ordered phase partitioning.

9.3.4. Labeling affects binding of GM1 to CTxB

The B subunit of cholera toxin (CTxB) is known to specifically bind to GM1, preferably in the ordered phase [123]. We therefore investigated how the mis-partitioning of fluorescently labeled GM1 influences its binding to CTxB. We labeled GPMVs derived from RBL cells with DiD (as a reference for the disordered phase) and GM1 with BD-FL at the end of a C5 acyl chain linker (BD-FL-C5 GM1 (AC)), then added Alexa555-labeled CTxB to determine the phase preference of the labeled CTxB from the simultaneously recorded multicolor confocal scanning images (Figure 9.5). BD-FL-C5 GM1 has a slight preference for the Lo phase (%Lo \approx 65%, Figure 9.3 and see Appendix). CTxB binding to GM1 was observed in both phases, with an unexpected enrichment in the disordered phase (Figure 9.5A); however, it was impossible to make a clear assignment for the binding to the labeled GM1, since the GPMVs derived from RBL cells contained native GM1

in addition to the exogenous GM1 analog. To isolate the effect of labeled GM1 from native GM1, we measured CTxB binding to GPMVs isolated from a Chinese Hamster Ovary subtype (CHO-K1) that does not produce complex gangliosides [223]. In the absence of exogenous GM1, CTxB did not bind to these vesicles, consistent with their lack of native GM1 (data not shown). When labeled GM1 was added to these CHO-K1 derived GPMVs, we observed partitioning of BD-FL-C5 GM1 similar to RBL GPMVs (%Lo = 66%). However, while there was still weak binding of CTxB to Lo phase in RBL GPMVs presumably due to the native GM1, we observed a very selective binding of CTxB to the Ld phase and no Lo binding in CHO GPMVs (Figure 9.5B). Thus, since labeled GM1 is present in both phases while CTxB signal is only observed in the Ld phase, CTxB can only bind the Ld, but not the Lo pool of BD-FL-C5 GM1. All of these results were the same when using Alexa647 instead of Alexa555 as a label for CTxB. To confirm this conclusion in a controlled system, we produced GUVs containing only labeled GM1, or both labeled and unlabeled GM1, and determined the phase preference of CTxB binding (Figure 9.5C-E). In GUVs (with or without native GM1), the labeled GM1 mainly partitioned into the Ld phase with 20% of the molecules entering the Lo phase. In presence of native GM1, CTxB bound highly preferentially to the Lo domain (Figure 9.5C), consistent with partitioning of its native ganglioside receptor to the ordered phase. When only labeled GM1 was included in the GUVs, CTxB bound exclusively to the Ld domain, despite the presence of BD-FL-C5 GM1 in the ordered phase (Figure 9.5D and green line in Figure 9.5F). Thus, the addition of the fluorescent dye label to the ganglioside GM1 acyl chain not only affects the phase partitioning of the lipid, but also impairs the binding of ligand to its head group. We speculate that for the labeled GM1, the conformation of the polar headgroup is different in the Lo than in the Ld phase. The headgroup may be tilted in the Lo phase [224, 225], accounting for the perturbed binding. CTxB cooperatively binds up five GM1 lipids and this multivalency may be disturbed in case of the altered conformation. Most importantly, this effect demonstrates that bulk membrane properties (in this case, the ordering or molecular packing) have an effect on the interaction of a ligand with its membrane-bound lipid receptor in biologically-complex environments which will be discussed in the following chapter.

9.3.5. Partitioning of lipid analogs is uncorrelated with its nanoscale diffusion in living cells

Several novel imaging methods have recently been developed to probe live cells at spatial resolutions well below the limit imposed by diffraction. These methods can reveal nanometer-scale structures on the order of the proposed spatiotemporal scales of lipid

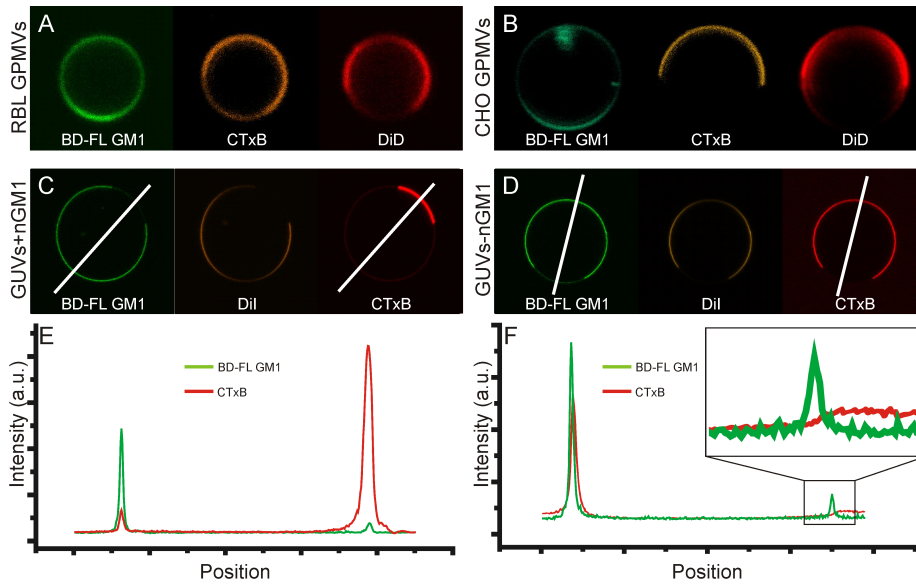


Figure 9.5. Phase specific binding of GM1 to CTxB. Representative scanning confocal fluorescence images of phase separated GPMVs (A,B) and GUVs (C,D) stained with BD-FL-C5 GM1 (green), Alexa555 labeled CTxB (orange) and the disorder marker DiI (red) along with (E) intensity profile along the lines marked in (D) for BD-FL-C5 and CTxB. In GPMVs (A,B), the labeled GM1 partitions in Lo phase (%Lo \approx 65%). In RBL-cell derived GPMVs (A), which contain native GM1, CTxB binds both phases, while in CHO-K1-cell derived GPMVs (B), which lack native GM1, CTxB binds exclusively to the Ld phase. In GUVs containing both labeled and native GM1 (C, GUVs+nGM1), CTxB is highly enriched in the Lo phase (presumably containing the native GM1) with some Ld binding (presumably to the labeled GM1, intensity line profile in E). In GUVs lacking native GM1 and having only BD-FL-C5 GM1 (D, GUVs-nGM1), CTxB exclusively binds to the Ld domain. As a consequence, while CTxB binds unlabeled GM1 in the Lo phase, it binds labeled GM1 only in the Ld phase.

rafts. We used the combination of STED nanoscopy [51, 54, 211] and FCS, STED-FCS [15, 217], to determine the affinity of several of the previously mentioned fluorescent lipid analogs to transient nanoscale complexes previously observed in the plasma membrane of living cells [15, 212]. A great advantage of the STED method is the ability to continuously tune the size of the effective focal spot through which lipid molecules may diffuse, from diffraction-limited $d = 240$ nm (or 180 nm depending on the excitation wavelength) down to molecular scales, and to determine their average transit times τ_D using FCS, as shown in Figure 9.6A. While freely diffusing molecules show a linear dependence of the focal transit time τ_D on the focal area ($\approx d^2$), transient trapping leads to relatively increased values of τ_D for smaller focal spots [226]. This is because the focal spot size becomes adequately small to ensure that the time of trapping sufficiently exceeds the focal dwelling time of free diffusion [15]. As a consequence, the description of the FCS data of such heterogeneous diffusion has to include an anomaly coefficient $\alpha < 1$ (Equation 9.4). Figure 9.6A depicts exemplary STED-FCS data of several fluorescent SM and GM1 lipid analogs, which all congruently showed the mentioned characteristic behavior

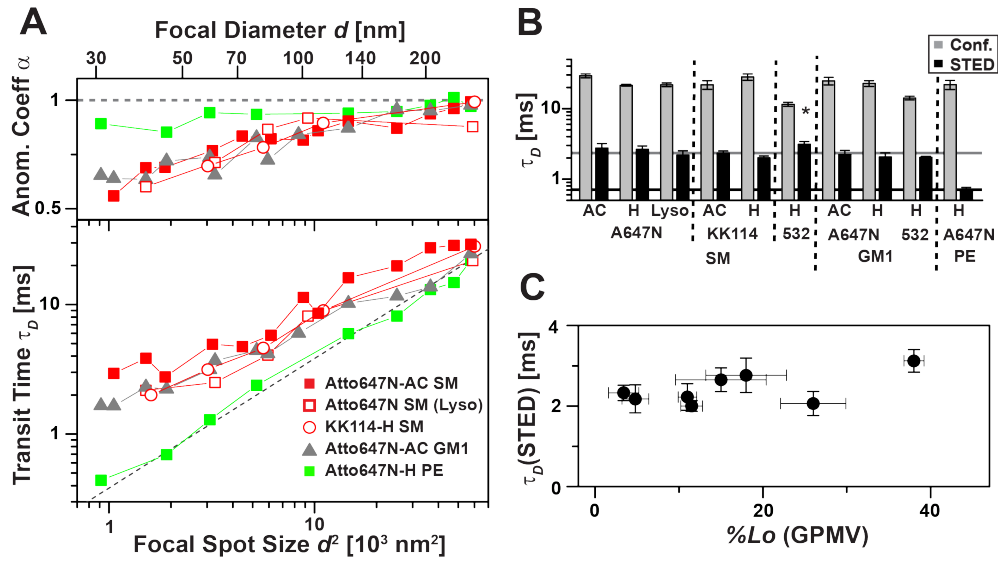


Figure 9.6. STED-FCS measurements of fluorescent raft lipid analogs in the plasma membrane of living cells and comparison to phase partitioning. (A) Anomaly coefficient α and average transit time τ_D for different fluorescent SM and GM1 lipids and for a fluorescent PE lipid determined by fitting Eq. 4 to the FCS data recorded for different focal spots tuned by STED. An anomaly coefficient $\alpha=1$ and a linear dependence of τ_D on the focal spot size (proportional diameter-squared d^2) indicated free diffusion (dotted line, diffusion coefficient $D = 0.45 \mu\text{m}^2/\text{s}$), while $\alpha < 1$ and a deviation of τ_D towards larger values for small focal spots indicated transient trapping events. (B) Average transit time τ_D of different fluorescent SM, GM1 and PE lipid analogs for confocal ($d \approx 240 \text{ nm}$ or $\approx 180 \text{ nm}$, grey columns) and STED recordings ($d \approx 40 \text{ nm}$, black columns). The SM and GM1 analogs showed increased transit times τ_D for the STED recordings indicating trapping (grey line) while a PE analog and the SM analog labeled at the acyl chain with the very hydrophilic dye Atto532 (532 AC) showed a low τ_D in accordance with almost free diffusion (black line). The confocal recordings failed to report this difference. Values and error bars represent the average and the standard deviation of the mean from at least 30 measurements on different spots of different cells ($A = \text{Atto}$). (C) Nanoscale trapping as probed by STED-FCS and phase partitioning are uncorrelated: Comparison of transit times (STED-FCS, $d \approx 40 \text{ nm}$) and Lo partitioning coefficient %Lo in GPMVs (see Appendix) for the lipids presented in B (red dot: Atto532-SM (AC)).

for transient trapping, while an Atto647N labeled phosphoethanolamine (PE) exhibited the characteristic linear dependence of τ_D on d^2 and $\alpha \approx 1$ of close to free diffusion. Screening of several differently labeled SM and GM1 molecules showed no dependence of their dynamical and trapping characteristics on the dye and its position (Figure 9.6B), indicating a negligible influence of the dye. We only investigated the lipid analogs labeled with Atto647N, KK114 and Atto532 with STED-FCS, because the absorption and emission spectrum of these dyes were the only ones that suited the present STED-FCS setups.

All SM and GM1 analogs used for STED-FCS were Ld-preferring in both GUVs and GPMVs with a significant variety in quantitative partitioning values (see Appendix, %Lo of 2 - 50%). This variable partitioning was in striking contrast to the parity of diffusion behavior observed for the very same dyes with STED-FCS (Figure 9.6B). Indeed, no

quantitative correlation between these two parameters could be discerned (Figure 9.6C). Most strikingly, SM labeled at the acyl chain with the very hydrophilic dye Atto532 (Atto532 SM (AC)) showed the largest Lo affinity of all lipid analogs investigated by STED-FCS (%Lo(GPMV) = 47%), but its diffusion characteristics was strongly biased in the plasma membrane of intact living cells: diffusion of Atto532 SM (AC) was much faster than for the other SM analogs and trapping was almost abolished, probably due to its high polarity and the resulting weak membrane anchoring of the analog (Figure 9.6B,C). These results suggest a different physical nature for the nanoscale trapping observed in intact living cells using STED-FCS and phase partitioning in isolated phase-separated plasma membrane.

9.4. Conclusion

To better understand the behavior of widely used fluorescent lipid analogs [68, 205], this study systematically investigates the partitioning of a multitude of fluorescent cholesterol, SM and GM1 analogs in two different model systems (fully synthetic GUVs and cell-derived GPMVs), and relates it to their nanoscale dynamics in intact cellular plasma membranes. Our results reveal: (i) In agreement with several previous observations [65, 67, 68, 202, 205–208], most fluorescently labeled analogs of raft lipids do not partition into ordered phases, in contrast to their native counterparts. (ii) The partitioning of a lipid analog is a complex function of type, size, polarity, charge and position of the dye tag, with a tendency of smaller and uncharged dye tags more likely preserving ordered phase partitioning. (iii) Labeling may not only affect the phase preference of a lipid, but also directly modulates its biological activity in a phase-specific manner, as shown for the CTxB-GM1 interaction. While CTxB preferably binds unlabeled GM1 in the Lo phase, the binding affinity between acyl-chain labeled GM1 and CTxB is higher in the Ld phase. (iv) Mis-partitioning of raft lipid analogs is much less pronounced in cell-derived GPMVs than in DOPC/BSM/Chol GUVs, suggesting that GPMVs are more appropriate models for biological systems. In spite of their value for studying membrane phase separation in general, commonly used DOPC/SM/Chol GUVs appear to be rather problematic models to mimic the cell membrane heterogeneity, not only because of their limited complexity, but due to the seemingly quite different physical nature of the domains. (v) Nanoscale diffusion and trapping of fluorescent raft lipids in the plasma membrane of intact living cells as observed by STED-FCS and phase partitioning in model membranes are uncorrelated, i.e., STED-FCS may be probing a property of the membrane that is not related to phase separation in GUVs and GPMVs.

It is important to point out that both model membrane systems are likely in a state of thermodynamic equilibrium, while the plasma membrane of living cells is dynamic

and non-equilibrated. Interactions in a dynamic and un-equilibrated system such as the plasma membrane of intact living cells, may be destroyed in GPMVs by the absence of some important cellular structures, such as the cytoskeleton and/or by equilibrating the system as, for example, done by reducing the temperature [227–229]. As a consequence, as already discussed for the difference between GUVs and GPMVs, the difference in order (or other physical properties) between lipid domains in living, non-equilibrated cellular membranes may be smaller than of any currently available model system. It is important to stress that although phase coexistence in lipid model systems is often viewed as an analog of raft behavior in the cell membrane, it may not necessarily be accurate to assign the "native behavior" of a lipid analog based on its partitioning in these systems. As we have shown, probe geometry and chemistry are important factors for the partitioning behavior of lipid analogs, while their confined diffusion in intact living cells indicates that the chemistry behind the confining interactions is unaffected by labeling. Most likely, in intact living cells, STED-FCS has probed the formation of transient, chemically specific interactions between raft lipids and other membrane constituents (such as other lipids and proteins) that may comprise the physicochemical basis of lipid-protein platforms. Lo-preferring fluorescent raft analogs are then used observe the coalesced (i.e., large, long-lived, equilibrium domains) state of these platforms. Taking these results into consideration, we will ask the question in the next chapter: how could the cell membrane heterogeneity in living cell be?

Continuously Variable Lipid Packing

Here, we present a new concept for the cell membrane lateral heterogeneity, continuously variable lipid packing. We propose that cell membrane does not simply have one kind of raft and non-raft domain. Instead, there are several types of rafts and non-rafts each having different lipid packing which modulates the orientation of membrane molecules, thus their activity.

10.1. Introduction

Since the introduction of the raft concept which proposes a heterogeneous structure of the cell membrane [7, 200], many processes taking place at the cell membrane were linked to these nano-entities [230, 231, 231–235]. Although having such an practical impact on the membrane field, the physicochemical nature of this heterogeneity is still controversial. Rafts have been studied extensively by detergent resistance assay [126] for a long time. This method yields a detergent-soluble and detergent insoluble fractions of the membrane. Thus, it was long assumed that there were only two distinct lipidic states of the membrane, raft (detergent-resistant fraction) and non-raft (detergent soluble fraction). Rafts were also mimicked by the liquid-liquid phase coexistence in the model membranes. A liquid ordered (Lo) phase is formed when saturated lipids and sterols condense which separates from an unsaturated lipid-enriched liquid disordered (Ld) phase. Similarly, this system also supported the idea of binary states of membrane (i.e., single kind of raft and non-raft). However as mentioned in Chapter 9, the cellular membrane heterogeneity is well beyond the two-phases observed in model membranes. This has been supported by a few recent reports [17, 18, 34, 236]. First, it was shown that the coexisting phases in three component phase separated Giant Unilamellar Vesicles (GUVs) and cell derived Giant Plasma Membrane Vesicles (GPMVs) are dramatically different [34] and this difference is biologically functional [106]. Later, it was found that the lipid packing of ordered and disordered phases in GPMVs can be tuned [17]. This finding triggered the discussion on the existence of multiple states of the cell membrane. Recently, this idea was supported with laurdan generalized fluctuation analysis showing that there could be multiple entities in the cell membrane having different lipid packing and size [18].

Here, we propose a new concept for the cellular membrane heterogeneity, continuously variable lipid packing which suggests that there are multiple raft and non-raft domains in the cell membrane each having different lipid packing. In our study, we show that both GUVs and GPMVs have the ability to form domains with different lipid packing. This varying lipid packing is functionally important in receptor-ligand binding as it regulates the geometrical configuration of the molecules in the membrane. We showed that Cholera toxin binding to its lipid receptor GM1 is highly regulated by the lipid packing of the domains. Finally, we demonstrated that cells can regulate the plasma membrane lipid packing by different mechanisms. Taking previous studies with our new findings together, we believe that the continuously variable lipid packing is the principle of functional cell membrane heterogeneity.

10.2. Materials and Methods

GUVs and GPMVs were prepared as described in Section 6.2.3 and Section 6.2.4 respectively. Lo partitioning of the molecules were determined as described in Section 9.2.2. Confocal microscopy was carried out as in Section 6.2.6. Information about all lipid probes can be found in Section 9.2.1.

10.3. Results and Discussion

10.3.1. Order of phases can be tuned in GUVs and GPMVs

We prepared GUVs from various mixtures having different saturated/unsaturated components or different cholesterol amount (Figure 10.1) all of which showed phase separation at room temperature. We measured the lipid packing of ordered and disordered domains (Generalized Polarization(GP)) of the GUVs with C-Laurdan (see Chapter 3). We found out that as more cholesterol included in the lipid mixture GP value of ordered phase decreased, i.e., it became more disordered (Fig 10.1A). Moreover, the GP of disordered domain increased slightly with increasing cholesterol which confirms the idea that cholesterol adjusts the ordering of both phases. We also checked the effect of saturated component on lipid packing. Commonly used DOPC with a sphingomyelin yielded a very tightly packed Lo phase and very loosely packed Ld phase (Figure 10.1B). However, when sphingomyelin was replaced by DPPC, GP of the ordered phase decreased dramatically. When DOPC (a synthetic, double unsaturated lipid) is also replaced by Liver PC (LPC, a natural lipid extracted from liver), GP of disordered domain increased slightly. Having seen that the order of the domains can be tuned in GUVs by changing the composition, we next investigated the tunability of the packing of domains in GPMVs derived from CHO cells which was previously reported for RBL cells [17]. We found that varying the

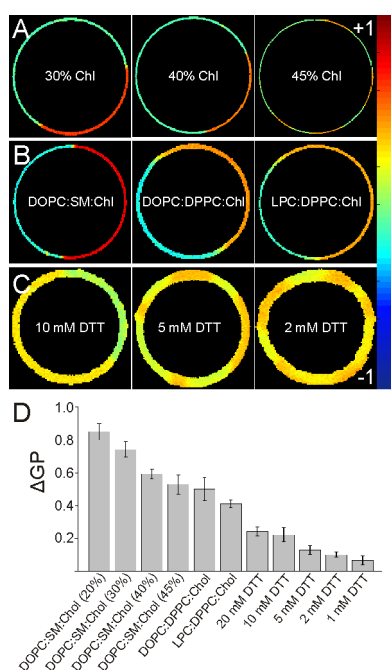


Figure 10.1. Laurdan images of the phases in GUVs and GPMVs which can be tuned. (A,B) Different mixtures in GUVs give different Lo and Ld phases having different lipid packing. Changing (A) cholesterol percentage (B) saturated or unsaturated components changes the lipid packing. (C) Preparation conditions changes the lipid packing in GPMVs. Changing DTT concentration in preparation changes the packing of the phases formed. (D) Lipid packing difference between Lo and Ld phases in different GUV and GPMVs shown in (A,B,C). Instead of having one kind of Lo and Ld phases, an order spectrum is obtained.

DTT concentration in preparation condition changes the lipid packing of the domains of CHO derived GPMVs presumably due to the depalmitoylation effect of DTT [124]. It is vital to highlight that the GP of GPMV domains are notably different than those of GUVs [106]. The ordered phase of the GPMVs are relatively disordered compared to GUV Lo domains. More importantly, disordered phase of the GPMVs are much more ordered than the Ld domains of any GUV mixture (Figure 10.1C). Figure 10.1D shows the lipid packing difference between Lo and Ld phases (ΔGP) of different GUV mixtures or GPMV preparations. It shows that the domains are variable in terms of lipid packing. Instead of a single Lo or Ld domain, there is a spectrum of ordered and disordered domains. Furthermore, as the system gets more biological (biological lipids (LPC) instead of synthetic ones (DOPC) or less DTT disturbance) the difference between ordered and disordered phases gets less pronounced.

10.3.2. Lipid packing affects the membrane related binding

Having obtained the spectrum of lipid packing, we investigated the effect of lipid packing on membrane related interactions. In order to do it, we have applied the phenomenon we

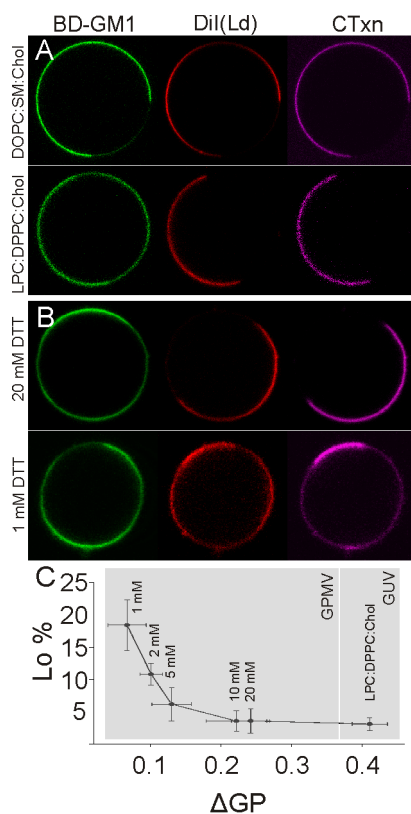


Figure 10.2. Effect of lipid packing on BD-GM1-CTxB binding. (A) CTxB does not recognize Lo pool of BD-GM1 in GUVs prepared from DOPC:SM:Chol and LPC:DPPC:Chol mixtures. (B) CTxB does not bind the Lo pool of BD-GM1 in GPMVs prepared with 20 mM DTT where ΔGP is around 0.24 while it starts recognizing the Lo phase in GPMVs prepared with 1 mM DTT which has a ΔGP of 0.07 (Figure 1). (C) CTxB-BD-GM1 binding is quantified by calculating the Lo percentage of CTxB. As ΔGP gets lower, BD-GM1 recognition of CTxB in ordered phase increases.

previously observed in the last chapter. In Chapter 9, we reported that Bodipy labeled ganglioside GM1 (BD-GM1) prefers the Ld phase in DOPC:SM:Chol vesicles however there is still a significant pool which prefers Lo phase (Lo% is 20 %). Interestingly, when cholera toxin (CTxB), bacterial ligand for GM1 added into the GUV suspension having BD-GM1, CTxB recognizes solely the Ld pool of BD-GM1 even though the environment is saturated with CTxB (see Figure 9.5). We investigated the recognition of BD-GM1 by CTxB on the continuously variable lipid packing spectrum we obtained. First, we tried to observe how this interaction is influenced in GUVs. Therefore, we have used two GUV systems, DOPC:SM:Chol (2:2:1) which has extremely ordered Lo and extremely disordered Ld phase (thus, a dramatic ΔGP (0.85)) and LPC:DPPC:Chol (2:2:1) which has a moderate ΔGP (0.43).

However, we did not observe any Lo binding in either cases (Figure 10.2A). Having shown that the lipid packing difference between ordered and disordered phases in GPMVs is much less pronounced than GUVs, we also tested this binding on GPMV. Moreover,

BD-GM1 partitions into Ld phase in GUVs which could be the reason of Ld binding of CTxB. However, as we reported previously BD-GM1 prefers Lo phase (Lo % of around 65 %) in GPMVs (Chapter 9, Appendix). We used two kinds of GPMVs, the ones prepared with 20 mM having ΔGP of 0.24 and 1 mM DTT having ΔGP of 0.07. The binding was observed exclusively in Ld phase in 20 mM DTT GPMVs although BD-GM1 was Lo enriched. It suggests that the binding is modulated by the lipid environment but not the probe concentration. Moreover, significant Lo binding was observed with 1 mM DTT GPMVs (Figure 10.2B) although BD-GM1 partitioning is almost the same in both preparations. In order to check if this effect is continuous, we prepared GPMVs with 10 mM, 5 mM and 2 mM DTT. We observed that after 5 mM DTT, the binding starts and continuously increases as DTT concentration decreases (Figure 10.2C). We postulate that lipid packing influences the geometry of the molecules embedded in the membrane so that their interactions driven by geometry (as in the example of CTxB-BD-GM1 or in most of receptor-ligand interactions [237]) could also be affected.

10.3.3. Lipid environment influences the geometry of membrane molecules

In order to understand how lipid packing influences the CTxB-BD-GM1 binding, we simulated this binding in two different lipid environments. Namely, DOPC environment which mimics the Ld phase and SM:Chol (1:1) mixture which mimics the Lo phase. We observed that the headgroup orientation is greatly affected by the lipid environment (Figure 10.3). As CTxB is a pentameric protein, geometrical fit is essential for its interaction with GM1 molecules. The freedom of movement in the Ld phase makes the molecules more flexible in term of their orientation. This increases the probability of interactions while the rigid structure in Lo phase constrains the movement of the molecules. If the optimal orientation is reached in this limited flexibility that the ordered phase allows, binding successfully happens. However, if the optimal orientation cannot be reached within the limited orientation flexibility, interaction could preferentially happen in Ld phase as there is more chance to get the optimal orientation in Ld phase.

When all the BD-GM1 molecules in Ld phase are bound by the CTxB and if the Lo phase orientation of BD-GM1 is still favoring the interaction even if it is weak, then excess CTxB should bind to the Lo phase BD-GM1. We tested this hypothesis experimentally by adding a gradient of CTxB to the GUVs (DOPC:SM:Chol and LPC:DPPC:Chol) and GPMVs (20 mM and 1 mM DTT preparations) doped with the same amount of BD-GM1 (Figure 10.4). At low amount of CTxB, it bound to only the Ld pool of BD-GM1 in GUVs as there is a dramatic order difference between Lo and Ld phases in both GUV systems. However at a high concentration we observed also Lo binding of CTxB on LPC:DPPC:Chol GUVs while there was still only Ld binding in DOPC:SM:Chol

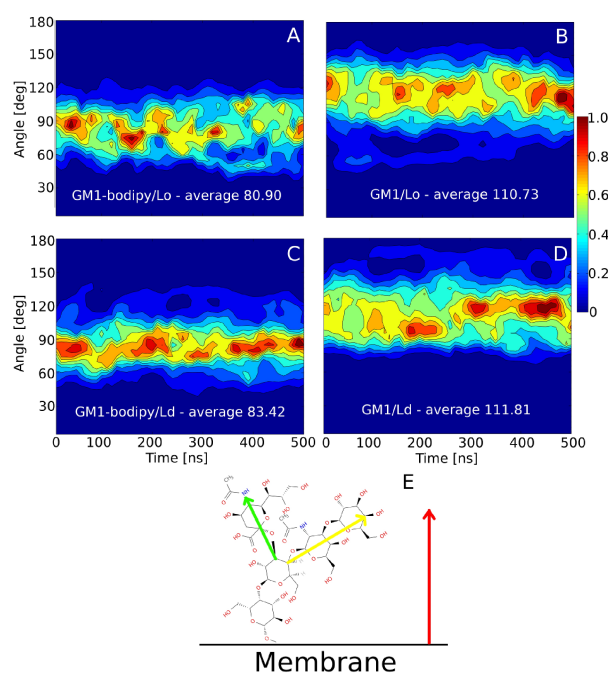


Figure 10.3. Probability of angle between membrane normal and plane of GM1 headgroup “thumb” in time as schematically shown in panel (E) angle between green and red vectors. (A) Lo system with GM1-bodipy, (B) Lo system with native GM1, (C) Ld system with native GM1-bodipy, (D) Lo system with native GM1. Angle between “forefinger” and membrane normal – angle between yellow and red arrows in panel (E) does not show differences between membranes.

GUVs. We attribute this difference to the large ΔGP difference between two systems. In GPMVs, a situation was observed. There was no Lo binding of CTxB in 20 mM DTT GPMVs at very low concentration of CTxB (see Figure 10.2). The Lo binding started at moderate concentrations and increased with increasing CTxB concentration. In 1 mM DTT GPMVs, there was already binding at very low concentrations due to the very small ΔGP between Lo and Ld phases as discussed earlier (See Figure 10.2). It increased gradually as the amount of CTxB increased. This confirms the hypothesis that CTxB binds Ld pool of BD-GM1 preferentially, but when all BD-GM1 molecules in disordered phase are occupied with CTxB, it binds the Lo phase BD-GM1 only if the configuration allows the binding (presumably it does not allow in DOPC:SM:Chol GUVs, thus, no interaction was observed in these vesicles even if the environment was saturated with CTxB).

10.3.4. Cells can tune their lipid packing

Although the lipid packing can be tuned in model membrane systems (Figure 10.1), it is crucial to know whether/how living cells can modulate their lipid packing upon cellular processes. In order to check whether the lipid order of the cell membrane is changed by

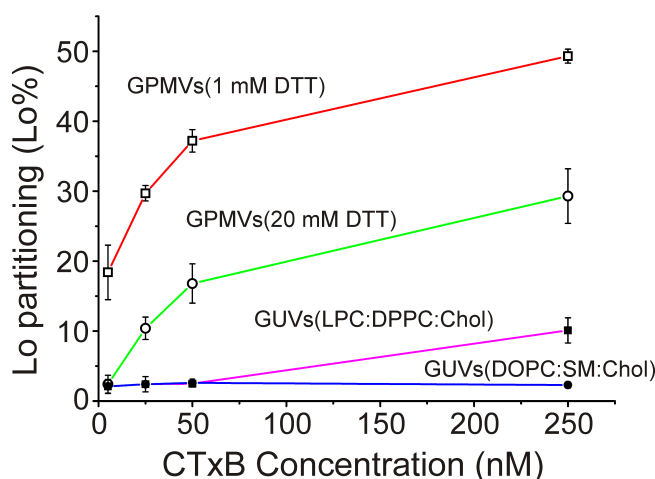


Figure 10.4. CTxB Lo binding with concentration gradient.

certain membrane event, such as endocytosis and exocytosis, we used insuloma cells (Ins1) secreting insulin upon glucose stimulation. We checked the plasma membrane packing upon time course high glucose stimulation by preparing GPMVs from stimulated cells at different time points. We observed that short after the stimulation by high glucose, the GP value of the cell membrane increases (Figure 10.5). After 20 min of stimulation, GP value started decreasing. We attribute the first increase of the GP value to secretory insulin granule exocytosis while the later decrease is presumably due to the re-endocytosis of the granular membrane. As a second environmental factor, we tested the temperature effect on membrane lipid packing. We grew cells in their normal conditions (37 °C) for 2 days. Then, we moved one group of cells to 25 °C and kept another group as control at 37 °C. After 20 hours of incubation, we prepared GPMVs and checked the lipid packing. We observed that the membrane of the cells grown in 25 °C is dramatically more disordered than that of the ones grown in 37 °C. This is presumably due to the fact that cells try to keep the membrane order homeostasis. Therefore, when temperature decreases which thermodynamically makes membrane more ordered, cells react this to make their membrane more disordered. As we prepared the GPMVs and carried out the lipid packing measurements under the same conditions, we observed such a contrast.

10.4. Conclusion

Although it is known that there is a functional heterogeneity in the cell membrane, the details about this heterogeneity are not fully clear. Here, we propose a new principle, continuously variable lipid packing. In this work, we showed that the lipid packing in model and cellular membrane can be altered by lipid/protein composition of the membrane. Therefore, instead of a single order and disorder domain, we obtained a spectrum

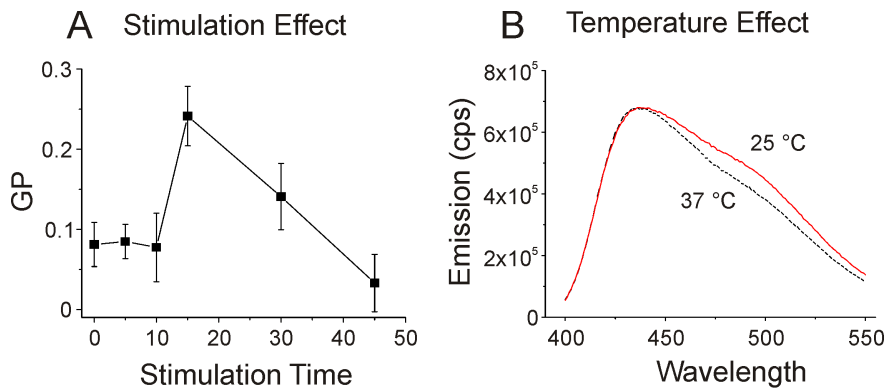


Figure 10.5. Cells can react their environment by changing their membrane lipid packing. The order of the Ins1 cell membrane changes with (A) glucose stimulation (B) varying growth temperature.

of lipid packings for both phases. We also observed that this lipid packing spectrum has a functional role in membrane related bindings. Cholera toxin binding to BD-GM1 was influenced by the lipid packing of the domains in a continuous way, i.e., we obtained a spectrum of binding with a spectrum of lipid packing. We further investigated the mechanism of lipid packing effect on CTxB-BD-GM1 binding. We simulated the BD-GM1 in ordered and disordered environment. We found out that lipid environment modulates the orientation of the molecules which is vital for their geometrical fit to their ligands. Showing all these, it was still a question how cells do regulate their lipid packing and obtain a lipid packing spectrum. We presented here two important environmental parameters that the cells can react by changing their membrane lipid packing.

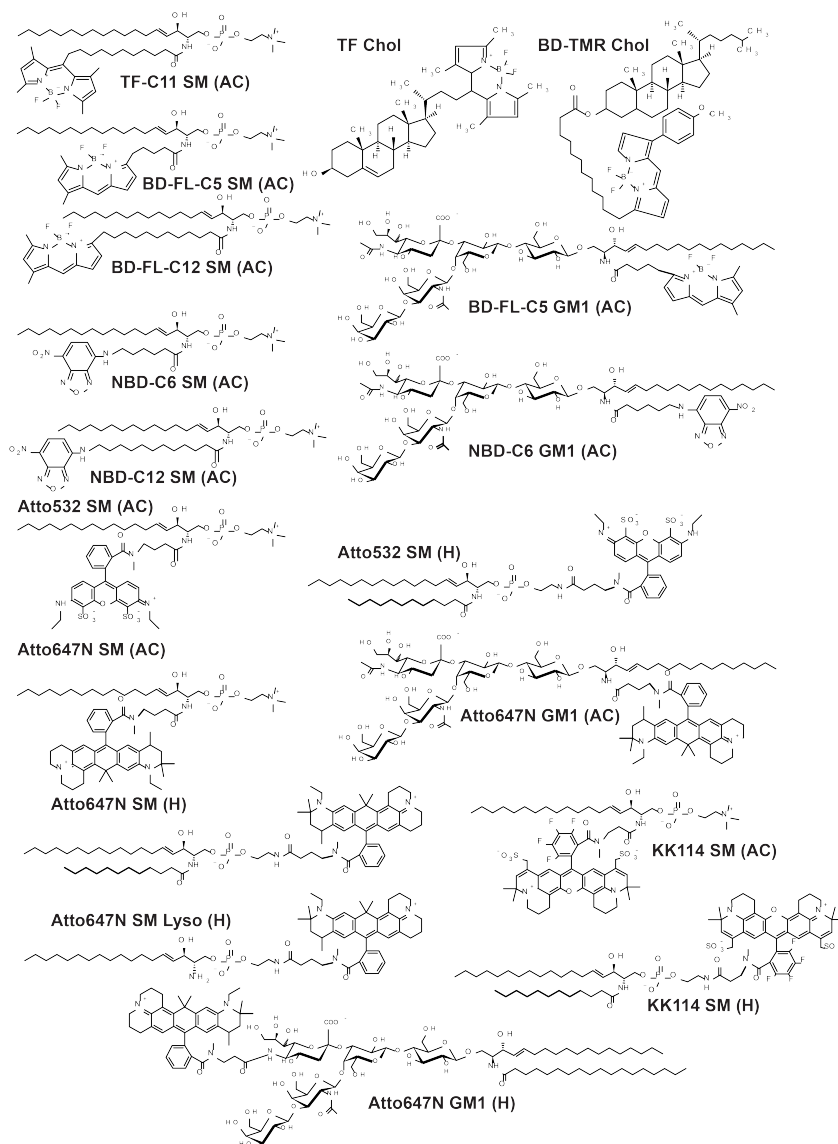
In the work presented in this thesis, we systematically investigated the physicochemical properties of membrane heterogeneity by employing fluorescence techniques, probes and model membranes. First of all, we discussed the potential fluorescent techniques with their advantages and disadvantages. Then, we focused on the fluorescent probes which could be used to elucidate the membrane structure. We also discussed the most widely used model membranes, particularly Giant Plasma Membrane Vesicles, highlighting their strong and weak sides. We showed some biological applications where model membranes could be useful. First, we showed that they could mimic the cell membrane to test the membrane penetration of the small molecules by testing the membrane penetration of typical hydrophilic quantum dots and amphiphilic quantum dots that we synthesized. Later, we showed the potential of GPMVs to investigate the lipid-protein dynamics in the cell membrane by showing how LRP6 protein distribution in the plasma membrane is modulated by the Lypd6 GPI-anchored protein. As another application for model systems, we investigated how the order of the prokaryotic membranes are modulated without cholesterol. We applied phase separated GUV systems to show that Hopanoid, a class of prokaryotic lipids, is capable of regulating the order of prokaryotic membranes as cholesterol for eukaryotic cell membranes. After showing the applications and potentials/limits of the model systems, we finally employed them to answer the key question of the thesis: how is the nature of the eukaryotic cell membrane heterogeneity? To figure that out, we first investigated the partitioning of fluorescent lipid analogs in GUVs and GPMVs and compared it with their nanoscale diffusion in the cell membrane measured by STED-FCS. We found out that GPMVs are more biological model systems especially for the raft related questions as the lipid packing of GPMV domains represents the live cell membrane better. Moreover, we concluded that the heterogeneity in living cells is much more complicated than two-phase state that we observed in model membranes. To this end, we started to investigate the membrane lateral heterogeneity. We showed that lipid packing of the domains in GUVs and GPMVs can be modulated by changing the lipid composition. This points out that cell membrane has the potential to form multiple domains having different properties, but not only one kind of rafts and non-rafts. Indeed, we obtained a continuous lipid packing spectrum instead of a binary (raft and non-raft)



Figure 11.1. An artistic depiction of cell membrane heterogeneity. Left panel shows the binary picture of the cell membrane which, we believe, does not represent the actual nature of membrane heterogeneity. Right panel shows the continuously variable lipid packing concept. There are many rafts and non-rafts and there is not a dramatic differences between raft and non-raft domains.

system. In the next step, we showed that this continuous lipid packing spectrum is functional for membrane related processes. We showed that the binding of Cholera toxin to its lipid ligand GM1 (we used Bodipy labeled GM1) is regulated by the lipid packing of the domains in a continuous way. With simulations, we found out that lipid packing regulates the geometry of the membrane molecules which determines their bioactivity. Finally, we showed different ways how the living cells regulate their membrane order.

With all these studies, we concluded that the cell membrane structure is not a binary structure as extensively pictured so far. It has many domains having many different characteristics. Instead of classifying these entities with Boolean approach which yields a binary picture (raft and non-raft), more quantitative approaches that can probe the exact physicochemical properties of the lipid environment and its effects on geometry/activity of membrane molecules should be considered.



Chemical Structures of the Raft Lipid Analogs

| Lipid Analog | <i>Lo</i> % in GUVs | <i>Lo</i> % in GPMVs |
|----------------------|---------------------|----------------------|
| TF SM (AC) | 21±4 | 33±6 |
| TF Chol (AC) | 80±3 | 66±6 |
| BD-TMR Chol (AC) | 41±1 | 76±4 |
| BD-FL-C5 SM (AC) | 25±4 | – |
| BD-FL-C12 SM (AC) | 31±5 | 66±6 |
| BD- FL-C5 GM1 (AC) | 25±7 | 65±4 |
| NBD-C12 SM (AC) | 5±2 | 35±5 |
| NBD-C6 SM (AC) | 13±3 | 46±4 |
| NBD-C6 GM1 (AC) | 23±8 | 67±6 |
| Atto532 SM (AC) | 15±3 | 47±1 |
| Atto532 SM (H) | 16±4 | 38±2 |
| Atto647N SM (AC) | 4±1 | 18±5 |
| Atto647N SM (H) | 3±1 | 18±6 |
| Atto647N GM1 (AC) | 6±2 | 11±1 |
| Atto647N GM1 (H) | 8±1 | 26±4 |
| Atto647N SM Lyso (H) | 3±1 | 5±2 |
| KK114 SM (AC) | 2±1 | 4±2 |
| KK114 SM (H) | 5±2 | 12±1 |

Partitioning of fluorescent raft lipid analogs in GUVs and GPMVs

Bibliography

- [1] E. Overton. The probable origin and physiological significance of cellular osmotic properties. *Vierteljahrsschrift der Naturforschende Gesellschaft*, 44:88–135, 1899.
- [2] R. B. Park. Translation of "The probable origin and physiological significance of cellular osmotic properties". *Biological Membrane Structure (Little, Brown & Co., Boston)*, 45-52, 1968.
- [3] S. J. Singer and G. L. Nicolson. The fluid mosaic model of the structure of cell membranes. *Science*, 175(4023):720, 1972.
- [4] J. Yu, D. A. Fischman, and T. L. Steck. Selective solubilization of proteins and phospholipids from red blood cell membranes by nonionic detergents. *Journal of Supramolecular Structure*, 1(3):233–248, 1973.
- [5] G. Vanmeer, E. H. K. Stelzer, R. W. Wijnaendtsvanresandt, and K. Simons. Sorting of sphingolipids in epithelial (madin-darby canine kidney) cells. *Journal of Cell Biology*, 105(4):1623–1635, 1987.
- [6] D. A. Brown and J. K. Rose. Sorting of GPI-anchored proteins to glycolipid-enriched membrane subdomains during transport to the apical cell surface. *Cell*, 68(3):533–544, 1992.
- [7] K. Simons and E. Ikonen. Functional rafts in cell membranes. *Nature*, 387(6633):569–572, 1997.
- [8] J. Korlach, P. Schwille, W. W. Webb, and G. W. Feigenson. Characterization of lipid bilayer phases by confocal microscopy and fluorescence correlation spectroscopy. *PNAS*, 96(15):8461–8466, 1999.
- [9] L. A. Bagatolli and E. Gratton. Two photon fluorescence microscopy of coexisting lipid domains in giant unilamellar vesicles of binary phospholipid mixtures. *Biophysical Journal*, 78(1):290–305, 2000.
- [10] E. Sezgin and P. Schwille. Fluorescence techniques to study lipid dynamics. *Cold Spring Harbor Perspectives in Biology*, 3(11), 2011.

- [11] M. Brameshuber, J. Weghuber, V. Ruprecht, I. Gombos, I. Horvath, L. Vigh, P. Eckerstorfer, E. Kiss, H. Stockinger, and G. J. Schuetz. Imaging of mobile long-lived nanoplateforms in the live cell plasma membrane. *J Biol Chem*, 285(53):41765–41771, 2010.
- [12] K. Gowrishankar, S. Ghosh, S. Saha, R. C. S. Mayor, and M. Rao. Active remodeling of cortical actin regulates spatiotemporal organization of cell surface molecules. *Cell*, 149(6):1353–1367, 2012.
- [13] M. Lozano, Z. Liu, K. Kumar, and S. Boxer. Partitioning of cholesterol and ganglioside gm1 in phase separated lipid bilayers imaged by secondary ion mass spectrometry. *Biophysical Journal*, 102:222, 2011.
- [14] M. Kraft, J. F. Frisz, K. Lou, H. Klitzing, W. Hanafin, P. Weber, P. K., and J. Zimmerberg. Chemical imaging of the lipid and cholesterol distribution in the plasma membranes of intact cells. *Biophysical Journal*, 102:26, 2011.
- [15] C. Eggeling, C. Ringemann, R. Medda, G. Schwarzmann, K. Sandhoff, S. Polyakova, V. N. Belov, B. Hein, C. von Middendorff, A. Schonle, and S. W. Hell. Direct observation of the nanoscale dynamics of membrane lipids in a living cell. *Nature*, 457(7233):1159–U121, 2009.
- [16] A. Kusumi, I. Koyama-Honda, and K. Suzuki. Molecular dynamics and interactions for creation of stimulation-induced stabilized rafts from small unstable steady-state rafts. *Traffic*, 5(4):213–230, 2004.
- [17] I. Levental, M. Grzybek, and K. Simons. Raft domains of variable properties and compositions in plasma membrane vesicles. *PNAS*, 108(28):11411–11416, 2011.
- [18] S. A. Sanchez, M. A. Triccerri, and E. Gratton. Laurdan generalized polarization fluctuations measures membrane packing micro-heterogeneity in vivo. *PNAS*, 109(19):7314–7319, 2012.
- [19] G. J. Brakenhoff, P. Blom, and P. Barends. Confocal scanning light-microscopy with high aperture immersion lenses. *Journal of Microscopy-Oxford*, 117(NOV):219–232, 1979.
- [20] Davidovi.P and M. D. Egger. Photomicrography of corneal endothelial cells in-vivo. *Nature*, 244(5415):366–367, 1973.
- [21] M. D. Egger and M. Petran. New reflected-light microscope for viewing unstained brain and ganglion cells. *Science*, 157(3786):305–, 1967.

- [22] D. K. Hamilton and T. Wilson. Scanning optical microscopy by objective lens scanning. *Journal of Physics E-Scientific Instruments*, 19(1):52–54, 1986.
- [23] C. J. R. Sheppard and T. Wilson. Effect of spherical-aberration on the imaging properties of scanning optical microscopes. *Applied Optics*, 18(7):1058–1063, 1979.
- [24] W. B. Amos and J. G. White. How the confocal laser scanning microscope entered biological research. *Biology of the Cell*, 95(6):335–342, 2003.
- [25] M. Goppert. Ueber die wahrscheinlichkeit des zusammenwirkens zweier lichtquanten in einem elementarakt. *Naturwissenschaften*, 17:932–932, 1929.
- [26] W. Kaiser and C. G. B. Garrett. 2-photon excitation in $\text{CaF}_2 - \text{Eu}^{2+}$. *Physical Review Letters*, 7(6):229, 1961.
- [27] R. Hellwarth and P. Christensen. Nonlinear optical microscope using second-harmonic generation. *Applied Optics*, 14(2):247–248, 1975.
- [28] W. Denk, J. H. Strickler, and W. W. Webb. 2-photon laser scanning fluorescence microscopy. *Science*, 248(4951):73–76, 1990.
- [29] C. Dietrich, L. A. Bagatolli, Z. N. Volovyk, N. L. Thompson, M. Levi, K. Jacobson, and E. Gratton. Lipid rafts reconstituted in model membranes. *Biophysical Journal*, 80(3):1417–1428, 2001.
- [30] L. A. Bagatolli, S. A. Sanchez, T. Hazlett, and E. Gratton. Giant vesicles, laurdan, and two-photon fluorescence microscopy: Evidence of lipid lateral separation in bilayers. *Biophotonics, Pt A*, 360:481–500, 2003.
- [31] L. A. Bagatolli and E. Gratton. Two-photon fluorescence microscopy observation of shape changes at the phase transition in phospholipid giant unilamellar vesicles. *Biophysical Journal*, 77(4):2090–2101, 1999.
- [32] L. A. Bagatolli and E. Gratton. A correlation between lipid domain shape and binary phospholipid mixture composition in free standing bilayers: A two-photon fluorescence microscopy study. *Biophysical Journal*, 79(1):434–447, 2000.
- [33] L. A. Bagatolli. Direct observation of lipid domains in free standing bilayers: from simple to complex lipid mixtures. *Chemistry and Physics of Lipids*, 122(1-2):137–145, 2003.
- [34] H. J. Kaiser, D. Lingwood, I. Levental, J. L. Sampaio, L. Kalvodova, L. Rajendran, and K. Simons. Order of lipid phases in model and plasma membranes. *PNAS*, 106(39):16645–16650, 2009.

- [35] H. M. Kim, H. J. Choo, S. Y. Jung, Y. G. Ko, W. H. Park, S. J. Jeon, C. H. Kim, T. H. Joo, and B. R. Cho. A two-photon fluorescent probe for lipid raft imaging: C-laurdan. *Chembiochem*, 8(5):553–559, 2007.
- [36] T. Parasassi, E. Gratton, W. M. Yu, P. Wilson, and M. Levi. Two-photon fluorescence microscopy of laurdan generalized polarization domains in model and natural membranes. *Biophysical Journal*, 72(6):2413–2429, 1997.
- [37] A. Gasecka, T. J. Han, C. Favard, B. R. Cho, and S. Brasselet. Quantitative imaging of molecular order in lipid membranes using two-photon fluorescence polarimetry. *Biophysical Journal*, 97(10):2854–2862, 2009.
- [38] L. Jin, A. C. Millard, J. P. Wuskell, X. M. Dong, D. Q. Wu, H. A. Clark, and L. M. Loew. Characterization and application of a new optical probe for membrane lipid domains. *Biophysical Journal*, 90(7):2563–2575, 2006.
- [39] H. M. Kim, B. H. Jeong, J. Y. Hyon, M. J. An, M. S. Seo, J. H. Hong, K. J. Lee, C. H. Kim, T. H. Joo, S. C. Hong, and B. R. Cho. Two-photon fluorescent turn-on probe for lipid rafts in live cell and tissue. *Journal of the American Chemical Society*, 130(13):4246, 2008.
- [40] A. S. Klymchenko, S. Oncul, P. Didier, E. Schaub, L. Bagatolli, G. Duportail, and Y. Mely. Visualization of lipid domains in giant unilamellar vesicles using an environment-sensitive membrane probe based on 3-hydroxyflavone. *Biochimica Et Biophysica Acta-Biomembranes*, 1788(2):495–499, 2009.
- [41] K. Bacia, D. Scherfeld, N. Kahya, and P. Schwille. Fluorescence correlation spectroscopy relates rafts in model and native membranes. *Biophysical Journal*, 87(2):1034–1043, 2004.
- [42] P. Schwille, J. Korch, and W. W. Webb. Fluorescence correlation spectroscopy with single-molecule sensitivity on cell and model membranes. *Cytometry*, 36(3):176–182, 1999.
- [43] E. L. Elson and D. Magde. Fluorescence correlation spectroscopy 1: Conceptual basis and theory. *Biopolymers*, 13(1):1–27, 1974.
- [44] D. Magde, W. W. Webb, and E. Elson. Thermodynamic fluctuations in a reacting system - measurement by fluorescence correlation spectroscopy. *Physical Review Letters*, 29(11):705, 1972.
- [45] D. Magde, E. L. Elson, and W. W. Webb. Fluorescence correlation spectroscopy 2: Experimental realization. *Biopolymers*, 13(1):29–61, 1974.

- [46] D. Magde, W. W. Webb, and E. L. Elson. Fluorescence correlation spectroscopy 3: Uniform translation and laminar-flow. *Biopolymers*, 17(2):361–376, 1978.
- [47] R. Rigler, U. Mets, J. Widengren, and P. Kask. Fluorescence correlation spectroscopy with high count rate and low-background - analysis of translational diffusion. *European Biophysics Journal with Biophysics Letters*, 22(3):169–175, 1993.
- [48] M. Eigen and R. Rigler. Sorting single molecules - application to diagnostics and evolutionary biotechnology. *PNAS*, 91(13):5740–5747, 1994.
- [49] E. Petrov and P. Schwille. *State of the art and novel trends in fluorescence correlation spectroscopy*. Springer, Verlag Berlin Heidelberg, 2007.
- [50] S. A. Kim, K. G. Heinze, and P. Schwille. Fluorescence correlation spectroscopy in living cells. *Nature Methods*, 4:963–973, 2007.
- [51] S. W. Hell and J. Wichmann. Breaking the diffraction resolution limit by stimulated-emission - stimulated-emission-depletion fluorescence microscopy. *Optics Letters*, 19(11):780–782, 1994.
- [52] T. A. Klar and S. W. Hell. Subdiffraction resolution in far-field fluorescence microscopy. *Optics Letters*, 24(14):954–956, 1999.
- [53] T. A. Klar, S. Jakobs, M. Dyba, A. Egner, and S. W. Hell. Fluorescence microscopy with diffraction resolution barrier broken by stimulated emission. *PNAS*, 97(15):8206–8210, 2000.
- [54] T. A. Klar, E. Engel, and S. W. Hell. Breaking Abbe’s diffraction resolution limit in fluorescence microscopy with stimulated emission depletion beams of various shapes. *Physical Review E*, 64(6), 2001.
- [55] R. Kasper, B. Harke, C. Forthmann, P. Tinnefeld, S. W. Hell, and M. Sauer. Single-molecule sted microscopy with photostable organic fluorophores. *Small*, 6(13):1379–1384, 2010.
- [56] G. Y. Mitronova, V. N. Belov, M. L. Bossi, C. A. Wurm, L. Meyer, R. Medda, G. Moneron, S. Bretschneider, C. Eggeling, S. Jakobs, and S. W. Hell. New fluorinated rhodamines for optical microscopy and nanoscopy. *Chemistry-a European Journal*, 16(15):4477–4488, 2010.
- [57] K. S. Morozova, K. D. Piatkevich, T. J. Gould, J. H. Zhang, J. Bewersdorf, and V. V. Verkhusha. Far-red fluorescent protein excitable with red lasers for flow cytometry and superresolution sted nanoscopy. *Biophysical Journal*, 99(2):L13–L15, 2010.

- [58] S. Deng, L. Liu, Y. Cheng, R. Li, and Z. Xu. Effects of primary aberrations on the fluorescence depletion patterns of STED microscopy. *Optics Express*, 18(2):1657–1666, 2010.
- [59] C. A. Wurm, D. Neumann, R. Schmidt, A. Egner, and S. Jakobs. Sample preparation for STED microscopy. *Live Cell Imaging: Methods and Protocols*, pages 185–199, 2010.
- [60] I. A. Boldyrev, X. H. Zhai, M. M. Momsen, H. L. Brockman, R. E. Brown, and J. G. Molotkovsky. New bodipy lipid probes for fluorescence studies of membranes. *Journal of Lipid Research*, 48(7):1518–1532, 2007.
- [61] M. Holtta-Vuori, R. L. Uronen, J. Repakova, E. Salonen, I. Vattulainen, P. Panula, Z. G. Li, R. Bittman, and E. Ikonen. Bodipy-cholesterol: A new tool to visualize sterol trafficking in living cells and organisms. *Traffic*, 9(11):1839–1849, 2008.
- [62] D. L. Marks, R. Bittman, and R. E. Pagano. Use of bodipy-labeled sphingolipid and cholesterol analogs to examine membrane microdomains in cells. *Histochemistry and Cell Biology*, 130(5):819–832, 2008.
- [63] J. Oreopoulos and C. M. Yip. Probing membrane order and topography in supported lipid bilayers by combined polarized total internal reflection fluorescence-atomic force microscopy. *Biophysical Journal*, 96(5):1970–1984, 2009.
- [64] D. Tyteca, L. D’Auria, P. Van Der Smissen, T. Medts, S. Carpentier, J. C. Monbaliu, P. de Diesbach, and P. J. Courtoy. Three unrelated sphingomyelin analogs spontaneously cluster into plasma membrane micrometric domains. *Biochimica Et Biophysica Acta-Biomembranes*, 1798(5):909–927, 2010.
- [65] O. Coban, M. Burger, M. Laliberte, A. Ianoul, and L. J. Johnston. Ganglioside partitioning and aggregation in phase-separated monolayers characterized by bodipy GM1 monomer/dimer emission. *Langmuir*, 23(12):6704–6711, 2007.
- [66] I. Mikhalyov, N. Gretskeya, and L. B. A. Johansson. Fluorescent bodipy-labelled g(m1) gangliosides designed for exploring lipid membrane properties and specific membrane-target interactions. *Chem. Phys. Lipids*, 159(1):38–44, 2009.
- [67] T. Baumgart, A. T. Hammond, P. Sengupta, S. T. Hess, D. A. Holowka, B. A. Baird, and W. W. Webb. Large-scale fluid/fluid phase separation of proteins and lipids in giant plasma membrane vesicles. *PNAS*, 104(9):3165–3170, 2007.

- [68] J. Juhasz, J. H. Davis, and F. J. Sharom. Fluorescent probe partitioning in giant unilamellar vesicles of 'lipid raft' mixtures. *Biochemical Journal*, 430(3):415–23, 2010.
- [69] J. L. Middlebrook and R. B. Dorland. Bacterial toxins - cellular mechanisms of action. *Microbiological Reviews*, 48(3):199–221, 1984.
- [70] E. Rusinova, V. Tretyachenko-Ladokhina, O. E. Vele, D. F. Senear, and J. B. A. Ross. Alexa and Oregon green dyes as fluorescence anisotropy probes for measuring protein-protein and protein-nucleic acid interactions. *Analytical Biochemistry*, 308(1):18–25, 2002.
- [71] A. Gidwani, D. Holowka, and B. Baird. Fluorescence anisotropy measurements of lipid order in plasma membranes and lipid rafts from RBL-2H3 mast cells. *Biochemistry*, 40(41):12422–12429, 2001.
- [72] M. Engelke, P. Bojarski, R. Bloss, and H. Diehl. Tamoxifen perturbs lipid bilayer order and permeability: comparison of dsc, fluorescence anisotropy, laurdan generalized polarization and carboxyfluorescein leakage studies. *Biophys. Chem.*, 90(2):157–173, 2001.
- [73] C. Thiele and J. Spandl. Cell biology of lipid droplets. *Curr. Opin. Cell Biol.*, 20(4):378–385, 2008.
- [74] L. Kuerschner, C. S. Ejsing, K. Ekroos, A. Shevchenko, K. I. Anderson, and C. Thiele. Polyene-lipids: A new tool to image lipids. *Nature Methods*, 2(1):39–45, 2005.
- [75] J. Spandl, D. J. White, J. Peychl, and C. Thiele. Live cell multicolor imaging of lipid droplets with a new dye, LD540. *Traffic*, 10(11):1579–1584, 2009.
- [76] P. Schwille and S. Diez. Synthetic biology of minimal systems. *Critical Reviews in Biochemistry and Molecular Biology*, 44(4):223–242, 2009.
- [77] P. Schwille. Bottom-up synthetic biology: engineering in a tinkerer's world. *Science*, 333(6047):1252–1254, 2011.
- [78] S. Arumugam, G. Chwastek, and P. Schwille. Protein-membrane interactions: the virtue of minimal systems in systems biology. *Wiley Interdisciplinary Reviews-Systems Biology and Medicine*, 3(3):269–280, 2011.
- [79] C. Tanford. *Ben Franklin Stilled the Waves: An Informal History of Pouring Oil on Water with Reflections on the Ups and Downs of Scientific Life in General*. Oxford University Press, 2004.

- [80] E. Gorter and F. Grendel. On bimolecular layers of lipoids on the chromocytes of the blood. *J. Exp. Med.*, 41:439–443, 1925.
- [81] I. Langmuir. The constitution and fundamental properties of solids and liquids. II. Liquids. *J. Amer. Chem. Soc.*, 39:1848–1906, 1917.
- [82] A. D. Bangham and R. W. Horne. Negative staining of phospholipids and their structural modification by surface-active agents as observed in the electron microscope. *J. Mol. Biol.*, 8(5):660, 1964.
- [83] H. M. McConnell, L. K. Tamm, and R. M. Weis. Periodic structures in lipid monolayer phase transitions. *PNAS*, 81(10):3249–3253, 1984.
- [84] L. K. Tamm and H. M. McConnell. Supported phospholipid-bilayers. *Biophysical Journal*, 47(1):105–113, 1985.
- [85] M. I. Angelova and D. S. Dimitrov. Liposome electroformation. *Faraday Discussions*, 81(81):303–+, 1986.
- [86] K. Bacia, C. G. Schuette, N. Kahya, R. Jahn, and P. Schwille. SNAREs prefer liquid-disordered over "raft" (liquid-ordered) domains when reconstituted into giant unilamellar vesicles. *Journal of Biological Chemistry*, 279(36):37951–37955, 2004.
- [87] P. Girard, J. Pecreaux, G. Lenoir, P. Falson, J. L. Rigaud, and P. Bassereau. A new method for the reconstitution of membrane proteins into giant unilamellar vesicles. *Biophysical Journal*, 87(1):419–429, 2004.
- [88] N. Kahya, D. A. Brown, and P. Schwille. Raft partitioning and dynamic behavior of human placental alkaline phosphatase in giant unilamellar vesicles. *Biochemistry*, 44(20):7479–7489, 2005.
- [89] R. Scott. Plasma membrane vesiculation: a new technique for isolation of plasma membranes. *Science*, 194:743–745, 1976.
- [90] D. L. Richmond, E. M. Schmid, S. Martens, J. C. Stachowiak, N. Liska, and D. A. Fletcher. Forming giant vesicles with controlled membrane composition, asymmetry, and contents. *PNAS*, 108(23):9431–9436, 2011.
- [91] N. Kahya, E. I. Pecheur, W. P. de Boeij, D. A. Wiersma, and D. Hoekstra. Reconstitution of membrane proteins into giant unilamellar vesicles via peptide-induced fusion. *Biophysical Journal*, 81(3):1464–1474, 2001.

- [92] S. Chiantia, N. Kahya, and P. Schwille. Raft domain reorganization driven by short- and long-chain ceramide: A combined AFM and FCS study. *Langmuir*, 23(14):7659–7665, 2007.
- [93] S. Chiantia, J. Ries, G. Chwastek, D. Carrer, Z. Li, R. Bittman, and P. Schwille. Role of ceramide in membrane protein organization investigated by combined AFM and FCS. *Biochimica Et Biophysica Acta-Biomembranes*, 1778(5):1356–1364, 2008.
- [94] R. P. Richter, R. Berat, and A. R. Brisson. Formation of solid-supported lipid bilayers: An integrated view. *Langmuir*, 22(8):3497–3505, 2006.
- [95] A. C. Simonsen and L. A. Bagatolli. Structure of spin-coated lipid films and domain formation in supported membranes formed by hydration. *Langmuir*, 20(22):9720–9728, 2004.
- [96] M. Loose and P. Schwille. Biomimetic membrane systems to study cellular organization. *J. Struct. Biol.*, 168(1):143–151, 2009.
- [97] M. L. Wagner and L. K. Tamm. Tethered polymer-supported planar lipid bilayers for reconstitution of integral membrane proteins: Silane-polyethyleneglycol-lipid as a cushion and covalent linker. *Biophysical Journal*, 79(3):1400–1414, 2000.
- [98] A. Honigmann, C. Walter, F. Erdmann, C. Eggeling, and R. Wagner. Characterization of horizontal lipid bilayers as a model system to study lipid phase separation. *Biophysical Journal*, 98(12):2886–2894, 2010.
- [99] A. V. Samsonov, I. Mihalyov, and F. S. Cohen. Characterization of cholesterol-sphingomyelin domains and their dynamics in bilayer membranes. *Biophysical Journal*, 81(3):1486–1500, 2001.
- [100] C. Hennesthal, J. Drexler, and C. Steinem. Membrane-suspended nanocompartments based on ordered pores in alumina. *Chemphyschem*, 3(10):885–889, 2002.
- [101] A. Simon, A. Girard-Egrot, F. Sauter, C. Pudda, N. P. D’Hahan, L. Blum, F. Chatelain, and A. Fuchs. Formation and stability of a suspended biomimetic lipid bilayer on silicon submicrometer-sized pores. *Journal of Colloid and Interface Science*, 308(2):337–343, 2007.
- [102] F. Heinemann and P. Schwille. Preparation of micrometer-sized free-standing membranes. *Chemphyschem*, 12:2568–2571, 2011.
- [103] M. I. Angelova and D. S. Dimitrov. A mechanism of liposome electroformation. *Prog Colloid Polymer Sci*, 76:59–67, 1988.

- [104] A. J. Garcia-Saez, D. C. Carrer, and P. Schwille. Fluorescence correlation spectroscopy for the study of membrane dynamics and organization in giant unilamellar vesicles. *Liposomes: Methods and Protocols*, 606:493–508, 2010.
- [105] N. F. Morales-Pennington, J. Wu, E. R. Farkas, S. L. Goh, T. M. Konyakhina, J. Y. Zheng, W. W. Webb, and G. W. Feigenson. GUV preparation and imaging: Minimizing artifacts. *Biochim. Biophys. Acta-Biomembr.*, 1798(7):1324–1332, 2010.
- [106] E. Sezgin, H. J. Kaiser, T. Baumgart, P. Schwille, K. Simons, and I. Levental. Elucidating membrane structure and protein behavior using giant plasma membrane vesicles. *Nature Protocols*, 7(6):1042–1051, 2012.
- [107] G. T. Charras, M. Coughlin, T. J. Mitchison, and L. Mahadevan. Life and times of a cellular bleb. *Biophysical Journal*, 94(5):1836–1853, 2008.
- [108] S. A. Johnson, B. M. Stinson, M. S. Go, L. M. Carmona, J. I. Reminick, X. Fang, and T. Baumgart. Temperature-dependent phase behavior and protein partitioning in giant plasma membrane vesicles. *Biochim. Biophys. Acta-Biomembr.*, 1798(7):1427–1435, 2010.
- [109] H. Keller, M. Lorizate, and P. Schwille. PI(4,5)P-2 degradation promotes the formation of cytoskeleton-free model membrane systems. *Chemphyschem*, 10(16):2805–2812, 2009.
- [110] D. Lingwood, J. Ries, P. Schwille, and K. Simons. Plasma membranes are poised for activation of raft phase coalescence at physiological temperature. *PNAS*, 105(29):10005–10010, 2008.
- [111] S. Chiantia, P. Schwille, A. S. Klymchenko, and E. London. Asymmetric GUVs prepared by m-beta CD-mediated lipid exchange: An FCS study. *Biophysical Journal*, 100(1):LO1–LO3, 2011.
- [112] M. D. Collins and S. L. Keller. Tuning lipid mixtures to induce or suppress domain formation across leaflets of unsupported asymmetric bilayers. *PNAS*, 105(1):124–128, 2008.
- [113] M. Montal and P. Mueller. Formation of bimolecular membranes from lipid monolayers and a study of their electrical properties. *PNAS*, 69(12):3561–3566, 1972.
- [114] D. Lingwood and K. Simons. Lipid rafts as a membrane-organizing principle. *Science*, 327(5961):46–50, 2010.

- [115] K. Gaus, E. Chklovskaya, B. Fazekas de St Groth, W. Jessup, and T. Harder. Condensation of the plasma membrane at the site of T lymphocyte activation. *J Cell Biol*, 171(1):121–131, 2005.
- [116] R. Scott and P. Maercklein. Plasma membrane vesiculation in 3T3 and SV3T3 cells II: Factors affecting the process of vesiculation. *Journal of Cell Science*, 35:245–252, 1979.
- [117] D. W. Tank, E. S. Wu, and W. W. Webb. Enhanced molecular diffusibility in muscle membrane blebs: release of lateral constraints. *Journal of Cell Biology*, 92:207–212, 1982.
- [118] M. Ge, A. Gidwani, H. A. Brown, D. Holowka, B. Baird, and J. H. Freed. Ordered and disordered phases coexist in plasma membrane vesicles of RBL-2H3 mast cells. an ESR study. *Biophysical Journal*, 85(2):1278–1288, 2003.
- [119] D. Holowka and B. Baird. Lactoperoxidase-catalyzed iodination of the receptor for immunoglobulin e at the cytoplasmic side of the plasma membrane. *J Biol Chem*, 259(6):3720–3728, 1984.
- [120] A. Dubavik, E. Sezgin, V. Lesnyak, N. Gaponik, P. Schwille, and A. Eychmueller. Penetration of amphiphilic quantum dots through model and cellular plasma membranes. *ACS Nano*, 6(3):2150–2156, 2012.
- [121] P. Saeaelik, A. Niinep, J. Pae, M. Hansen, D. Lubenets, U. Langel, and M. Pooga. Penetration without cells: membrane translocation of cell-penetrating peptides in the model giant plasma membrane vesicles. *J Control Release*, 153(2):117–125, 2011.
- [122] P. Sengupta, A. Hammond, D. Holowka, and B. Baird. Structural determinants for partitioning of lipids and proteins between coexisting fluid phases in giant plasma membrane vesicles. *Biochimica Et Biophysica Acta-Biomembranes*, 1778(1):20–32, 2008.
- [123] I. Levental, F. J. Byfield, P. Chowdhury, F. Gai, T. Baumgart, and P. A. Janmey. Cholesterol-dependent phase separation in cell-derived giant plasma-membrane vesicles. *Biochemical Journal*, 424:163–167, 2009.
- [124] I. Levental, M. Grzybek, and K. Simons. Greasing their way: Lipid modifications determine protein association with membrane rafts. *Biochemistry*, 49(30):6305–6316, 2010.

- [125] S. L. Veatch, P. Cicuta, P. Sengupta, A. Honerkamp-Smith, D. Holowka, and B. Baird. Critical fluctuations in plasma membrane vesicles. *ACS Chemical Biology*, 3(5):287–293, 2008.
- [126] D. Lingwood and K. Simons. Detergent resistance as a tool in membrane research. *Nat Protoc*, 2(9):2159–2165, 2007.
- [127] K. Roeper, D. Corbeil, and W. B. Huttner. Retention of prominin in microvilli reveals distinct cholesterol-based lipid micro-domains in the apical plasma membrane. *Nat Cell Biol*, 2(9):582–592, 2000.
- [128] S. Schuck, M. Honsho, K. Ekroos, A. Shevchenko, and K. Simons. Resistance of cell membranes to different detergents. *PNAS*, 100(10):5795–5800, 2003.
- [129] S. L. Veatch and S. L. Keller. Separation of liquid phases in giant vesicles of ternary mixtures of phospholipids and cholesterol. *Biophysical Journal*, 85(5):3074–3083, 2003.
- [130] S. L. Veatch and S. L. Keller. Organization in lipid membranes containing cholesterol. *Physical Review Letters*, 89(26):1–6, 2002.
- [131] D. Holowka and B. Baird. Structural studies on the membrane-bound immunoglobulin e-receptor complex. 1. characterization of large plasma membrane vesicles from rat basophilic leukemia cells and insertion of amphipathic fluorescent probes. *Biochemistry*, 22:3466–3474, 1983.
- [132] H.-J. Kaiser, A. Orłowski, T. Rog, T. K. M. Nyholm, W. Chai, T. Feizi, D. Lingwood, I. Vattulainen, and K. Simons. Lateral sorting in model membranes by cholesterol-mediated hydrophobic matching. *PNAS*, 108(40):16628–16633, 2011.
- [133] A. G. Ayuyan and F. S. Cohen. Lipid peroxides promote large rafts: effects of excitation of probes in fluorescence microscopy and electrochemical reactions during vesicle formation. *Biophysical Journal*, 91(6):2172–2183, 2006.
- [134] D. M. Owen, C. Rentero, A. Magenau, A. Abu-Siniyeh, and K. Gaus. Quantitative imaging of membrane lipid order in cells and organisms. *Nature Protocols*, 7(1):24–35, 2012.
- [135] J. Nikolaus, S. Scolari, E. Bayraktarov, N. Jungnick, S. Engel, A. P. Plazzo, M. Stockl, R. Volkmer, M. Veit, and A. Herrmann. Hemagglutinin of influenza virus partitions into the nonraft domain of model membranes. *Biophysical Journal*, 99(2):489–498, 2010.

- [136] X. Michalet, F. F. Pinaud, L. A. Bentolila, J. M. Tsay, S. Doose, J. J. Li, G. Sundaresan, A. M. Wu, S. S. Gambhir, and S. Weiss. Quantum dots for live cells, in vivo imaging, and diagnostics. *Science*, 307(5709):538–544, 2005.
- [137] I. L. Medintz, H. T. Uyeda, E. R. Goldman, and H. Mattoussi. Quantum dot bioconjugates for imaging, labelling and sensing. *Nature Mater.*, 4(6):435–446, 2005.
- [138] U. Resch-Genger, M. Grabolle, S. Cavaliere-Jaricot, R. Nitschke, and T. Nann. Quantum dots versus organic dyes as fluorescent labels. *Nat. Methods*, 5(9):763–775, 2008.
- [139] A. Derfus, W. Chan, and S. Bhatia. Intracellular delivery of quantum dots for live cell labeling and organelle tracking. *Adv. Mater.*, 16(12):961–966, 2004.
- [140] I. Nabiev, S. Mitchell, A. Davies, Y. Williams, D. Kelleher, R. Moore, Y. K. Gun’ko, S. Byrne, Y. P. Rakovich, J. F. Donegan, A. Sukhanova, J. Conroy, D. Cottell, N. Gaponik, A. Rogach, and Y. Volkov. Nonfunctionalized nanocrystals can exploit a cell’s active transport machinery delivering them to specific nuclear and cytoplasmic compartments. *Nano Lett.*, 7(11):3452–3461, 2007.
- [141] A. J. Garcia-Saez, J. Ries, M. Orzaez, E. Perez-Paya, and P. Schwille. Membrane promotes tBID interaction with BCLXL. *Nature Structural & Molecular Biology*, 16(11):1178–U9, 2009.
- [142] S. P. Gordon, S. Berezhna, D. Scherfeld, N. Kahya, and P. Schwille. Characterization of interaction between cationic lipid-oligonucleotide complexes and cellular membrane lipids using confocal imaging and fluorescence correlation spectroscopy. *Biophysical Journal*, 88(1):305–316, 2005.
- [143] A. Dubavik, V. Lesnyak, W. Thiessen, N. Gaponik, T. Wolff, and A. Eychmeuller. Synthesis of amphiphilic cdte nanocrystals. *J. Phys. Chem. C*, 113(12):4748–4750, 2009.
- [144] A. Dubavik, V. Lesnyak, N. Gaponik, and A. Eychmeuller. One-phase synthesis of gold nanoparticles with varied solubility. *Langmuir*, 27(16):10224–10227, 2011.
- [145] R. G. Shimmin, A. B. Schoch, and P. V. Braun. Polymer size and concentration effects on the size of gold nanoparticles capped by polymeric thiols. *Langmuir*, 20(13):5613–5620, 2004.

- [146] A. L. Rogach, T. Franzl, T. A. Klar, J. Feldmann, N. Gaponik, V. Lesnyak, A. Shavel, A. Eychmueller, Y. P. Rakovich, and J. F. Donegan. Aqueous synthesis of thiol-capped CdTe nanocrystals: state-of-the-art. *J. Phys. Chem. C*, 111(40):14628–14637, 2007.
- [147] N. Gaponik, D. V. Talapin, A. L. Rogach, K. Hoppe, E. V. Shevchenko, A. Kornowski, A. Eychmueller, and H. Weller. Thiol-capping of cdte nanocrystals: an alternative to organometallic synthetic routes. *J. Phys. Chem. B*, 106(29):7177–7185, 2002.
- [148] M. Grabolle, M. Spieles, V. Lesnyak, N. Gaponik, A. Eychmueller, and U. Resch-Genger. Determination of the fluorescence quantum yield of quantum dots: suitable procedures and achievable uncertainties. *Anal. Chem.*, 81(15):6285–6294, 2009.
- [149] C. Reichardt. WILEY-VCH Verlag GmbH & Co. KGaA, Weinheim, 2003.
- [150] Y. Volkov, S. Mitchell, N. Gaponik, Y. P. Rakovich, J. F. Donegan, D. Kelleher, and A. L. Rogach. In-situ observation of nanowire growth from luminescent cdte nanocrystals in a phosphate buffer solution. *Chemphyschem*, 5(10):1600–1602, 2004.
- [151] A. P. Liu, F. Aguet, G. Danuser, and S. L. Schmid. Local clustering of transferrin receptors promotes clathrin-coated pit initiation. *J. Cell Biol.*, 191(7):1381–1393, 2010.
- [152] H. Clevers. Wnt/beta-catenin signaling in development and disease. *Cell*, 127(3):469–480, 2006.
- [153] H. Huang and X. He. Wnt/beta-catenin signaling: new (and old) players and new insights. *Curr Opin Cell Biol*, 20(2):119–125, 2008.
- [154] C. Y. Logan and R. Nusse. The wnt signaling pathway in development and disease. *Annu Rev Cell Dev Biol*, 20:781–810, 2004.
- [155] A. Klaus and W. Birchmeier. Wnt signalling and its impact on development and cancer. *Nat Rev Cancer*, 8(5):387–398, 2008.
- [156] B. T. MacDonald, K. Tamai, and X. He. Wnt/beta-catenin signaling: components, mechanisms, and diseases. *Dev Cell*, 17(1):9–26, 2009.
- [157] A. Kikuchi and H. Yamamoto. Regulation of wnt signalling by receptor-mediated endocytosis. *J Biochem*, 141(4):443–551, 2007.

- [158] H. Sakane, H. Yamamoto, and A. Kikuchi. Lrp6 is internalized by dkk1 to suppress its phosphorylation in the lipid raft and is recycled for reuse. *J Cell Sci*, 123(Pt 3):360–368, 2010.
- [159] T. Jowett and L. Lettice. Whole-mount in situ hybridizations on zebrafish embryos using a mixture of digoxigenin- and fluorescein-labelled probes. *Trends Genet*, 10(3):73–74, 1994.
- [160] B. Kagermeier-Schenk, D. Wehner, G. Ozhan-Kizil, H. Yamamoto, J. Li, K. Kirchner, C. Hoffmann, P. Stern, A. Kikuchi, A. Schambony, and G. Weidinger. Waif1/5t4 inhibits Wnt/beta-catenin signaling and activates noncanonical Wnt pathways by modifying LRP6 subcellular localization. *Dev Cell*, 21(6):1129–43, 2011.
- [161] A. Bamezai. Mouse Ly-6 proteins and their extended family: markers of cell differentiation and regulators of cell signaling. *Arch Immunol Ther Exp (Warsz)*, 52(4):255–266, 2004.
- [162] M. Mallya, R. D. Campbell, and B. Aguado. Characterization of the five novel ly-6 superfamily members encoded in the mhc, and detection of cells expressing their potential ligands. *Protein Sci*, 15(10):2244–2256, 2006.
- [163] G. Davidson, W. Wu, J. Shen, J. Bilic, U. Fenger, P. Stannek, A. Glinka, and C. Niehrs. Casein kinase 1 gamma couples Wnt receptor activation to cytoplasmic signal transduction. *Nature*, 438(7069):867–872, 2005.
- [164] A. I. Magee and I. Parmryd. Detergent-resistant membranes and the protein composition of lipid rafts. *Genome Biol*, 4(11):234, 2003.
- [165] X. L. Xu and E. London. The effect of sterol structure on membrane lipid domains reveals how cholesterol can induce lipid domain formation. *Biochemistry-US*, 39(5):843–849, 2000.
- [166] G. van Meer, D. R. Voelker, and G. W. Feigenson. Membrane lipids: where they are and how they behave. *Nat Rev Mol Cell Bio*, 9(2):112–124, 2008.
- [167] A. Pearson, S. R. F. Page, T. L. Jorgenson, W. W. Fischer, and M. B. Higgins. Novel hopanoid cyclases from the environment. *Environ Microbiol*, 9(9):2175–2188, 2007.
- [168] M. Rohmer, P. Bouviernave, and G. Ourisson. Distribution of hopanoid triterpenes in prokaryotes. *J Gen Microbiol*, 130(May):1137–1150, 1984.

- [169] M. Rohmer, P. Bouvier, and G. Ourisson. Molecular evolution of biomembranes - structural equivalents and phylogenetic precursors of sterols. *P Natl Acad Sci USA*, 76(2):847–851, 1979.
- [170] K. U. Wendt, K. Poralla, and G. E. Schulz. Structure and function of a squalene cyclase. *Science*, 277(5333):1811–1815, 1997.
- [171] G. Ourisson, M. Rohmer, and K. Poralla. Prokaryotic hopanoids and other polyterpenoid sterol surrogates. *Annu Rev Microbiol*, 41:301–333, 1987.
- [172] M. Grzybek, J. Kubiak, A. Lach, M. Przybylo, and A. F. Sikorski. A raft-associated species of phosphatidylethanolamine interacts with cholesterol comparably to sphingomyelin. a langmuir-blodgett monolayer study. *Plos One*, 4(3), 2009.
- [173] J. H. Ipsen, G. Karlstrom, O. G. Mouritsen, H. Wennerstrom, and M. J. Zuckermann. Phase-equilibria in the phosphatidylcholine-cholesterol system. *Biochim Biophys Acta*, 905(1):162–172, 1987.
- [174] K. Bacia, P. Schwille, and T. Kurzchalia. Sterol structure determines the separation of phases and the curvature of the liquid-ordered phase in model membranes. *PNAS*, 102(9):3272–3277, 2005.
- [175] M. A. F. Hermans, B. Neuss, and H. Sahn. Content and composition of hopanoids in zymomonas-mobilis under various growth-conditions. *J Bacteriol*, 173(17):5592–5595, 1991.
- [176] D. M. Doughty, R. C. Hunter, R. E. Summons, and D. K. Newman. 2-methylhopanoids are maximally produced in akinetes of nostoc punctiforme: geobiological implications. *Geobiology*, 7(5):524–532, 2009.
- [177] U. J. Jurgens, P. Simonin, and M. Rohmer. Localization and distribution of hopanoids in membrane systems of the cyanobacterium synechocystis pcc-6714. *Fems Microbiol Lett*, 92(3):285–288, 1992.
- [178] I. C. Hancock and K. M. Williams. The outer-membrane of methylobacterium-organophilum. *J Gen Microbiol*, 132:599–610, 1986.
- [179] H. Nikaido and M. Vaara. Molecular-basis of bacterial outer-membrane permeability. *Microbiol Rev*, 49(1):1–32, 1985.
- [180] K. Brandenburg and U. Seydel. Investigation into the fluidity of lipopolysaccharide and free lipid-a membrane systems by fourier-transform infrared-spectroscopy and differential scanning calorimetry. *Eur J Biochem*, 191(1):229–236, 1990.

- [181] P. V. Welander, R. C. Hunter, L. C. Zhang, A. L. Sessions, R. E. Summons, and D. K. Newman. Hopanoids play a role in membrane integrity and pH homeostasis in *rhodospseudomonas palustris* TIE-1. *J Bacteriol*, 191(19):6145–6156, 2009.
- [182] C. L. Schmerk, M. A. Bernards, and M. A. Valvano. Hopanoid production is required for low-ph tolerance, antimicrobial resistance, and motility in *burkholderia cenocepacia*. *J Bacteriol*, 193(23):6712–6723, 2011.
- [183] D. S. Jones, H. L. Albrecht, K. S. Dawson, I. Schaperdoth, K. H. Freeman, Y. D. Pi, A. Pearson, and J. L. Macalady. Community genomic analysis of an extremely acidophilic sulfur-oxidizing biofilm. *Isme J*, 6(1):158–170, 2012.
- [184] M. P. Cooke, H. M. Talbot, and P. Farrimond. Bacterial populations recorded in bacteriohopanepolyol distributions in soils from northern england. *Org Geochem*, 39(9):1347–1358, 2008.
- [185] Y. P. Xu, M. P. Cooke, H. M. Talbot, and M. J. Simpson. Bacteriohopanepolyol signatures of bacterial populations in western canadian soils. *Org Geochem*, 40(1):79–86, 2009.
- [186] J. P. Saenz, T. I. Eglinton, and R. E. Summons. Abundance and structural diversity of bacteriohopanepolyols in suspended particulate matter along a river to ocean transect. *Org Geochem*, 42(7):774–780, 2011.
- [187] A. Pearson and D. B. Rusch. Distribution of microbial terpenoid lipid cyclases in the global ocean metagenome. *Isme J*, 3(3):352–363, 2009.
- [188] J. P. Saenz. Hopanoid enrichment in a detergent resistant membrane fraction of *crocosphaera watsonii*: Implications for bacterial lipid raft formation. *Org Geochem*, 41(8):853–856, 2010.
- [189] D. Lopez and R. Kolter. Functional microdomains in bacterial membranes. *Gene Dev Gene Dev*, 24(17):1893–1902, 2010.
- [190] S. Rexroth, C. W. Mullineaux, D. Ellinger, E. Sendtko, M. Rogner, and F. Koenig. The plasma membrane of the cyanobacterium *gloeobacter violaceus* contains segregated bioenergetic domains. *Plant Cell Plant Cell*, 23(6):2379–2390, 2011.
- [191] S. Neunlist, O. Holst, and M. Rohmer. Prokaryotic triterpenoids - the hopanoids of the purple non-sulfur bacterium *rhodomicrobium-vanniellii* - an aminotriol and its aminoacyl derivatives, n-tryptophanyl and n-ornithinyl aminotriol. *Eur J Biochem*, 147(3):561–568, 1985.

- [192] W. W. Fischer, R. E. Summons, and A. Pearson. Targeted genomic detection of biosynthetic pathways: anaerobic production of hopanoid biomarkers by a common sedimentary microbe. *Geobiology*, 3(1):33–40, 2005.
- [193] T. Haertner, K. Straub, and E. L. Kannenberg. Occurrence of hopanoid lipids in anaerobic geobacter species. *FEMS Microbiology Letters*, 243:59–64, 2005.
- [194] J. S. Sinninghe Damste, W. I. C. Rijpstra, S. Schouten, J. A. Fuerst, M. S. M. Jetten, and M. Strous. The occurrence of hopanoids in planctomycetes: implications for the sedimentary biomarker record. *Org Geochem*, 35(5):561–566, 2004.
- [195] M. I. Angelova, S. Soleau, P. Meleard, F. Faucon, and P. Bothorel. Preparation of giant vesicles by external ac electric fields. kinetics and applications. *Prog Colloid Polymer Sci*, 89:127–131, 1992.
- [196] N. Kahya, D. Scherfeld, K. Bacia, B. Poolman, and P. Schwille. Probing lipid mobility of raft-exhibiting model membranes by fluorescence correlation spectroscopy. *Journal of Biological Chemistry*, 278(30):28109–28115, 2003.
- [197] N. Kahya, D. Scherfeld, K. Bacia, and P. Schwille. Lipid domain formation and dynamics in giant unilamellar vesicles explored by fluorescence correlation spectroscopy. *Journal of Structural Biology*, 147(1):77–89, 2004.
- [198] R. Scott, P. Maercklein, and L. Furcht. Plasma membrane intramembranous particle topography in 3T3 and SV3T3 cells: The effect of cytochalasin B. *Journal of Cell Science*, 23:173–192, 1977.
- [199] T. Baumgart, G. Hunt, E. R. Farkas, W. W. Webb, and G. W. Feigenson. Fluorescence probe partitioning between l-o/l-d phases in lipid membranes. *Biochimica Et Biophysica Acta-Biomembranes*, 1768:2182–2194, 2007.
- [200] U. Coskun and K. Simons. Membrane rafting: From apical sorting to phase segregation. *Febs Letters*, 584(9):1685–1693, 2010.
- [201] C. Schultz, A. B. Neef, T. W. Gadella Jr, and J. Goedhart. Imaging lipids in living cells. *Cold Spring Harb. Protoc.*, pages –, 2010.
- [202] J. E. Shaw, R. F. Epanand, R. M. Epanand, Z. G. Li, R. Bittman, and C. M. Yip. Correlated fluorescence-atomic force microscopy of membrane domains: Structure of fluorescence probes determines lipid localization. *Biophysical Journal*, 90(6):2170–2178, 2006.

- [203] C. Wan, V. Kiessling, and L. K. Tamm. Coupling of cholesterol-rich lipid phases in asymmetric bilayers. *Biochemistry*, 47(7):2190–2198, 2008.
- [204] A. R. Burns, D. J. Frankel, and T. Buranda. Local mobility in lipid domains of supported bilayers characterized by atomic force microscopy and fluorescence correlation spectroscopy. *Biophysical Journal*, 89(2):1081–1093, 2005.
- [205] N. Kahya. Light on fluorescent lipids in rafts: a lesson from model membranes. *Biochemical Journal*, 430(3):e7–9, 2010.
- [206] O. Maier, V. Oberle, and D. Hoekstra. Fluorescent lipid probes: some properties and applications (a review). *Chemistry and Physics of Lipids*, 116(1-2):3–18, 2002.
- [207] D. Wustner. Fluorescent sterols as tools in membrane biophysics and cell biology. *Chemistry and Physics of Lipids*, 146(1):1–25, 2007.
- [208] T. Y. Wang and J. R. Silvius. Different sphingolipids show differential partitioning into sphingolipid/cholesterol-rich domains in lipid bilayers. *Biophysical Journal*, 79(3):1478–1489, 2000.
- [209] A. Kusumi, H. Ike, C. Nakada, K. Murase, and T. Fujiwara. Single-molecule tracking of membrane molecules: plasma membrane compartmentalization and dynamic assembly of raft-philic signaling molecules. *Semin. Immunol.*, 17(1):3–21, 2005.
- [210] A. Kusumi, Y. M. Shirai, I. Koyama-Honda, K. G. N. Suzuki, and T. K. Fujiwara. Hierarchical organization of the plasma membrane: Investigations by single-molecule tracking vs. fluorescence correlation spectroscopy. *Febs Letters*, 584(9):1814–1823, 2010.
- [211] S. W. Hell. Far-field optical nanoscopy. *Science*, 316(5828):1153–1158, 2007.
- [212] V. Mueller, C. Ringemann, A. Honigmann, G. Schwarzmann, R. Medda, M. Leutenegger, S. Polyakova, V. Belov, S. Hell, and C. Eggeling. STED nanoscopy reveals molecular details of cholesterol- and cytoskeleton-modulated lipid interactions in living cells. *Biophysical Journal*, 101:1651–1660, 2011.
- [213] K. Kolmakov, V. N. Belov, J. Bierwagen, C. Ringemann, V. Muller, C. Eggeling, and S. W. Hell. Red-emitting rhodamine dyes for fluorescence microscopy and nanoscopy. *Chemistry-a European Journal*, 16(1):158–166, 2010.

- [214] S. M. Polyakova, V. N. Belov, S. F. Yan, C. Eggeling, C. Ringemann, G. Schwarzmann, A. de Meijere, and S. W. Hell. New GM1 ganglioside derivatives for selective single and double labelling of the natural glycosphingolipid skeleton. *European Journal of Organic Chemistry*, 30(30):5162–5177, 2009.
- [215] G. Schwarzmann and K. Sandhoff. Lysogangliosides: synthesis and use in preparing labeled gangliosides. *Methods in Enzymology*, 138:319–341, 1987.
- [216] S. L. Veatch and S. L. Keller. Miscibility phase diagrams of giant vesicles containing sphingomyelin. *Phys Rev Lett*, 94(14):148101, 2005.
- [217] C. Ringemann, B. Harke, C. V. Middendorff, R. Medda, A. Honigmann, R. Wagner, M. Leutenegger, A. Schoenle, S. Hell, and C. Eggeling. Exploring single-molecule dynamics with fluorescence nanoscopy. *New J Phys*, 11:103054, 2009.
- [218] T. Harder, P. Scheiffele, P. Verkade, and K. Simons. Lipid domain structure of the plasma membrane revealed by patching of membrane components. *J Cell Biol*, 141(4):929–942, 1998.
- [219] D. M. C. Ramirez, W. W. Ogilvie, and L. J. Johnston. NBD-cholesterol probes to track cholesterol distribution in model membranes. *Biochim. Biophys. Acta-Biomembr.*, 1798(3):558–568, 2010.
- [220] L. A. Bagatolli. To see or not to see: Lateral organization of biological membranes and fluorescence microscopy. *Biochimica Et Biophysica Acta-Biomembranes*, 1758(10):1541–1556, 2006.
- [221] O. A. Kucherak, S. Oncul, Z. Darwich, D. A. Yushchenko, Y. Arntz, P. Didier, Y. Mely, and A. S. Klymchenko. Switchable Nile red-based probe for cholesterol and lipid order at the outer leaflet of biomembranes. *Journal of the American Chemical Society*, 132(13):4907–4916, 2010.
- [222] A. Chattopadhyay and E. London. Parallax method for direct measurement of membrane penetration depth utilizing fluorescence quenching by spin-labeled phospholipids. *Biochemistry*, 26(1):39–45, 1987.
- [223] M. Rusnati, C. Urbinati, E. Tanghetti, P. Dell’Era, H. Lortat-Jacob, and M. Presta. Cell membrane GM(1) ganglioside is a functional coreceptor for fibroblast growth factor 2. *PNAS*, 99(7):4367–4372, 2002.
- [224] D. Lingwood, B. Binnington, T. Rog, I. Vattulainen, M. Grzybek, U. Coskun, C. A. Lingwood, and K. Simons. Cholesterol modulates glycolipid conformation and receptor activity. *Nature Chemical Biology*, 7(5):260–262, 2011.

- [225] N. Yahi, A. Aulas, and J. Fantini. How cholesterol constrains glycolipid conformation for optimal recognition of alzheimer's beta amyloid peptide (A beta(1-40)). *Plos One*, 5(2):e9079, 2010.
- [226] L. Wawrezinieck, H. Rigneault, D. Marguet, and P. F. Lenne. Fluorescence correlation spectroscopy diffusion laws to probe the submicron cell membrane organization. *Biophysical Journal*, 89(6):4029–4042, 2005.
- [227] L. A. Bagatolli, J. H. Ipsen, A. C. Simonsen, and O. G. Mouritsen. An outlook on organization of lipids in membranes: Searching for a realistic connection with the organization of biological membranes. *Progress in Lipid Research*, 49(4):378–389, 2010.
- [228] M. Fidorra, A. Garcia, J. H. Ipsen, S. Hartel, and L. A. Bagatolli. Lipid domains in giant unilamellar vesicles and their correspondence with equilibrium thermodynamic phases: A quantitative fluorescence microscopy imaging approach. *Biochimica Et Biophysica Acta-Biomembranes*, 1788(10):2142–2149, 2009.
- [229] J. Juhasz, F. J. Sharom, and J. H. Davis. Quantitative characterization of coexisting phases in dopc/dppc/cholesterol mixtures: Comparing confocal fluorescence microscopy and deuterium magnetic resonance. *Biochimica Et Biophysica Acta-Biomembranes*, 1788(12):2541–2552, 2009.
- [230] S. Engel, S. Scolari, B. Thaa, N. Krebs, T. Korte, A. Herrmann, and M. Veit. Flim-fret and frap reveal association of influenza virus haemagglutinin with membrane rafts. *Biochemical Journal*, 425:567–573, 2010.
- [231] S. Mayor and M. Rao. Rafts: Scale-dependent, active lipid organization at the cell surface. *Traffic*, 5(4):231–240, 2004.
- [232] M. Rao and S. Mayor. Use of forster's resonance energy transfer microscopy to study lipid rafts. *Biochimica Et Biophysica Acta-Molecular Cell Research*, 1746(3):221–233, 2005.
- [233] F. Pinaud, X. Michalet, G. Iyer, E. Margeat, H. P. Moore, and S. Weiss. Dynamic partitioning of a glycosyl-phosphatidylinositol-anchored protein in glycosphingolipid-rich microdomains imaged by single-quantum dot tracking. *Traffic*, 10(6):691–712, 2009.
- [234] C. Depry, M. D. Allen, and J. Zhang. Visualization of pka activity in plasma membrane microdomains. *Mol Biosyst*, 7(1):52–58, 2011.

- [235] K. Simons, U. Coskun, M. Grzybek, D. Lingwood, I. Levental, and H. J. Kaiser. Lipid-protein interactions governing raft partitioning in membranes. *Chemistry and Physics of Lipids*, 163:S10–S10, 2010.
- [236] E. Sezgin, I. Levental, M. Grzybek, G. Schwarzmann, V. Mueller, A. Honigmann, V. N. Belov, C. Eggeling, U. Coskun, K. Simons, and P. Schwille. Partitioning, diffusion, and ligand binding of raft lipid analogs in model and cellular plasma membranes. *Biochimica Et Biophysica Acta-Biomembranes*, 1818(7):1777–1784, 2012.
- [237] J. J. Adams, S. Narayanan, B. Liu, M. E. Birnbaum, A. C. Kruse, N. A. Bowerman, W. Chen, A. M. Levin, J. M. Connolly, C. Zhu, D. M. Kranz, and K. C. Garcia. T cell receptor signaling is limited by docking geometry to peptide-major histocompatibility complex. *Immunity*, 35(5):681–693, 2011.

Acknowledgments

This work would not be possible without the contribution of several people. First of all, I would like to thank Petra Schwille for giving me the perfect environment that I needed for my science. Independence that she provides is, I believe, what keeps the spirit in the lab. I also would like to thank Kai Simons for being always a great support. He is not only a great scientist that inspires me, but also a great person with modesty and wisdom that makes him a role model for me. I am grateful to Michele Solimena and Stefan Diez for their support and valuable comments during my thesis committee meetings.

Thanks to all the members of Schwille Lab and Simons lab for their support and friendship. Particularly I would like to thank Grzegorz, Jens and Senthil(Dada) for teaching me how to play kicker, being very helpful to me and all the fun we had together. Karin, Sarah, Sabine, Anke, thank you for making my life a lot easier in the lab. Also I want to thank Unal (Dr. Cosi) for his being like a "big" brother to me. He was always ready to help whenever I needed. I would also like to thank my collaborators who provided me excellent questions and different visions. Thanks to Christian Eggeling, Alf Honigmann, Ron Dirkx, Aliaksei Dubavik, Vladimir Lesnyak, James Saenz and Gunes Ozhan.

I thank all friends of mine who supported me mentally during my thesis. First, the people who changed my social life in Neustadt: The Shouting Men. Tobi, Hannes, Konrad and Philipp filled it with street music, skat (with German cards, of course) and friendship. The days that police came three times to disperse the crowd listening to us in Assi-eck were among my best days in Dresden. I would also like to thank the WG: Lena and Maja for being great flatmates. We had many marvelous days full of joy and deep conversation. Also, thanks to Olli, Isa, Sonja, Marija, Nikos, Ana, Tiago, Juan, Miguel, Aida, Matias and Julieta for giving me great time outside the work. I want to thank the Turkish gang who created a homy environment for me. Thanks to Caghan, Gamze, Nehir, Ozlem, Fatih, Songul, Vahap, Muge, Aylin, Dilce and Gokcan. Sagolun gencler. And finally Zeynep and Gunes who were always with me during my difficult days with their great smiles which made me forget about all my troubles.

After all, it is most certain that this work would not be possible without Ilya Levental. He was always helpful to me even while he was yelling at me because of my awful writing. He taught me how to set the balance between the enthusiasm and the criticism

which shaped my scientific vision dramatically. He was a great scientific tutor, but more importantly a great friend who introduced me plenty of new things. He taught me, for instance, that country music is not from California (although I am not completely convinced) or how to distinguish different whiskies with its wood or seaweed smell. I owe him thousands of thanks for all the things he did for me.

Finally many thanks to Ilya, Gunes and Lena for reading and correcting the parts of the thesis.

And thanks to all my family and friends who were always with me...

**Erklärung gemäß § 5 (5) der Promotionsordnung der
Fakultät Mathematik und Naturwissenschaften der
Technischen Universität Dresden**

(Declaration required according to § 5 (5) of the *regulations for obtaining a doctoral degree* of the Faculty of Science of the TU Dresden)

Hiermit versichere ich, dass ich die vorliegende Arbeit ohne unzulässige Hilfe Dritter und ohne Benutzung anderer als der angegebenen Hilfsmittel angefertigt habe; die aus fremden Quellen direkt oder indirekt übernommenen Gedanken sind als solche kenntlich gemacht. Die Arbeit wurde bisher weder im Inland noch im Ausland in gleicher oder ähnlicher Form einer anderen Prüfungsbehörde vorgelegt.

Diese Dissertation wurde unter der Betreuung von Prof. Dr. Petra Schwille im Zeitraum vom Dezember 2008 bis August 2012 am Biotechnologischen Zentrum der Technischen Universität Dresden angefertigt.

Ich erkenne die Promotionsordnung der Fakultät Mathematik und Naturwissenschaften der Technischen Universität Dresden an.

I herewith declare that I have produced this paper without the prohibited assistance of third parties and without making use of aids other than those specified; notions taken over directly or indirectly from other sources have been identified as such. This paper has not previously been presented in identical or similar form to any other German or foreign examination board.

The thesis work was conducted from November 2009 to December 2012 under the supervision of Prof. Dr. Petra Schwille at Biotechnologischen Zentrum der Technischen Universität Dresden.

I declare that I have not undertaken any previous unsuccessful doctorate proceedings.

I declare that I recognize the doctorate regulations of the Fakultät für Mathematik und Naturwissenschaften of the Technische Universität Dresden.

Erdinc Sezgin

Dresden, November 2012